THE MECHANISTIC AND STRUCTURAL BASIS OF VERAPAMIL AND DIGOXIN INTERACTIONS WITH THE P-GLYCOPROTEIN TRANSPORTER

by

KAITLYN V. LEDWITCH

(Under the Direction of Arthur G. Roberts)

ABSTRACT

Molecular "efflux" pumps belonging to the ATP-binding cassette (ABC) superfamily such as P-glycoprotein use energy from ATP hydrolysis to drive drug export across cell membranes back to the extracellular space. The Pgp transporter is widely recognized for its unusual ability to bind many clinically relevant drugs that are chemically and functionally diverse. This drug promiscuity poses challenges in the clinic because Pgp confers multidrug resistance (MDR) in cancer cells and mediates drug-drug interactions (DDIs). One of the most recognized DDIs with the Pgp transporter is between the two cardiovascular ion channel inhibitors verapamil and digoxin. Despite many *in vitro* and *in vivo* studies, the mechanistic and structural basis of verapamil and digoxin interactions with the P-glycoprotein transporter and how drug binding is coupled to ATP hydrolysis is quite elusive. To shed light on this Pgp-mediated DDI, we probed verapamil and digoxin interactions with Pgp using several NMR techniques (STDD NMR, PRE NMR), fluorescence and the kinetic fitting software COPASI. From this work, we generated a comprehensive molecular model of the DDI between verapamil and digoxin with Pgp encompassing competitive and noncompetitive inhibition of digoxin transport by verapamil. We also showed that coupling between verapamil and ATP binding to

the transporter and verapamil-induced ATP hydrolysis occurs in a cooperative fashion. Excitingly, a model of digoxin bound to Pgp was determined using PRE NMR derived distance restraints to drive molecular docking in the HADDOCK software. To our knowledge, this will be the first model demonstrating the bound location of a drug to the Pgp transporter. This information will guide the rational design of effective cancer drugs and Pgp inhibitors and guide better predictions of safe multidrug regimens that bypass Pgp-mediated DDIs in the clinic.

INDEX WORDS: P-glycoprotein, drug-drug interactions (DDIs), cardiovascular, verapamil, digoxin, nuclear magnetic resonance (NMR)

THE MECHANISTIC AND STRUCTURAL BASIS OF VERAPAMIL AND DIGOXIN INTERACTIONS WITH THE P-GLYCOPROTEIN TRANSPORTER

by

KAITLYN V. LEDWITCH

BS Chemistry, Valdosta State University, 2012

A Dissertation Submitted to the Graduate Faculty of The University of Georgia in Partial Fulfillment of the Requirements for the Degree

DOCTOR OF PHILOSOPHY

ATHENS, GEORGIA

2017

THE MECHANISTIC AND STRUCTURAL BASIS OF VERAPAMIL AND DIGOXIN INTERACTIONS WITH THE P-GLYCOPROTEIN TRANSPORTER

by

KAITLYN V. LEDWITCH

Major Professor:	Arthur G. Roberts
Committee:	Brian Cummings
	Jason Zastre
	Eileen Kennedy
	James Prestegard

Electronic Version Approved:

Suzanne Barbour
Dean of the Graduate School
The University of Georgia
August 2017

DEDICATION

I dedicate this dissertation to my grandparents, Gwen Love, Jerry Love, Grace Ledwitch and my late grandfather as of July 2016, John William Ledwitch II. As he would never fail to mention how proud of me he was, even to passing strangers—this is especially for you Peepaw.

ACKNOWLEDGEMENTS

"It will not be simple, it will not be long, it will take little time, it will take all your thought, it will take all your heart, it will take all your breath, it will be short, it will not be simple—Adrienne Rich." Although this adventure was far from simple and now, seemingly short, there are many who made the toughest and longest of days seem easy.

To my partner, Breanna Miller, you have been my anchor throughout this entire journey. You gave me strength when I was weak and courage when I was scared. You were my peace in times of chaos and my ambition when I would lose sight of my motivation. You are hands down my better half and I could not have done this without you, I love you.

To my doggie children, Harbor and Coasta, you both never fail to have dance parties for me every time I walk through the door. Not only do these make my heart smile, but also, they instantly made the bad days good. I am so lucky to be your human.

To my Mom and Dad, and brothers, John and Paxton, the support you have shown throughout my education has been instrumental in my successes. I love, love you all.

To Jason Simpson, I cannot imagine a better best friend coming into my life at such the right time. Thank you for always being down for some porch sittin' and late night conversations. I should also mention my ladies of the night, Lishann Ingram and Dr. Octavia Goodwin, your words of wisdom during these times kept my laughter alive. These moments never failed to restore my spirits. I adore each and every one of you.

To my Graduate Committee, I sincerely appreciate all of your time, guidance and support

during this process. You have challenged me to be a better thinker, a better scientist and ultimately, prepared me for the next chapter in my career. For this, I am forever grateful.

To my advisor, Audie Roberts, although you may never actually read this, thank you for all of your support and patience over the past five years. It has been a wild journey, but I am so proud to have done this under your direction. The impact you have made on my graduate career is priceless.

And last, to the city of Athens, you have never failed to energize my soul with your beauty, music and array of delectable eateries. You are truly an extraordinary place to live and I have been so proud to call you home.

TABLE OF CONTENTS

Page

LIST OF TABLES

Page

LIST OF FIGURES

Page

ABBREVIATIONS

ABC: ATP binding cassette

ADRs: adverse drug reactions

AMPPNP: adenosine 5'-(β,γ-imido)triphosphate

COPASI: complex pathway simulator

DDIs: drug-drug interactions

DDM: *n*-dodecyl-β-*D*-maltoside

DLCs: digitalis-like compounds

DOSY: diffusion ordered spectroscopy

EGTA: ethylene glycol tetraacetic acid

$F_{0,H}$: initial fluorescence intensity at the high concentration phase

$F_{0,L}$: initial fluorescence intensity at the low concentration phase

HADDOCK: High Ambiguity Driven DOCKing

ICLs: intracellular loops

K_A: Association constant

K_D: Dissociation constant

K_H: equilibrium constant at high concentration

K_L: equilibrium constant at low concentration

K_m: Michaelis-Menton constant

K_{SV}: Stern-Volmmer quenching constant

L: ligand

NATA: *N*-acetyl-*L*-tryptophanamide

NTA: nickel-nitrilotriacetic acid

PAGE: polyacrylamide gel electrophoresis

Pgp: P-glycoprotein

Pi: inorganic phosphate

PRE: paramagnetic relaxation enhancement

RF: radio frequency

SDS: sodium dodecylsulfate

Q: quenching ligand

STD: saturation transfer difference

STDD: saturation transfer double difference

TMHs: transmembrane helices

TMDs: transmembrane domains

CHAPTER 1

CARDIOVASCULAR ION CHANNEL INHIBITOR DRUG-DRUG INTERACTIONS WITH THE P-GLYCOPROTEIN TRANSPORTER[1]

[1] Ledwitch, K. V. and A. G. Roberts (2017). *The AAPS Journal.* 19, 409-420. Reprinted here with permission of publisher.

1.1. ABSTRACT

P-glycoprotein (Pgp) is an ATP-binding cassette (ABC) transporter that plays a major role in cardiovascular drug disposition by effluxing a chemically and structurally diverse range of cardiovascular therapeutics. Unfortunately, drug-drug interactions (DDIs) with the transporter have become a major roadblock to effective cardiovascular drug administration because they can cause adverse drug reactions (ADRs) or reduce the efficacy of drugs. Cardiovascular ion channel inhibitors are particularly susceptible to DDIs and ADRs with Pgp because they often have low therapeutic indexes and are commonly coadministered with other drugs that are also Pgp substrates. DDIs from cardiovascular ion channel inhibitors with the transporter occur because of inhibition or induction of the transporter and the transporter's tissue and cellular localization. Inhibiting Pgp can increase absorption and reduce excretion of drugs, leading to elevated drug plasma concentrations and drug toxicity. In contrast, inducing Pgp can have the opposite effect by reducing the drug plasma concentration and its efficacy. A number of *in vitro* and *in vivo* studies have already demonstrated DDIs from several cardiovascular ion channel inhibitors with human Pgp and its animal analogs, including verapamil, digoxin, and amiodarone. In this review, Pgp-mediated DDIs and their effects on pharmacokinetics for different categories of cardiovascular ion channel inhibitors are discussed. This information is essential for improving pharmacokinetic predictions of cardiovascular therapeutics, for safer cardiovascular drug administration and for mitigating ADRs emanating from Pgp.

1.2. INTRODUCTION

Cardiovascular drug prescriptions have significantly increased over the past decade with over 15% of patients on multidrug regimens (a.k.a. polypharmacy) (Kantor *et al.*, 2015). Of

hospitalized patients on cardiovascular medications, ~4% exhibited serious adverse drug reactions (ADRs) (Zaidenstein *et al.*, 2002). Cardiovascular ion channel inhibitors, which are used to treat cardiac arrhythmia and hypertension, represent a major contributor of cardiovascular drug ADRs (Gholami *et al.*, 2008; Tabrizchi, 2010). These drugs target channels and enzymes that control the flow of ions in vascular smooth muscle cells and the cardiomyocytes (Tabrizchi, 2010). This serves to regulate cardiac inotropy, maintain the resting potential of cardiovascular cells, and control blood pressure (Tabrizchi, 2010). Unfortunately, many of these drugs such as digoxin have a low therapeutic index, so any changes to their plasma concentration can potentially lead to ADRs (Tabrizchi, 2010). Many cardiovascular drug fatalities from ADRs are the result of drug-drug interactions (DDIs) with cardiovascular ion channel inhibitors (Karimzadeh *et al.*, 2011; N. Mohebbi *et al.*, 2010; Mowry *et al.*, 2015). In one study, the cardiovascular ion channel inhibitor digoxin was implicated in a majority of preventable DDIs (Karimzadeh *et al.*, 2011). In another study, the cardiovascular ion channel inhibitor amiodarone, which is known to have several significant DDIs, had the second highest frequency of ADRs (Niayesh Mohebbi *et al.*, 2010).

One of the main contributors to cardiovascular ion channel inhibitor DDIs and ADRs is the ATP-binding cassette (ABC) P-glycoprotein (Pgp) transporter (Aller *et al.*, 2009). In general, Pgp is a promiscuous drug transporter that can bind multiple drugs simultaneously (Glaeser, 2011), which includes interactions with a chemically and structurally diverse range of cardiovascular drugs (Seelig, 1998; Wessler *et al.*, 2013). These interactions in combination with the narrow therapeutic indexes make Pgp particularly susceptible to cardiovascular DDIs. The transporter is also prone to DDIs because of its function in absorption, elimination, and distribution of drugs (Wessler *et al.*, 2013). This function leads to changes in cardiovascular ion

inhibitor drug plasma concentrations and results in ADRs or reduced drug efficacy (Glaeser, 2011).

A general overview of cardiovascular drugs and Pgp was published (Wessler *et al.*, 2013), but no recent comprehensive review has been published that discusses Pgp-mediated DDIs from cardiovascular ion channel inhibitors and their clinical consequences. This review discusses a wider range of cardiovascular ion channel inhibitors and provides a more detailed analysis of the observed pharmacokinetics than (Wessler *et al.*, 2013). This review also describes the pharmacodynamics of cardiovascular ion channel inhibitors including their targets and mechanisms of action. Then, we discuss Pgp-mediated transport of the cardiovascular ion channel inhibitor and DDIs observed with the drug. This is followed by a discussion and comments on the observed pharmacokinetics of coadministering the drug.

1.3. CARDIOVASCULAR DISEASES AND CURRENT TREATMENTS

Cardiovascular disease (CVD) is a leading cause of death worldwide (Luepker, 2011). CVD represents a class of diseases of the vascular system that can involve blood vessels such as coronary artery disease and stroke, or the heart, which includes congestive heart failure and hypertension (Luepker, 2011). A number of treatments have been developed to treat CVD that target receptors, channels, and enzymes of the cardiovascular system (Atlas, 2007; Giovannitti *et al.*, 2015; Grant, 2009; Harter *et al.*, 2015; Helfand *et al.*, 2009; Jensen *et al.*, 2011; Smith *et al.*, 2009). Since hypertension represents a major risk factor for several diseases within CVD (Padwal *et al.*, 2001), several drug classes have been developed to lower blood pressure [*e.g.*, (Atlas, 2007)]. Some of the most effective treatments for hypertension have targeted the angiotensin-renin-aldosterone system, which is the signaling pathway for regulating blood pressure and fluid balance (Atlas, 2007). There are also antihypertensive drugs that target the α-

and β-adrenergic receptors that affect the action of catecholamines, norepinephrine and epinephrine (Giovannitti *et al.*, 2015; Helfand *et al.*, 2009; Jensen *et al.*, 2011). Loop diuretics represent a third class of antihypertensive drugs that reduce blood pressure by decreasing fluid volume as a result of inhibiting the Na^+-K^+-$2Cl^-$ symporter in the kidneys (Roush and Sica, 2016). To treat strokes, cardiovascular drugs have been designed to reduce blood clotting by targeting proteins within the coagulation cascade or involved in platelet aggregation (Harter *et al.*, 2015). High cholesterol, which represents a major risk factor for CVD, is most often treated with statin drugs (Smith *et al.*, 2009). These drugs lower high cholesterol by targeting 3-hydroxy-3-methyl-glutaryl (HMG)-CoA reductase, which is the rate-limiting enzyme in cholesterol biosynthesis (Smith *et al.*, 2009). The cardiovascular drugs that are the focus of this review are cardiovascular ion channel inhibitors. These drugs are used to treat a range of diseases within CVD, including hypertension, cardiac dysrhythmias, and atrial fibrillation (Grant, 2009). These drugs affect vascular physiology by directly inhibiting the flow of ions through Ca^{2+}, K^+, or Na^+ channels or indirectly by increasing intracellular Ca^{2+} concentration through inhibition of the Na^+/K^+ ATPase (Grant, 2009). In addition to the reviewed drugs, there are emerging therapies for CVD that target chemokines, high-density lipoproteins, and microRNA, and there has been some progress toward the actual regeneration of cardiomyocytes (Dimmeler, 2011).

1.4. CARDIOVASCULAR ION CHANNELS

Cardiovascular ion channels control the flow of ions and function to regulate the heart rhythm and blood pressure (Amin *et al.*, 2010; Martens and Gelband, 1998). They are found in cardiomyocytes of the heart and vascular smooth muscle cells of the arteries and veins where heterogeneous expression of these channels promotes proper heart rhythms and blood pressure

(Amin *et al.*, 2010; Martens and Gelband, 1998). Mutations in genes that code for the ion channels or alterations in their expression level lead to inherited or acquired cardiac arrhythmia (Amin *et al.*, 2010). Table 1.1 shows several types of cardiovascular ion channels, including Ca^{2+}, K^{+}, and Na^{+} channels. The table also shows the channel isoforms, their general functions, and cardiovascular diseases associated with them.

1.4.1. Calcium Channels

Cardiovascular Ca^{2+} channels are voltage-dependent channels that control the flux of Ca^{2+} into vascular smooth muscle cells and cardiomyocytes (Catterall, 2011). Inward flux of Ca^{2+} ions by the channel triggers additional Ca^{2+} release from the sarcoplasmic reticulum (Catterall, 2011). Calcium binds and induces a conformational change in the troponin-tropomyosin complex that facilitates interaction between the actin filament and myosin, and leads to a muscle contraction (Catterall, 2011). There are two types of cardiovascular Ca^{2+} channels, long-lasting (L)-type and transient (T)-type Ca^{2+} channels, that activate the inward flux of Ca^{2+} ions through relatively high and low voltage potentials, respectively (Catterall, 2011). The L-type Ca^{2+} channels function to excite and contract muscle cells, while T-type Ca^{2+} channels serve a cardiac pacemaking function and regulate arterial resistance (Catterall, 2011). Defects in the ion channel have been associated with various cardiovascular disorders, including arrhythmias and hypertension (J. B. Kim, 2014).

1.4.2. Potassium Channels

Potassium ion transport by these proteins is accomplished by several mechanisms including Ca^{2+} activation, voltage, and ATP (Giudicessi and Ackerman, 2012). These channels

Table 1.1. Types and function of cardiovascular ion channels.

Ion Channel	Relevant Types	Physiological Function	Associated Cardiovascular Diseases	References
Ca^{2+} channels	• Long-lasting (L-type) • Transient (T-type)	• L-type: excite and contract muscle cells • T-type: cardiac pacemaking function and regulate arterial resistance	arrhythmias, Brugada syndrome, hypertension	(Catterall, 2011; J. B. Kim, 2014)
K^+ channels	• Calcium-activated (BK_{Ca}) • Voltage-gated (K_V) • ATP-dependent (K_{ATP}) • Inwardly rectifying (K_{IR})	• Mediate membrane and resting potential • Regulate cardiac action potential	atrial fibrillation, Brugada syndrome, hypertension, long and short QT syndrome	(Giudicessi and Ackerman, 2012; J. B. Kim, 2014)
Na^+ channels	• Voltage-gated (Na_V)	• Initial fast upstroke of the cardiac action potential • Contractile response of vascular smooth muscle cells	atrial standstill, Brugada syndrome, cardiac conduction disorders, dilated cardiomyopathy, erthromelalgia, long QT syndrome, nonprogressive familial heart block	(Giudicessi and Ackerman, 2012; Ho *et al.*, 2013; J. B. Kim, 2014)
Na^+/K^+ ATPases	• α and β isoforms	• Resting potential, cell volume and $[Ca^{2+}]$	atrial fibrillation, heart failure	(Suhail, 2010)

are a major regulator of vascular smooth muscle cell voltage and resting potential (Giudicessi and Ackerman, 2012). The channels also function to regulate the duration of the action potential in the cardiac muscle (Giudicessi and Ackerman, 2012). Abnormal functioning of this channel has been associated with hypertension and Brugada syndrome, which leads to increased risk of cardiac death (Giudicessi and Ackerman, 2012; J. B. Kim, 2014).

1.4.3. Sodium Channels

Voltage-gated sodium channels (Na_V) control the Na^+ ion flux through Na^+-induced conformational changes (Remme and Bezzina, 2010). In the heart, influx by these channels is responsible for the initial fast upstroke of the cardiac action potential (Remme and Bezzina, 2010). There is also recent evidence that these channels contribute to the contractile response of vascular smooth muscle cells (Ho *et al.*, 2013). Defects in this channel are associated with a number of cardiomyopathies including long QT syndrome (J. B. Kim, 2014; Remme and Bezzina, 2010).

1.4.4. Na/K^+ ATPase

This ATP-dependent enzyme effluxes Na^+ ions out while pumping K^+ ions into cardiovascular cells (Suhail, 2010). The enzymes help maintain the resting potential and cell volume through osmosis and indirectly decrease intracellular Ca^{2+} concentration through the Na^+/Ca^{2+} exchanger (Suhail, 2010). Defects in the energy-dependent transporter are associated with heart failure and atrial fibrillation (Suhail, 2010).

1.5. ION CHANNEL INHIBITORS AND THEIR MECHANISMS OF ACTION

Ion channel inhibitors are used to redistribute ions and restore the natural rhythm of the heart by inhibiting specific channels and transporters of the cardiovascular system (Amin *et al.*, 2010). These inhibitors can be classified as calcium, sodium, or potassium channel inhibitors and cardiac glycosides, but may fit into multiple ion channel inhibitor categories and may have an array of electrophysiological actions (Dan M. Roden *et al.*, 2007). For example, the antiarrhythmic drug quinidine is a well-known sodium channel blocker, but it also exerts action against potassium channels and α-adrenergic receptors (Dan M. Roden *et al.*, 2007). For simplicity, ion channel inhibitors in this review will be discussed according to their main site of action. Table 1.2 summarizes the general categories of cardiovascular inhibitors, their mechanism of action, clinical uses, and ADRs.

1.5.1. Calcium Channel Inhibitors

These drugs are used to treat a range of cardiovascular disorders including hypertension and arrhythmias (Buckley *et al.*; McDonagh *et al.*, 2005). Calcium channel inhibitors (or blockers) disrupt the flow of L- and/or T-type Ca^{2+} channels (Buckley *et al.*; Grant, 2009; McDonagh *et al.*, 2005). This disruption increases the intracellular Ca^{2+} concentration in vascular smooth muscle cells and cardiomyocytes, which leads to vasodilation and promotes a regular heart rhythm (Buckley *et al.*; McDonagh *et al.*, 2005). ADRs from toxic concentrations of calcium channel inhibitors result in bradycardia (abnormally slow heart rate) and hypotension that can lead to serious complications including death (Buckley *et al.*; McDonagh *et al.*, 2005).

Table 1.2. Characteristics of cardiovascular ion channel inhibitors.

Inhibitor Class	Examples	Mechanism	Clinical Uses	ADRs	References
Ca^{2+} channel inhibitors	amlodipine diltiazem mibefradil nicardipine nifedipine verapamil	Inhibit or interfere with Ca^{2+} influx by binding to specific sites on the channel	angina, arrhythmias, hypertension, coronary artery disease	bradycardia, hypotension	(Buckley *et al.*, 2007; Grant, 2009; McDonagh *et al.*, 2005)
K^+ channel inhibitors	amiodarone dronedarone	Interfere with K^+ ion flow	cardiomyopathy, atrial fibrillation and flutter	arrhythmias, blue-gray hyperpigmentation, hepatotoxicity, pulmonary fibrosis	(Grant, 2009; Siddoway, 2003; Wulff *et al.*, 2009)
Na^+ channel inhibitors	flecainide phenytoin quinidine	Stabilize the inactivated channel conformation through fast and slow mechanisms	atrial flutter, tachycardias	bradyarrhythmias, slow atrial flutter, proarrhythmia	(Dan M. Roden *et al.*, 2007)
Cardiac Glycosides	digitoxin digoxin ouabain	Inhibit Na^+/K^+ ATPase and indirectly increase intracellular $[Ca^{2+}]$	atrial fibrillation and heart failure	atrioventricular block, bradycardia, gastrointestinal and neurological disorders, ventricular arrhythmias,	(Fuerstenwerth, 2014; Hauptman and Kelly, 1999; Ziff and Kotecha, 2016)

1.5.2. Potassium Channel Inhibitors

Potassium channel inhibitors prolong repolarization and the action potential duration in cardiomyocytes by interfering with conduction through potassium channels (Grant, 2009; Wulff *et al.*, 2009). In general, these inhibitors are used to treat cardiomyopathy and atrial fibrillation (Grant, 2009; Wulff *et al.*, 2009). They have also been used to treat ventricular tachycardia during cardiac arrest (Wulff *et al.*, 2009). These drugs exhibit a range of ADRs including worsening arrhythmias, blue-gray hyperpigmentation, and sudden cardiac arrest (Siddoway, 2003).

1.5.3. Sodium Channel Inhibitors

Sodium channel blockers are used to suppress heart tachycardias and atrial flutter by decreasing the flow of Na^+ ions through the sodium channel and reducing the action potential duration (D. M. Roden, 2004). Reduction of Na^+ ion flow by these inhibitors is accomplished by stabilizing the inactivated state of the Na^+ channel through fast and slow mechanisms (D. M. Roden, 2004). ADRs from these inhibitors include bradyarrhythmias (slowed heart rate) and slow atrial flutter (D. M. Roden, 2004).

1.5.4. Cardiac Glycosides

Cardiac glycosides are a special type of ion channel inhibitor and include digitalis glycosides such as digoxin, digitoxin, and ouabain (Fuerstenwerth, 2014). Clinically, these drugs are used to treat atrial fibrillation and flutter and some cases of heart failure (Hauptman and Kelly, 1999; Ziff and Kotecha, 2016). These drugs target the Na^+/K^+ ATPase in the heart, which indirectly increases intracellular Ca^{2+} concentration by the effect of decreasing intracellular Na^+

levels on the sodium-calcium exchanger (Fuerstenwerth, 2014). The increase in intracellular Ca^{2+} corresponds with an increase in inotropy or force of contraction of the heart (Fuerstenwerth, 2014). In addition to cardiovascular ADRs, gastrointestinal and neurological disorders are commonly observed with this class of drug (Hauptman and Kelly, 1999; Ziff and Kotecha, 2016).

1.6. CHARACTERISTICS OF PGP AND ITS EFFECT ON ION CHANNEL INHIBITOR DISPOSITION

Pgp is a member of the ABC transporter superfamily and can efflux a chemically and structurally diverse range of molecules (Seelig, 1998; Wessler *et al.*, 2013). Figure 1.1 A shows the X-ray crystal structure of mouse Pgp, which consists of two nucleotide-binding domains (NBDs), 12 transmembrane (TM) helices, and a large 6000-$Å^3$ drug binding cavity (Aller *et al.*, 2009). Figure 1.1 B shows the generally accepted model for ATP-driven drug efflux by Pgp. The left side of the panel depicts drugs binding to Pgp from the cell membrane or the cytosol within the TM region of Pgp with the NBDs separated (Aller *et al.*, 2009; Sharom, 2014). The binding of two ATP molecules shifts the NBDs together (right side of Figure 1.1 B) and releases the drug to the extracellular side of the membrane (Aller *et al.*, 2009; Sharom, 2014). ATP is hydrolyzed into ADP and inorganic phosphate (P_i) resetting the NBDs back to their initial conformation for another round of drug binding and transport (left side of Figure 1.1 B) (Aller *et al.*, 2009; Sharom, 2014).

Pgp plays a key role in cardiovascular ion channel inhibitor DDIs by altering drug plasma concentrations and distribution and by its cellular localization and expression levels. The transporter is found at relatively high concentrations on the lumenal side of enterocytes and

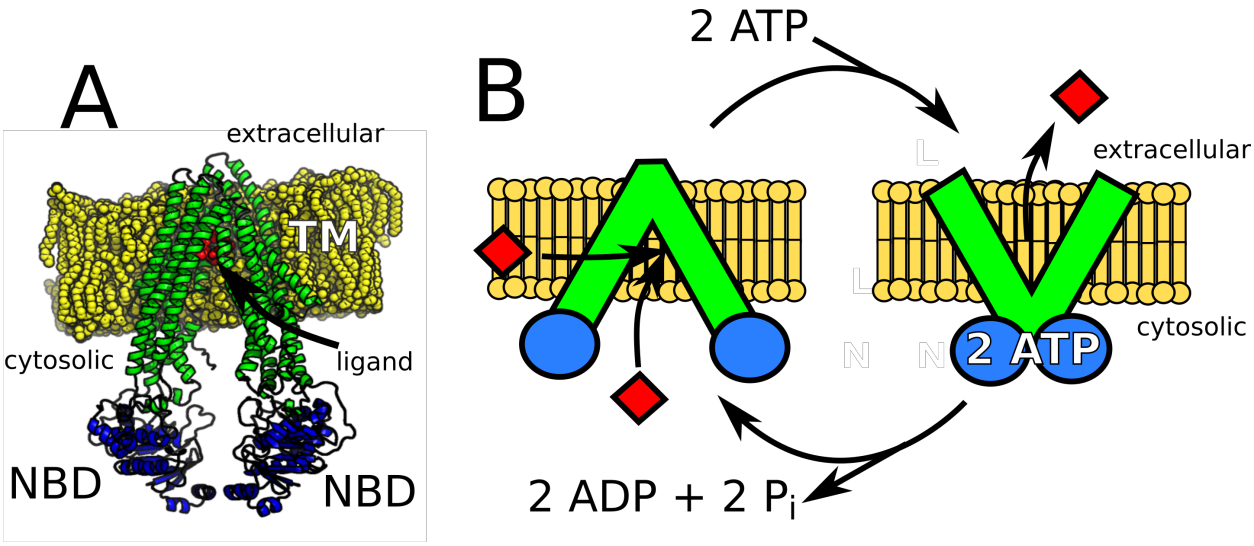

Figure 1.1. Structure and ATP-driven transport mechanism of Pgp. A) The X-ray crystal structure of mouse Pgp showing the transmembrane (TM, green), nucleotide-binding domains (NBDs, blue) and the position of QZ59-RRR, which is labeled "ligand" (red) in a phosphatidylcholine lipid bilayer (yellow) (Aller *et al.*, 2009). B) Conformationally and ATP-driven model of efflux by Pgp. On the left of the panel, drug binding (red diamonds) occurs with the NBDs of Pgp separated. Binding of 2 ATP causes the NBDs to come together and leads to the release of drug (red diamonds) to the extracellular space. The extracellular and cytosolic sides of the cell membrane (yellow) are shown on the top and bottom of the membrane, respectively.

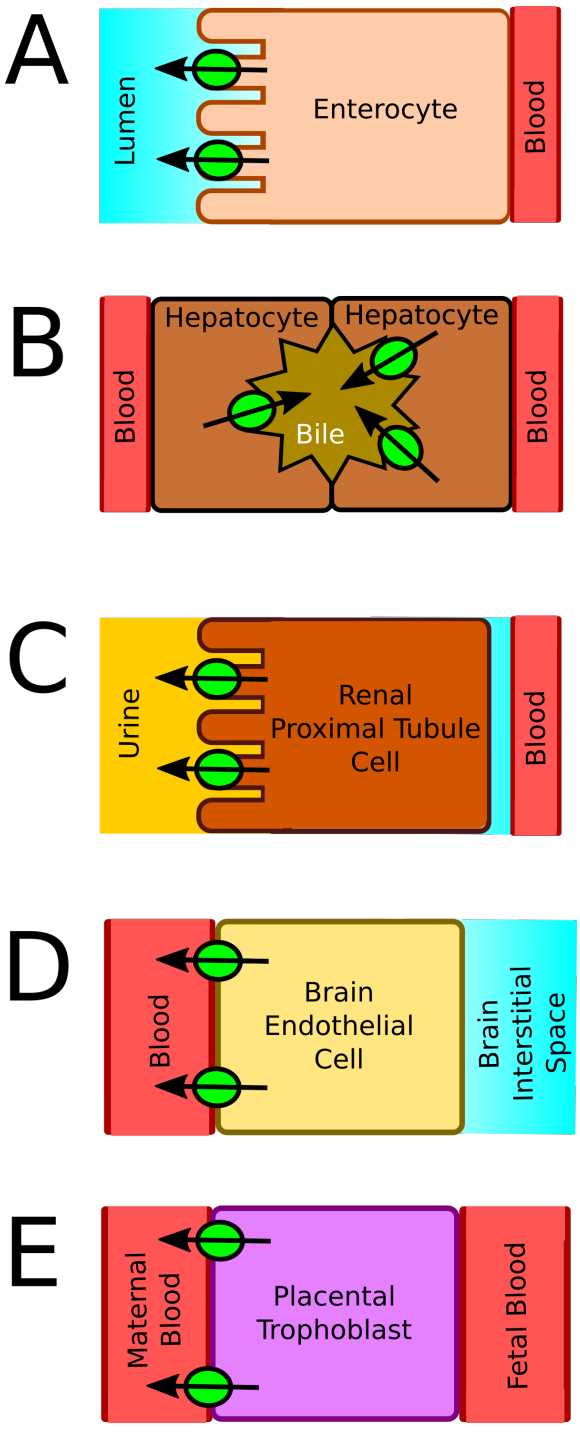

Figure 1.2. Pgp localization in A) an enterocyte, B) a hepatocyte, C) a kidney proximal tubule cell, D) a brain endothelial cell and E) a placental trophoblast. The green circles are Pgp and the arrows denote the direction of efflux.

reduces oral absorption and bioavailability by effluxing drugs back into the intestinal lumen (Figure 1.2 A) (Giacomini *et al.*, 2010). The transporter is also found at relatively high concentrations on the lumenal side of kidney proximal tubule cells and the bile canalicular surface of hepatocytes decreasing drug plasma concentrations by excretion (Figure 1.2 B, C) (Giacomini *et al.*, 2010). Pgp also affects drug distribution. Pgp is found on the blood side of epithelial cells located at the blood brain barrier (BBB) and reduces brain penetration of cardiovascular drugs (Figure 1.2 D) (Giacomini *et al.*, 2010). Pgp is also present on the maternal side of placental trophoblasts preventing entry of cardiovascular drugs and protecting the unborn fetus (Figure 1.2 E) (Staud *et al.*, 2012). Although there is Pgp present in the heart, it has little effect on drug disposition because of its relatively low concentration (Couture *et al.*, 2006). Moreover, Pgp expression levels in all of these tissues can be influenced by genetic polymorphisms of Pgp, cardiomyopathy, and different stages of pregnancy (Cascorbi *et al.*, 2004; F. S. Chung *et al.*, 2010; Meissner *et al.*, 2002).

Pgp-mediated DDIs result in significant changes in the drug pharmacokinetics by inhibition or induction of the transporter. Inhibition of intestinal Pgp is saturable and will lead to an increase in oral absorption of Pgp substrates, while inhibition of excretory cells in the kidneys and the liver will reduce the clearance and increase the terminal elimination half-life ($t_{1/2}$) of Pgp substrates (Lin and Yamazaki, 2003). The combined inhibition will result in a net increase in the drug plasma concentration and will lead to an increase in the peak drug plasma concentration (C_{max}) and the individual's exposure as reflected by the area under the curve (AUC) in the pharmacokinetics profile (Lin and Yamazaki, 2003). This is particularly problematic for several cardiovascular ion channel inhibitors because of their relatively low therapeutic indexes and because elevated drug plasma concentration can lead to toxic drug plasma concentrations and

serious ADRs (Ehle *et al.*, 2011). Inhibition of Pgp at the BBB or in the placental trophoblasts potentially increases penetration and toxic exposure to the brain and fetus, respectively (Lin and Yamazaki, 2003). Pgp inhibition there can lead to changes in the drug's distribution, which is reflected in the apparent volume of distribution (V_D) (Lin and Yamazaki, 2003). Induction of Pgp will have the opposite effect of Pgp inhibition by decreasing the drug plasma concentration and exposure, but might also significantly reduce a drugs' efficacy. This will lead to a decrease in the C_{max} and AUC in the pharmacokinetics profile (Lin and Yamazaki, 2003). Pregnancy, age, sex, and disease can also contribute to the pharmacokinetics and the clinically observed DDIs (Rowland and Tozer, 2010).

1.7. *IN VITRO* ION CHANNEL INHIBITOR DDIS WITH PGP AND THE CORRESPONDING CLINICAL OBSERVATIONS

A number of *in vitro* studies have demonstrated that several cardiovascular ion channel inhibitors are substrates of and exhibit DDIs with Pgp. In some cases, the observed pharmacokinetics with the cardiovascular ion channel inhibitors seem to correlate with *in vitro* studies implying the involvement of Pgp. In other cases, the *in vitro* Pgp studies and the pharmacokinetics seem to contradict. In this section, *in vitro* DDI studies with Pgp and specific ion channel inhibitors are discussed and compared to the observed pharmacokinetics. The pharmacokinetic details associated with each DDI are summarized in Table 1.3.

1.7.1. Amiodarone and Dronedarone

Amiodarone and dronedarone are potassium channel blockers used to treat cardiac dysrhythmias (Wegener *et al.*, 2006). Amiodarone is converted into the active metabolite

Table 1.3. Pgp-mediated DDIs of commonly prescribed cardiovascular ion channel inhibitors

Drug	Sub.[a]	Inh.[b]	Ind.	Digoxin PK	Other[d]	References
amiodarone	non	6 μM	NA	*AUC*: increases 66%[c] CL_R: no change C_{max}: increases 78%[c] V_D: no change or decreases	Apixaban[d] Dabigatran[d] Digitoxin[e] Daunorubicin[f] Flecainide[d] Rivaroxaban[g]	(Fenner *et al.*, 2009; Kakumoto *et al.*, 2002; Katoh *et al.*, 2001; Laer *et al.*, 1998; Robinson *et al.*, 1989; Stollberger and Finsterer, 2015)
amlodipine	non to good	NA	NA	*C_{ss}: No change*	Simvastatin[h]	(Nishio *et al.*, 2005; Rausl *et al.*, 2006; Schwartz, 1988)
digoxin	good	-	Yes	-	Quinidine[h]	(Elsby *et al.*, 2008; Fenner *et al.*, 2009; Haslam *et al.*, 2008; Mendell *et al.*, 2013; Rameis, 1985b; Riganti *et al.*, 2009)
diltiazem	weak	36 μM	NA	*AUC*: increases 34%[c] C_{max}: increases 31%[c]	Quinidine[h]	(Emi *et al.*, 1998; Fenner *et al.*, 2009; Polli *et al.*, 2001).
dronedarone	non	NA	NA	*AUC*: increases 150% CL_R: decreases 60%		(Vallakati *et al.*, 2013)
flecainide	good	NA	NA	C_{avg}: increased ~20%		(Horie *et al.*, 2014; G. P. Lewis and Holtzman, 1984)
mibefradil	non	7.5 μM	NA	*AUC*: increases 31% C_{max}: increases 41%	Atorvastatin[g]	(Fenner *et al.*, 2009; Holtzman *et al.*, 2006)
nicardipine	non	<1 μM	NA	*AUC*: increases 6% C_{max}: increases 6%		(Fenner *et al.*, 2009; Polli *et al.*, 2001)
nifedipine	non	<1 μM	NA	*AUC*: increases 21%[c] C_{max}: increases 5%[c]		(Fenner *et al.*, 2009; Polli *et al.*, 2001)
ouabain	X	No	Yes	NA		(Cavet *et al.*, 1996; Gozalpour *et al.*, 2016; Pauli-Magnus *et al.*, 2001;

						Riganti *et al.*, 2009)
phenytoin	non to good	NA	NA	*AUC*: decreases 23% *CL*: increases 27% CL_R: no change V_D: no change	Paclitaxel[i]	(Baltes *et al.*, 2007; Maines *et al.*, 2005; Rameis, 1985a; C. Zhang *et al.*, 2010)
quinidine	good	21 µM	Yes	*AUC:* increases 121%[c] *CL:* decreases 56% CL_R*:* decreases 51% C_{max}: increases 75% *F:* increases 16% $t_{1/2}$: decreases 47% V_D: decreases 38%	Edoxaban[d] Fentanyl[j] Flecainide[f] Methadone[j]	(Fenner *et al.*, 2009; Haslam *et al.*, 2008; Horie *et al.*, 2014; Evan D. Kharasch *et al.*, 2004b; E. D. Kharasch *et al.*, 2004; Mendell *et al.*, 2013; Munafo *et al.*, 1992; Pedersen *et al.*, 1983; Schenck-Gustafsson and Dahlqvist, 1981)
verapamil	non to good	1-200 µM	NA	*AUC*: increases 51% *CL*: decreases 34% CL_H: decreases 62% CL_R: decreases 21% C_{max}: increases 44% $t_{1/2}$*:* increases 31% V_D*:* decreases 23%	Colchicine[k] Dabigatran[d] Prazosin[l] Quinidine[h] Vinblastine[k]	(Edwards *et al.*, 1987; Fenner *et al.*, 2009; Hartter *et al.*, 2013; Ledwitch, Barnes*, et al.*, 2016; Pedersen *et al.*, 1981; Polli *et al.*, 2001; Rautio *et al.*, 2006; Schwab *et al.*, 2003)

– not applicable, *AUC* area under the curve, C_{avg} average drug plasma concentration, C_{ss} steady-state drug plasma concentration, *CL* total clearance, CL_H extrarenal clearance, CL_R renal clearance, C_{max} peak drug plasma concentration, *DEA* monodesethyl-amiodarone, *Ind*. inducer, *Inh*. inhibitor, *NA* not available, *Sub*. substrate, $t_{1/2}$ terminal elimination half time, V_D apparent volume of distribution

[a]Classification of a drug as a nonsubstrate (non), weak substrate (weak), good substrate (good), or nonligand (X) to Pgp. A nonsubstrate had an efflux ratio = 1, a weak substrate had an efflux ratio >1 and <2, a good substrate had an efflux ratio >2, and a nonligand was neither a substrate or inhibitor for Pgp

[b]*In vitro* inhibition concentration range of Pgp-mediated digoxin transport by the drug

[c]Average pharmacokinetic values

[d]The more severe ADR: myopathy (Feng *et al.*, 2012)

[e]The more severe ADR: digitalis-associated toxicities (Moss *et al.*, 1981)

[f]The more severe ADR: cardiotoxicity (Keefe, 2001; Ranger *et al.*, 1993)

[g]The more severe ADR: bleeding and thrombosis (Piazza *et al.*, 2011)

[h]The more severe ADR: thrombocytopenia (Lefkowitz and Shapiro, 1986)

[i]The more severe ADR: cardiac arrest (Ruiz-Casado *et al.*, 2006)

[j]The more severe ADR: respiratory depression (Hunt and Bruera, 1995; Smydo, 1979)

[k]The more severe ADR: neutropenia (Dixon and Wall, 2001; Makinson *et al.*, 2007)

[l]The more severe ADR: orthostatic hypotension (Thein *et al.*, 1977)

monodesethyl-amiodarone (DEA) by cytochromes P450 in the liver (Elsherbiny *et al.*, 2008). There is currently no evidence that amiodarone or dronedarone are actually transported by Pgp, but DEA was weakly transported by human Pgp in Caco-2 cells with an efflux ratio of 1.6 (Kimoto *et al.*, 2007). These drugs are particularly prone to Pgp-mediated DDIs because of their unusually long elimination $t_{1/2}$ (Latini *et al.*, 1984; Patel *et al.*, 2009). While dronedarone has a $t_{1/2}$ of ~24 h (Patel *et al.*, 2009), which is long by most standards, amiodarone and DEA have $t_{1/2}$ of several days to over a month due to accumulation in adipose tissue (Lafuente-Lafuente *et al.*, 2009; Latini *et al.*, 1984).

In vitro cell studies with porcine kidney epithelial cells overexpressing human Pgp have shown that both amiodarone and DEA inhibit the transport of digoxin and the anticancer drug daunorubicin (Kakumoto *et al.*, 2002; Katoh *et al.*, 2001). Amiodarone also inhibited the transport of the sodium channel inhibitor flecainide in porcine kidney epithelial cells overexpressing human Pgp and in human intestinal epithelial LS180 cells (Horie *et al.*, 2014).

These potassium channel inhibitors are also known to exhibit a number of DDIs in the clinic [*e.g.*, (Elsby *et al.*, 2008; Haslam *et al.*, 2008; Mendell *et al.*, 2013)]. The pharmacokinetic consequences of amiodarone-digoxin DDIs have been the most thoroughly evaluated [*e.g.*, (Elsby *et al.*, 2008; Rameis, 1985b)]. Amiodarone causes ~70% increases in the C_{max} and AUC of digoxin, while there were very little changes in V_D of digoxin and surprisingly no significant decrease in the renal clearance [*e.g.*, (Elsby *et al.*, 2008; Rameis, 1985b)]. The authors explained the lack of renal clearance to an increase in intestinal absorption and a decrease in extrarenal clearance (Robinson *et al.*, 1989) implying the preferential inhibition of Pgp in the intestines and liver. Amiodarone also showed very strong DDIs with the related cardiac glycoside digitoxin leading to drug toxicity in several cases (Laer *et al.*, 1998). Amiodarone was also found to

increase the oral bioavailability of the anticoagulants, dabigatran, rivaroxaban, and apixaban, by ~10% through inhibition of intestinal Pgp (Liesenfeld *et al.*, 2011; Stollberger and Finsterer, 2015). In contrast, dronedarone showed even stronger DDIs with digoxin than amiodarone (Vallakati *et al.*, 2013). The AUC of digoxin was almost 2-fold higher with dronedarone and there was a 60% decrease in renal clearance (Vallakati *et al.*, 2013).

1.7.2. Amlodipine, Nicardipine, and Nifedipine

The dihydropyridine drugs amlodipine, nicardipine, and nifedipine are typically used in the treatment of hypertension and target the L-type Ca^{2+} channels (McDonagh *et al.*, 2005). At pH 7.4, the drugs were Pgp ligands but were not transported by Pgp (Polli *et al.*, 2001; Rausl *et al.*, 2006). At pH 6.5, amlodipine was efficiently transported by Pgp with an efflux ratio of ~10 (Rausl *et al.*, 2006), but it is unknown if nicardipine or nifedipine are also transported under these conditions. Digoxin transport by Pgp was inhibited by submicromolar concentrations of nifedipine and nicardipine (Fenner *et al.*, 2009). In the clinic, coadministration of nifedipine and digoxin leads to an increase in the C_{max} and AUC in patients of 5% and 21%, respectively (Fenner *et al.*, 2009). DDIs from the coadministration of digoxin and nicardipine had a similar increase in C_{max}, but the increase in the AUC was only ~6% (Fenner *et al.*, 2009). In contrast, despite its molecular similarity to nicardipine and amlodipine, amlodipine did not show significant clinical DDIs with digoxin (Schwartz, 1988). However, amlodipine did show clinical DDIs with simvastatin, which is a recognized Pgp substrate (Hochman *et al.*, 2004), with significant increases in the C_{max} and AUC of simvastatin from 9.6 to 13.7 ng/ml and 34.3 to 43.9 ng h/ml, respectively (Nishio *et al.*, 2005).

1.7.3. Digoxin

Digoxin is the most commonly prescribed cardiac glycoside and inhibits the Na^+/K^+ ATPase (Ehle *et al.*, 2011). The drug is primarily eliminated through the kidneys unmetabolized (Ziff and Kotecha, 2016). Several *in vitro* studies with cells that express human Pgp have shown that digoxin is a good substrate for the transporter [*e.g.*, (Cavet *et al.*, 1996; Gozalpour *et al.*, 2016; Pauli-Magnus *et al.*, 2001)]. Because of digoxin's low therapeutic index, the drug is administered at doses that it is unlikely to affect the pharmacokinetic parameters of other drugs in the clinic (Ziff and Kotecha, 2016). For example, digoxin only had minimal effects on the exposure of the oral anticoagulant edoxaban (Mendell *et al.*, 2013). However, one study did find that the drug did increase the elimination $t_{1/2}$ by ~20% and decreased renal clearance of quinidine at elevated doses, although digoxin's effect on the AUC of quinidine was not statistically significant (Rameis, 1985b).

Therefore, most *in vitro* and *in vivo* studies have focused on inhibition of digoxin transport, which are known to occur with a number of Pgp ligands (Fenner *et al.*, 2009). *In vivo*, Pgp transport inhibition typically leads to significant increases in the AUC, C_{max}, and $t_{1/2}$ and decreases in renal and extrarenal clearance of digoxin (Fenner *et al.*, 2009). Inhibition of intestinal Pgp often leads to increased oral absorption and bioavailability of the drug (Fenner *et al.*, 2009). Because Pgp is found at relatively high concentrations at the BBB (Giacomini *et al.*, 2010), one might expect that the V_D of digoxin would increase significantly as well. In knockout mice lacking mouse Pgp, digoxin concentrations in the brain increased almost 30-fold *versus* wild-type mice (Schinkel *et al.*, 1997). Instead, the V_D of digoxin often decreases in the presence of another drug [*e.g.*, (Rameis, 1985a)]. One possibility is that Pgp inhibition at the BBB can be compensated by alternate efflux transporters including several isoforms of the multidrug

resistance-associated protein (MRP) and the breast cancer resistance protein (BCRP) (Eyal *et al.*, 2009). This hypothesis is supported by that fact that digoxin is also a substrate for MRP2 (Lowes *et al.*, 2003). To complicate the digoxin pharmacokinetics further, digoxin can induce Pgp (Riganti *et al.*, 2009), which explains why Pgp-mediated DDIs between verapamil and digoxin were reduced after long-term coadministration (Pedersen *et al.*, 1982).

1.7.4. Digitalis-Related Molecules

Digitalis-related molecules are functionally and structurally similar to digoxin (Fuerstenwerth, 2014)and include digitoxin, bufalin, and strophanthidin. These molecules are generally good substrates of human Pgp like digoxin (Gozalpour *et al.*, 2016; Pauli-Magnus *et al.*, 2001). Digitoxin and bufalin both inhibited digoxin transport in Caco-2 cells containing human Pgp (Cavet *et al.*, 1996). Digitoxin also inhibited Pgp-mediated secretion of quinidine in the rat small intestine (Emi *et al.*, 1998).

1.7.5. Diltiazem

Diltiazem is a benzothiazepine drug that targets L-type Ca^{2+} channels and is used in the treatment of hypertension and certain types of arrhythmia (McDonagh *et al.*, 2005). The drug is known to be a relatively weak substrate of the transporter with an efflux ratio of 1.64 (Polli *et al.*, 2001). Studies showed that diltiazem inhibited both quinidine and digoxin transport (Emi *et al.*, 1998; Fenner *et al.*, 2009). In the clinic, coadministration of diltiazem and digoxin to patients moderately increased the C_{max} and AUC by about 30% (Fenner *et al.*, 2009).

1.7.6. Flecainide

Flecainide is an antiarrhythmic agent that specifically inhibits the $Na_V1.5$ Na^+ channel, which affects the fast depolarization phase of the cardiac action potential (Ramos and O'Leary M, 2004; Dan M. Roden *et al.*, 2007). *In vitro* studies have shown that it is transported by Pgp with an efflux ratio of ~2 (Horie *et al.*, 2014), and a clinical study showed that it increased blood plasma concentrations of digoxin by ~20% (G. P. Lewis and Holtzman, 1984).

1.7.7. Mibefradil

Mibefradil is a nonspecific inhibitor of both L- and T-type voltage-gated Ca^{2+} channels (Leuranguer *et al.*, 2001). The drug was weakly transported by Pgp in porcine kidney epithelial cells overexpressing the human and mouse Pgp (Schwab *et al.*, 2003). The drug appears to inhibit digoxin transport in human Pgp containing Caco-2 cells with low micromolar potency (Fenner *et al.*, 2009). In the clinic, the drug increases the C_{max} and AUC of digoxin by 41 and 31%, respectively (Fenner *et al.*, 2009). The drug also shows strong Pgp-mediated DDIs with the cholesterol-lowering drug atorvastatin with a 4-fold increase in the AUC from 134 to 594 ng h/ml when coadministered with mibefradil (Holtzman *et al.*, 2006; Jacobson, 2004).

1.7.8. Ouabain

Ouabain functions like other digitalis drugs (Fuerstenwerth, 2014)and is similar in structure to digoxin but only has a single sugar functional group rather than three. No Pgp-mediated transport of ouabain has been observed with mammalian cells expressing human Pgp (Gozalpour *et al.*, 2016; Pauli-Magnus *et al.*, 2001). Ouabain also did not inhibit digoxin

transport in human epithelial Caco-2 cells (Cavet *et al.*, 1996). However, Pgp-mediated DDIs with this drug may occur indirectly through induction of the transporter (Riganti *et al.*, 2009).

1.7.9. Phenytoin

Phenytoin is a sodium channel inhibitor that is used to treat abnormal heart rhythms and is used as an alternative to digoxin (Eijkelkamp *et al.*, 2012). *In vitro* studies with human Pgp overexpressing cell lines and the drug have shown that it ranges from being a nonsubstrate to a substrate [*c.f.* (Keefe, 2001; Piazza *et al.*, 2011)]. *In vivo*, the drug has been shown to be a Pgp substrate with rats using Pgp-specific inhibitors (Potschka and Loscher, 2001). The drug inhibits transport of the anticancer drug paclitaxel in bovine retinal endothelial cells (Maines *et al.*, 2005). However, in the clinic, phenytoin-paclitaxel interactions do not appear to result from Pgp-mediated DDIs but from cytochrome P450-mediated DDIs due to cytochrome P450 induction (Baker and Dorr, 2001; Johannessen and Landmark, 2010). Coadministration of this drug with digoxin in patients decreased the AUC and increased the total clearance of digoxin around 20–30%, but no significant effects on the volume distribution or the renal clearance of digoxin were observed (Rameis, 1985a). This pharmacokinetic outcome is also consistent with cytochrome P450-mediated DDIs.

1.7.10. Quinidine

The sodium channel inhibitor quinidine is a stereoisomer of the antimalarial drug quinine (Dan M. Roden *et al.*, 2007). *In vitro* and *in vivo* studies have demonstrated that this drug is a good substrate for Pgp (Fromm *et al.*, 1999). Quinidine is known to inhibit the transport of several Pgp substrates [*e.g.*, (Cavet *et al.*, 1996; Nishio *et al.*, 2005)]. Several *in vitro* studies

with cells expressing human Pgp have demonstrated that quinidine inhibits digoxin transport (Fenner *et al.*, 2009). In the clinic, coadministration of digoxin with quinidine decreased the terminal elimination $t_{1/2}$, total and renal clearance, and the V_D of digoxin in patients while increasing its absorption and bioavailability (Fenner *et al.*, 2009; Pedersen *et al.*, 1983; Schenck-Gustafsson and Dahlqvist, 1981). In mammalian cells expressing Pgp, quinidine inhibited the transport of the sodium channel inhibitor flecainide (Polli *et al.*, 2001). In the clinic, quinidine reduced the renal clearance of flecainide from 10.6 to 8.1 ml/min/kg (Munafo *et al.*, 1992). Quinidine also increased the AUC and C_{max} of the oral anticoagulant edoxaban from 1577 to 2575 ng h/ml and 223 to 390 ng/ml, respectively (Mendell *et al.*, 2013), and increased the oral bioavailability of methadone and fentanyl (Evan D. Kharasch *et al.*, 2004a). In addition to Pgp inhibition, quinidine also exhibits DDIs through Pgp induction (Haslam *et al.*, 2008).

1.7.11. Verapamil

Verapamil is also one of the most investigated drugs with Pgp [e.g., (Polli *et al.*, 2001; Schwab *et al.*, 2003)]. In vitro studies with mammalian cells expressing human Pgp have revealed that the drug manifests a range of characteristics from being a good substrate to a nonsubstrate depending on the cell type [cf. (Polli *et al.*, 2001; Schwab *et al.*, 2003)]. A positron emission tomography rat brain imaging study with [11C]verapamil and Pgp-specific transport inhibitors has conclusively demonstrated that verapamil is transported by Pgp *in vivo* (J. W. Chung *et al.*, 2010). Verapamil is also a well-known inhibitor of Pgp-mediated transport [e.g., (Rautio *et al.*, 2006)]. The focus of many *in vivo* and *in vitro* studies has been on the effects of verapamil on digoxin transport, since digoxin is often coadministered with verapamil [e.g., (Fenner *et al.*, 2009; Holcberg *et al.*, 2003; Ledwitch, Barnes*, et al.*, 2016; Pedersen *et al.*,

1981)]. Except for a single *in vitro* study with the human placenta (Holcberg *et al.*, 2003), verapamil inhibits Pgp-mediated digoxin transport in the micromolar range (Fenner *et al.*, 2009). *In vitro* studies with mouse Pgp have suggested that digoxin transport inhibition occurs by both competitive and noncompetitive mechanisms (Ledwitch, Barnes*, et al.*, 2016). Clinical studies have shown that verapamil inhibits both renal and extrarenal digoxin clearance leading to an increase in the C_{max}, AUC, and terminal elimination $t_{1/2}$ of the drug, while the apparent V_D decreased (Fenner *et al.*, 2009; Pedersen *et al.*, 1981). A longitudinal clinical study with verapamil and digoxin revealed that the verapamil-mediated DDIs disappeared after several weeks (Pedersen *et al.*, 1982). There was no explanation posited by the authors in (Pedersen *et al.*, 1982), but we hypothesize that this clinical outcome is the result of Pgp induction by digoxin (Riganti *et al.*, 2009). An *in vitro* study with mammalian cells overexpressing human Pgp found that verapamil also inhibited Pgp-mediated transport of colchicine, prazosin, and vinblastine (Rautio *et al.*, 2006). An *in vitro* study with a rat small intestine showed that verapamil increased quinidine absorption through Pgp inhibition (Emi *et al.*, 1998). Verapamil was also found to increase the bioavailability, C_{max}, and AUC of the anticoagulant and Pgp substrate dabigatran (Hartter *et al.*, 2013).

1.8. CURRENT STRATEGIES FOR OVERCOMING PGP-MEDIATED DDIS IN THE CLINIC

In the clinic, finding alternative drug combinations to avoid DDIs all together is the most preferable strategy. For example, one can administer mibefradil and pravastatin, which does not elicit Pgp-mediated DDIs, instead of mibefradil and atorvastatin (Becquemont *et al.*, 1999;

Holtzman *et al.*, 2006). In many cases, this approach may not always be feasible, so methods have been developed to minimize ADR from DDIs.

The first step to minimize Pgp-mediated DDIs is to identify drugs that are known to exhibit DDIs (Rowland and Tozer, 2010; Shargel *et al.*, 2012). For drugs that are coadministered, low therapeutic index drugs can be administered at subtherapeutic doses and the pharmacodynamic response monitored to minimize the risk of ADRs from DDIs (Rowland and Tozer, 2010; Shargel *et al.*, 2012). Therapeutic drug monitoring (TDM) is another method to minimize ADRs from DDIs (Shargel *et al.*, 2012). In the method, the drug plasma concentration is measured directly in the blood or indirectly through biological fluids and correlated to a pharmacodynamic endpoint such as blood pressure (Shargel *et al.*, 2012). Although less common, another approach is to give a digitalizing dose, which is a series of small doses to control and achieve a therapeutic concentration and avoid ADRs (Rowland and Tozer, 2010).

Cardiovascular ion channel inhibitor DDIs and their observed pharmacokinetics discussed in the review are summarized in Table 1.3 The first column shows the name of the drug, while the next columns identify the substrates, inhibitors, and inducers of Pgp. Since many ion channel inhibitors have DDIs with digoxin [*e.g.*, (Rameis, 1985b)], their effects on digoxin PK parameters are shown in the next column. The penultimate column shows other observed DDIs and the last column are the corresponding references.

Table 1.3 shows that cardiovascular ion channel inhibitors range from being nonligands to good substrates for Pgp. Although digoxin is often considered the gold standard for measuring Pgp-mediated DDIs (Giacomini *et al.*, 2010), drugs with very similar molecular structures can have dramatically different inhibitory potency to digoxin transport such as nifedipine and amlodipine (Fenner *et al.*, 2009; Polli *et al.*, 2001; Schwartz, 1988). Some of the drugs are also

Pgp inducers (Haslam *et al.*, 2008; Riganti *et al.*, 2009). In the clinic, cardiovascular ion channel inhibitors show a large range of effects on digoxin pharmacokinetics. Large increases in digoxin exposure and drug plasma concentration are observed in the presence of dronedarone (Vallakati *et al.*, 2013), while decreases in digoxin plasma concentration are observed in the presence of phenytoin (Rameis, 1985a). Unfortunately, *in vitro* Pgp-mediated inhibition of digoxin transport and the observed pharmacokinetics are not well correlated. For example, despite being potent inhibitors of digoxin *in vitro*, nicardipine and nifedipine had relatively modest effects on digoxin pharmacokinetics *in vivo* (Fenner *et al.*, 2009; Polli *et al.*, 2001). The most studied cardiovascular ion channel inhibitors, digoxin, amiodarone, and verapamil, are known to exhibit DDIs with several Pgp ligands. On the other hand, only a few Pgp-mediated DDIs have been noted in the literature with the other drugs, and this reflects a significant gap in our understanding of Pgp-mediated DDIs. Bridging this knowledge gap will require additional Pgp DDI studies in the future.

1.9. CONCLUSIONS AND FUTURE PERSPECTIVES

This review was focused on DDIs-mediated by Pgp, but, in reality, clinically observed DDIs are multifactorial and reflect the complex interplay between drug-metabolizing enzymes and transporters (Pang *et al.*, 2010). For example, the pharmacokinetics profile from verapamil-quinidine DDIs reflects the combined inhibition of Pgp-mediated transport and drug metabolism by cytochromes P450 (Edwards *et al.*, 1987). Drug metabolites can also contribute significant Pgp-mediated DDIs (Pang *et al.*, 2010), such as in the case of amiodarone and its metabolite DEA (Kakumoto *et al.*, 2002; Katoh *et al.*, 2001). Alternative transporters such as MRP2 can potentially mitigate Pgp-mediated DDIs at the BBB and the placenta by effluxing the same drugs

(Eyal *et al.*, 2009; Holcberg *et al.*, 2003; Lowes *et al.*, 2003; Vahakangas and Myllynen, 2009). Influx transporters that actively transport Pgp inhibitors and are found in specific tissues can potentially increase Pgp's sensitivity to inhibitors skewing the pharmacokinetics. For example, amiodarone is a substrate of the organic anionic transporting polypeptide 2B1 (OAT2B1) influx transporter that is found at relatively high concentrations in hepatocytes and intestinal cells but relatively low concentrations in the kidneys (Pan *et al.*, 2013; Segawa *et al.*, 2013). Under these conditions, Pgp will be more sensitive to amiodarone inhibition in hepatocytes and intestinal cells than kidney cells because of the higher intracellular amiodarone concentration mediated by OAT2B1. Under these conditions, we anticipate relatively high intestinal absorption and decreased extrarenal clearance as a result of Pgp inhibition and relatively little effect on renal clearance of Pgp substrates. This is exactly what we observe pharmacokinetically with amiodarone and digoxin (Robinson *et al.*, 1989).

Because of the involvement of alternate transporters and drug-metabolizing enzymes in cardiovascular ion channel inhibitor disposition, extrapolating clinically observed DDIs to Pgp-mediated DDIs observed *in vitro* remains a significant challenge (Prueksaritanont *et al.*, 2013). To overcome this challenge, future *in vitro* studies with cardiovascular ion channel inhibitors will need to consider contributions from alternate transporters and drug-metabolizing enzymes in addition to Pgp.

CHAPTER 2

UNRAVELING THE COMPLEX DRUG-DRUG INTERACTION BETWEEN THE CARDIOVASCULAR DRUGS, VERAPAMIL AND DIGOXIN, WITH THE P-GLYCOPROTEIN TRANSPORTER[2]

[2] Ledwitch, K. V., Barnes, R. W. and A. G. Roberts. (2016). *Bioscience Reports.* 36, 1-14. Reprinted here with permission of publisher.

2.1. ABSTRACT

Drug–drug interactions (DDIs) and associated toxicity from cardiovascular drugs represents a major problem for effective co-administration of cardiovascular therapeutics. A significant amount of drug toxicity from DDIs occurs because of drug interactions and multiple cardiovascular drug binding to the efflux transporter P-glycoprotein (Pgp), which is particularly problematic for cardiovascular drugs because of their relatively low therapeutic indexes. The calcium channel antagonist, verapamil and the cardiac glycoside, digoxin, exhibit DDIs with Pgp through non-competitive inhibition of digoxin transport, which leads to elevated digoxin plasma concentrations and digoxin toxicity. In the present study, verapamil-induced ATPase activation kinetics were biphasic implying at least two verapamil-binding sites on Pgp, whereas monophasic digoxin activation of Pgp-coupled ATPase kinetics suggested a single digoxin-binding site. Using intrinsic protein fluorescence and the saturation transfer double difference (STDD) NMR techniques to probe drug–Pgp interactions, verapamil was found to have little effect on digoxin–Pgp interactions at low concentrations of verapamil, which is consistent with simultaneous binding of the drugs and non-competitive inhibition. Higher concentrations of verapamil caused significant disruption of digoxin–Pgp interactions that suggested overlapping and competing drug-binding sites. These interactions correlated to drug-induced conformational changes deduced from acrylamide quenching of Pgp tryptophan fluorescence. Also, Pgp-coupled ATPase activity kinetics measured with a range of verapamil and digoxin concentrations fit well to a DDI model encompassing non-competitive and competitive inhibition of digoxin by verapamil. The results and previous transport studies were combined into a comprehensive model of verapamil–digoxin DDIs encompassing drug binding, ATP hydrolysis, transport and conformational changes.

2.2. INTRODUCTION

Drug–drug interactions (DDIs) involving cardiovascular therapeutics and their related toxicity continue to represent serious challenges to effective treatment of patients with heart disease (Bailey and Dresser, 2004; Lattuca *et al.*, 2013; Mateti *et al.*, 2011; Mendell *et al.*, 2013; Zaidenstein *et al.*, 2002). In one previous (Zaidenstein *et al.*, 2002) study, DDIs from co-administration of cardiovascular drugs were implicated in ~50% of adverse drug reactions in patients receiving therapy. The P-glycoprotein (Pgp) transporter is an ATP-powered efflux pump that plays a major role in cardiovascular DDIs and effluxes a diverse range of cardiovascular therapeutics (Seelig, 1998; Wessler *et al.*, 2013). The transporter is expressed in the brain, intestines, liver, placenta and the kidneys (Ceckova-Novotna *et al.*, 2006; Lum and Gosland, 1995)and at relatively low levels in the heart (Couture *et al.*, 2006). The expression level is also influenced by genetic polymorphisms and cardiomyopathy (Cascorbi *et al.*, 2004; Meissner *et al.*, 2002).

DDIs with the transporter occur because many cardiovascular drugs are substrates for and functional inhibitors of the transporter (Marchetti *et al.*, 2007; Mendell *et al.*, 2013; Rodriguez *et al.*, 1999; Wessler *et al.*, 2013). This is particularly problematic for cardiovascular drugs with relatively low therapeutic indexes such as antiarrhythmic drugs and oral anticoagulants because co-administration with these drugs can lead to elevated drug plasma concentrations and increased toxicity (Wessler *et al.*, 2013).

The calcium channel blocker verapamil (Figure 2.1 A) which is commonly used to control hypertension, chest pain and arrhythmia (Fleckenstein, 1977; Gould *et al.*, 1982; G. R. Lewis *et al.*, 1978; G. R. Lewis *et al.*, 1979; Neugebauer, 1978), functions as a substrate and an inhibitor of the transporter (Wessler *et al.*, 2013). From results of *in vitro* studies, the drug is

known to activate Pgp-coupled ATP-hydrolysis (e.g. Aanismaa and Seelig, 2007). This drug manifests a spectrum of characteristics, ranging from being a good substrate to a non-substrate for the transporter, which depends on the cell type being evaluated in *in vitro* cell studies (Faassen *et al.*, 2003; Haslam *et al.*, 2008; Mahar Doan *et al.*, 2002; Pauli-Magnus *et al.*, 2000; Polli *et al.*, 2001; Schwab *et al.*, 2003) or host tissue type in *in vivo* studies (Cao *et al.*, 2005; Ke *et al.*, 2013; Romermann *et al.*, 2013). Although the actual molecular details of these interactions are currently unknown, the drug has been shown to inhibit the ATPase activity of a second drug by competitive, non-competitive and allosteric mechanisms in an *in vitro* study (Litman, Zeuthen*, et al.*, 1997a). Verapamil has also been shown to inhibit cardiovascular drug transport by human Pgp *in vivo* (Klein *et al.*, 1982; Mendell *et al.*, 2013; Pedersen *et al.*, 1982).

The cardiac glycoside digoxin (Figure 2.1 B), which has a relatively low therapeutic index, is widely used to treat atrial fibrillation and heart failure (Ehle *et al.*, 2011). The drug is primarily excreted by the Pgp transporter in the kidneys (Englund *et al.*, 2004; Tanigawara, 2000). Importantly, this drug is often co-administered with verapamil, which is known to non-competitively inhibit human Pgp-mediated digoxin transport based upon *in vitro* studies (Ito *et al.*, 1993; Verschraagen *et al.*, 1999). These findings strongly suggest that both drugs are simultaneously bound to the transporter. Inhibition of human Pgp transport by verapamil *in vivo* is known to decrease the extent of renal tubular elimination of digoxin. This finding correlated with increased digoxin blood plasma concentrations from 60 to 90% (Pedersen *et al.*, 1982; Verschraagen *et al.*, 1999) and lead to adverse drug reactions from digoxin toxicity (Gordon and Goldenberg, 1986; Klein *et al.*, 1982).

Because verapamil and digoxin have been the focus of a number of *in vitro* (e.g. Aanismaa and Seelig, 2007) and *in vivo* studies (e.g. Romermann *et al.*, 2013), these drugs are

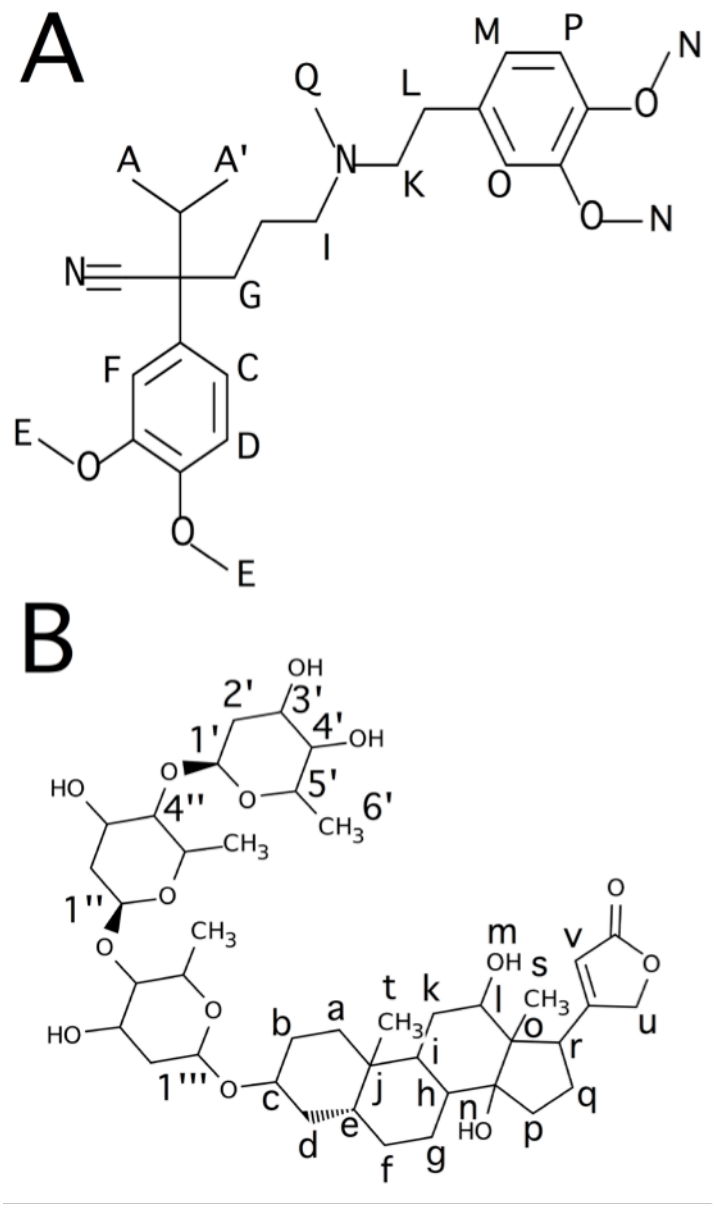

Figure 2.1. Molecular structures of (A) verapamil and (B) digoxin with the nuclei labeled.

ideal for studying DDIs with the transporter. Many molecular and mechanistic details of verapamil–digoxin DDIs with Pgp remain unresolved. This information is essential for defining a general DDI mechanism, for identifying therapeutics that have a high probability of exhibiting DDIs with Pgp and for ameliorating DDIs from commercially available therapeutics with Pgp.

The effect of verapamil and digoxin on the Pgp-coupled ATPase activity, the interactions of verapamil and digoxin with Pgp and the effect of verapamil and digoxin on Pgp conformation were investigated with Pgp reconstituted into liposomes. The drug-induced ATPase activation kinetics of Pgp in the presence of verapamil and digoxin allowed us to estimate the minimum number of drug-binding sites. To explore the effect of verapamil on the affinity of digoxin, digoxin's affinity to Pgp in the presence of several verapamil concentrations was estimated using intrinsic protein fluorescence. The molecular interactions between the drugs and Pgp were investigated by the saturation transfer double difference (STDD) NMR technique. Drug-induced effects on Pgp conformation were studied by acrylamide quenching of tryptophan fluorescence. Additionally, Pgp-coupled ATPase activity kinetics were measured with a panel of verapamil and digoxin concentrations, and fit to a DDI model of drug-induced ATPase activation. This information was combined with previous transport studies to produce a comprehensive mechanistic and molecular model of verapamil–digoxin DDIs.

2.3. MATERIALS AND METHODS

2.3.1. Materials

Verapamil hydrochloride was purchased from Fagron. Digoxin, ethylene glycol tetraacetic acid (EGTA) and imidazole were purchased from Alfa Aesar. The detergent used in protein purification, *n*-dodecyl-β-D-maltoside (DDM), was purchased from EMD Millipore

Corporation. *Escherichia coli* total lipid extract powder was purchased from Avanti Polar Lipids Inc. DTT was purchased from Gold Biotechnology. Deuterium oxide (^2H_2O) was purchased from Cambridge Isotope Laboratories. The remaining chemicals were purchased from Sigma–Aldrich.

2.3.2. Expression and Purification of the mouse Pgp transporter

The wild-type His-tagged mouse Pgp transporter was purified from *Pichia pastoris* as described with some modifications (Bai *et al.*, 2011; Lerner-Marmarosh *et al.*, 1999). The yeast cells were grown and induced with methanol at the Bioexpression and Fermentation Facility at the University of Georgia in a 32 l DCI-Biolafitte fermenter with a 20 l working volume using a similar strategy as (Lerner-Marmarosh *et al.*, 1999). Instead of using glass bead breaking or the French press to crack the yeast cells (Bai *et al.*, 2011; Lerner-Marmarosh *et al.*, 1999), the cells were cracked by a minimum of six passes by liquid nitrogen freezing and blending (Dunn and Wobbe, 2001). To reduce the amount of DDM in our activity assays and during liposome preparation, no additional DDM was added after the nickel-nitrilotriacetic acid (Ni-NTA) column step. Typical protein purification yields were 12±2 mg for 100 g of wet weight cells, which is similar to previous yields (Bai *et al.*, 2011). SDS/PAGE analysis of the protein showed that it was >95% pure. The protein was concentrated up to 150 μM in Amicon Ultra-15 100 kDa cut-off filters (EMD Millipore, Billerica, MA) and stored at −80°C in 10 mM Tris/HCl, 30% glycerol, pH 8.0. The concentration of detergent-solubilized Pgp was measured using the DC Protein Assay Kit II (Bio-Rad Laboratories) or using the molar absorption coefficient of 1.28 $ml \cdot mg^{-1} \cdot cm^{-1}$ (0.181 $\mu M^{-1} \cdot cm^{-1}$) (Bai *et al.*, 2011).

2.3.3. Reconstitution of Pgp into liposomes

Pgp was reconstituted into 400 nm unilamellar liposomes using the filter extrusion method (Mui *et al.*, 2003; Rigaud and Levy, 2003). The liposomes were composed of 80% w/v Avanti *E. coli* Total Lipid Extract (Avanti Polar Lipids) with a defined lipid profile and 20% w/v cholesterol. Lipids and cholesterol were mixed together in chloroform to a final volume and concentration of 10 ml and 10 $mg \cdot ml^{-1}$ respectively. This organic solution was evaporated to dryness in a Buchi Rotavapor Model R-114 (Buchi). This was resuspended in 10 ml of 0.1 mM EGTA and 50 mM Tris/HCl (pH 7.4). The suspension was freeze thawed at least 10 times using liquid nitrogen. The rehydrated lipid was put through a LIPEX extruder 11 times (Northern Lipids) with a 400 nm cutoff Millipore filter (EMD Millipore). Approximately 100 μM of Pgp was dialysed against HEPES buffer (20 mM HEPES, 100 mM sodium chloride, 5 mM magnesium chloride, 2 mM DTT, pH 7.4) for 2 h to remove residual detergent. Then 50 μM of dialysed protein and 4 $mg \cdot ml^{-1}$ liposomes were incubated for 1 h. This was then dialysed for another 2 h against HEPES buffer to promote integration of the protein into the liposomes. To remove aggregated Pgp, the reconstituted liposomes were centrifuged for 5 min at 100 ***g*** in a Sorvall Legend Micro 21 centrifuge (ThermoScientific). To determine the orientation of mouse Pgp in the liposomes, the permeability of the reconstituted liposomes was tested with CHAPS detergent to expose nucleotide-binding domains (NBDs) oriented within the liposome (Aanismaa and Seelig, 2007; Shapiro and Ling, 1995; Sharom *et al.*, 1993). Since there was no increase in the ATPase activity with increasing CHAPS concentrations, Pgp was assumed to be in an inside-out orientation.

2.3.4. ATPase activity measurements

The ATPase activity of the Pgp transporter was measured using the Chifflet method (Chifflet *et al.*, 1988). The method estimates the ATPase activity by measuring the concentration of free P_i after ATP hydrolysis through the formation of a P_i–molybdenum complex, which produces a strong absorbance signal at 850 nm. The absorbance at 850 nm was measured on a 96-well plate in a FlexStation 3 spectrometer (Molecular Devices). The ATPase activity of verapamil and digoxin was measured with 50 nM Pgp in Chifflet buffer (150 mM ammonium chloride, 5 mM magnesium sulfate, 0.02% w/v sodium azide, 50 mM Tris/HCl, 2 mM DTT, pH 7.4).

Traditionally, simple enzyme kinetics have been analysed using linear transformations such as the Lineweaver–Burk (double reciprocal), Hans–Woolf or Eadie–Hofstee plots (Cook and Cleland, 2007; Segel, 1975b). However, these plots suffer from a lack of variable independence across the axes and biasing of the error and the data points (Leatherbarrow, 1990; Martin, 1997; Ranaldi *et al.*, 1999). These methods have generally been superseded by non-linear regression methods that are significantly more accurate and no longer computationally inaccessible (Leatherbarrow, 1990). Therefore, for ATP hydrolysis kinetics that were monophasic, the ATP hydrolysis rate (v), the maximum ATP hydrolysis rate (V_{MAX}), the basal ATPase hydrolysis rate (v_{basal}) and the Michaelis–Menten constant (K_m) were estimated with the Michaelis–Menten equation (equation 1) (A. G. Roberts *et al.*, 2011; Segel, 1975b):

$$v = \frac{V_{MAX}\,[L]}{K_m + [L]} + v_{basal} \qquad (1)$$

For ATP hydrolysis kinetic curves showing biphasic substrate inhibition, the V_{MAX}, K_m and the inhibitory constant (K_i) were estimated with equation 2 (A. G. Roberts *et al.*, 2011; Segel, 1975b):

$$v = \frac{V_{MAX}}{1+\frac{K_m}{[L]}+\frac{[L]}{K_i}} + v_{basal} \qquad (2)$$

For more complicated kinetics, fitting equations have been developed in some cases, but may require specialized numerical methods to solve and may result in multiple solutions (Davydov *et al.*, 2005).

To overcome these challenges, a variety of advanced software modeling packages have been developed to fit arbitrary kinetic models including the free complex pathway simulator (COPASI) (Hoops *et al.*, 2006) and the proprietary Berkeley Madonna (University of California, Berkeley, CA). For ATP hydrolysis kinetics observed in the presence of both verapamil and digoxin, the ATPase activity curves were fit to kinetic models using the evolutionary programming fitting algorithm in the COPASI software (Hoops *et al.*, 2006).

2.3.5. Fluorescence spectroscopy

Quenching of intrinsic protein fluorescence has been used to measure the binding affinity of a chemically-diverse range of ligands with Pgp (Liu *et al.*, 2000; Sharom *et al.*, 2003). Drug-induced quenching of protein fluorescence with Pgp reconstituted in liposomes was investigated on an Olis DM 45 spectrofluorimeter (Olis Corp). All fluorescence samples contained 1 μM liposome-reconstituted Pgp in Chifflet buffer (pH 7.4). Fluorescence emission was measured at 333 nm following excitation between 260 and 295 nm to minimize inner filter effects and background fluorescence. Drug-induced fluorescence quenching was corrected ($F_{\text{corrected}}$) for background fluorescence, dilution and inner filter effects with equation 3 (Lakowicz, 1999):

$$F_{corrected} = (F - B)10^{\frac{(\varepsilon_{ex}\, b_{ex} + \varepsilon_{em} b_{em})[Q]}{2}} \qquad (3)$$

where F is the measured protein fluorescence, B is the background and $[Q]$ is the quenching ligand concentration. The molar absorption coefficients (ε) for excitation and emission are ε_{ex}

and ε_{em} respectively. Verapamil was transparent above 300 nm and had $\varepsilon_{280\ nm}$ and $\varepsilon_{295\ nm}$ of 4 and 0.27 $mM^{-1} \cdot cm^{-1}$ respectively. Digoxin was transparent above 250 nm. The pathlength (b) along the excitation and emission axes are b_{ex} and b_{em} respectively. Drug-induced quenching of protein fluorescence from complexation of the ligand to the protein is known as static quenching, and can be used to estimate the drug's affinity. Drug-induced fluorescence quenching from random collisions with the protein is known as dynamic quenching (Lakowicz, 1999). Regardless of the nature of the quenching, the fluorescence quenching curves were fit to equation 4 (Lakowicz, 1999):

$$F_{corrected} = \frac{F_{corrected,0}}{1+K[Q]} \qquad (4)$$

where $F_{\text{corrected,0}}$ is the protein fluorescence in the absence of a quenching ligand and K is the association constant (K_A) or the Stern–Volmer quenching constant (K_{SV}) in the case of a static and dynamic quenching processes respectively. The two different quenching mechanisms can be differentiated by measuring the protein's fluorescence life time in the presence of the quenching ligand or by performing the fluorescence titration experiments at two different temperatures (Lakowicz, 1999). In the latter case, the K will increase with increasing temperature for dynamic quenching by increasing the collisional frequency of the quencher and will decrease in the case of static quenching by decreasing the residence time of the quenching ligand.

Acrylamide is a neutral aqueous collisional quencher that has been widely used to probe the accessibility of tryptophans in proteins and probe changes in tertiary structure (Liu *et al.*, 2000; Sonveaux *et al.*, 1999). Dynamic quenching of intrinsic tryptophan fluorescence by acrylamide has been used to probe conformational changes of Pgp (Liu *et al.*, 2000; Russell and Sharom, 2006; Sonveaux *et al.*, 1999). For these experiments, fluorescence emission with Pgp reconstituted in liposomes was measured at 333 nm following excitation at 295 nm. Control

acrylamide titrations were performed in the presence of *N*-acetyl-L-tryptophanamide (NATA) to estimate the degree of non-specific quenching (Liu *et al.*, 2000). Fluorescence intensities were corrected for with equation 3 (Lakowicz, 1999). To produce the Stern–Volmer plots, the $F_{\text{corrected},0}/F_{\text{corrected}}$ was plotted as a function of the acrylamide concentration. The degree of dynamic tryptophan quenching was estimated from the slopes of the Stern–Volmer curves, which is related to K_{SV} by $F_{\text{corrected},0}/F_{\text{corrected}} = 1 + K_{SV}[Q]$ (Lakowicz, 1999).

2.3.6. NMR

All NMR experiments with verapamil and digoxin ^{1}H NMR spectra were performed on a 600 MHz Varian INOVA spectrometer at 25°C equipped with a 5 mm z-gradient ^{1}H{^{13}C/^{15}N} cryoprobe. The ^{1}H NMR peaks were assigned using standard ^{1}H 1D and 2D NMR techniques. NMR spectra were analysed using the iNMR software (http://www.inmr.net) and Igor Pro 6.2 (Wavemetrics). The ^{1}H NMR peak assignments for verapamil and digoxin are shown in Supplementary Figure S1 in the Supplementary Information and were essentially identical with previous ^{1}H NMR peak assignments (Maccotta *et al.*, 1991a; Tetreault and Ananthanarayanan, 1993).

The saturation transfer difference (STD) NMR technique is a well-established method for probing ligand–protein interactions (e.g. Leach and Hann, 2011). With this technique, the protein is selectively excited at a frequency outside of the ligand ^{1}H NMR peaks, the saturation is transferred from the excited protein to the ligand through spin diffusion and the ligand STD NMR signal is observed (Mayer and Meyer, 2001a). However, in the case of liposomes reconstituted with Pgp, there will be significant interference because of saturation transfer between the liposome membrane and the drugs. This interference can be subtracted from the

saturation transfer between the drug and the protein by the NMR technique called STDD (Claasen *et al.*, 2005b; Haselhorst *et al.*, 2007; Pereira *et al.*, 2009; Shirzadi *et al.*, 2008). The STDD NMR procedure for membrane proteins was performed as described in (R. Venkitakrishnan *et al.*, 2012). STDD NMR samples contained 1 μM Pgp reconstituted into liposomes in 100 mM potassium phosphate buffer [80% ^2H_2O (99.9%) and 20% ddH_2O, pH 7.4]. The STDD NMR experiments were performed with a double pulsed field gradient spin echo pulse sequence to suppress background water, a 2s train of 50 ms shaped saturation pulses to selectively excite the protein and a total relaxation delay of 5 s (Mayer and Meyer, 2001a). The number of transients collected for the on resonance and the off resonance spectra were 512. To minimize saturation transfer between the drugs and the liposomes, samples were selectively irradiated at a frequency of 10.5 ppm. Control experiments were performed under identical conditions with liposomes and the drugs. To produce the STDD NMR spectrum, ^{1}H STD NMR spectrum of liposomes with drugs was subtracted from the ^{1}H STD NMR spectrum of Pgp reconstituted in liposomes with drugs (ΔI). The STDD NMR subtraction procedure is demonstrated with verapamil in Supplementary Figure S2 in the Supplementary Information. The STDD amplification factor was calculated using the following equation based on the STD amplification factor (equation 5) (Mayer and Meyer, 2001a):

$$STDD\ Amplification\ Factor = \frac{[L]}{[P]}\frac{\Delta I}{I_0} \qquad (5)$$

where $[P]$ is the protein concentration and I_0 is the amplitude of the ^{1}H NMR peaks in the absence of saturating pulses.

2.4. RESULTS

2.4.1. The effect of verapamil and digoxin on the Pgp-coupled ATPase activity

Figure 2.2 shows the mouse Pgp-coupled ATPase activity of Pgp with verapamil and digoxin. In the absence of drugs, Pgp had basal ATPase activity of 512±151 nmol·min^{-1}·mg^{-1} at saturating 3.2 mM ATP, which is in the range of basal activity rates observed in the literature between 0 (Ritchie *et al.*, 2009) and 2600 nmol·min^{-1}·mg^{-1} (Borgnia *et al.*, 1996).

Kinetics of Pgp-coupled ATP hydrolysis in the presence of verapamil (Figure 2.2, open squares) was biphasic with substrate activation and inhibition of ATP hydrolysis reaching a maximum of 2106±98 nmol·min^{-1}·mg^{-1} or 3- to 4-fold activation at 8 μM verapamil. Fitting the kinetics to the substrate inhibition equation (equation 2) produced values for V_{MAX}, K_m and K_i of 2546±130 nmol·min^{-1}·mg^{-1}, 1.9±0.5 μM and 454±109 μM respectively. These results suggest that there is a high-affinity and a low-affinity verapamil-binding site on Pgp.

Biphasic verapamil kinetics with the transporter has been observed previously with hamster (Borgnia *et al.*, 1996; Litman, Zeuthen*, et al.*, 1997b; Orlowski *et al.*, 1996; Sharom *et al.*, 1995), human (Aanismaa and Seelig, 2007) and mouse (Litman, Nielsen*, et al.*, 1997) Pgp. These values are very similar to the average K_m and K_i values determined for mouse Pgp in Ehrlich membranes of 2.5 and 225 μM (Litman, Nielsen*, et al.*, 1997) and for human Pgp in NIH-MDR1-G185 cells of 1.0 and 843.6 μM respectively (Aanismaa and Seelig, 2007). The V_{MAX} was also similar to previous determinations with mouse Pgp and the half maximal ATPase activity of 4.2 μM with mouse Pgp was close to our estimates (Bai *et al.*, 2011).

However, in a previous study (Bai *et al.*, 2011), verapamil ATPase activation kinetics was monophasic and the maximum velocity was reached at 150 μM rather than 8 μM. Since the

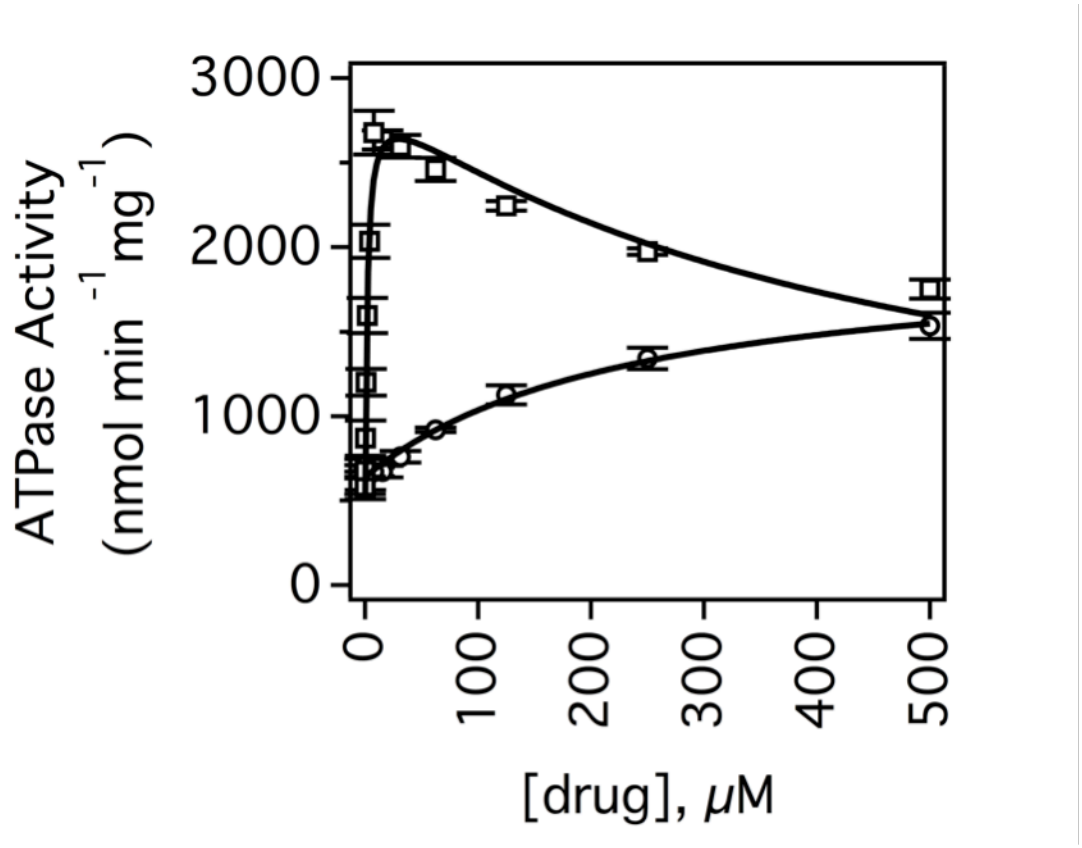

Figure 2.2. Verapamil and digoxin-induced ATPase activation of Pgp. The Pgp-coupled ATPase activity as a function of verapamil (open squares) and digoxin (open circles) concentrations. The fits are shown as solid lines. Error bars represent the standard deviation and the points represent an average of at least three independent experiments.

transporter is known to be sensitive to detergent and lipid composition (Doige *et al.*, 1993; Lerner-Marmarosh *et al.*, 1999; Romsicki and Sharom, 1998, 1999; Saeki *et al.*, 1992; Sharom, 2014; Sharom *et al.*, 1995), these differences in ATP hydrolysis kinetics were attributed to our procedure for reconstituting the transporter into the liposomes and our efforts to minimize the DDM during the protein purification process.

The digoxin-induced activation of ATP hydrolysis kinetics was monophasic and reached a maximum ~2-fold activation or ~1300 nmol·min^{-1}·mg^{-1} (Figure 2.2, open circles), which is in the range observed previously (Matsunaga *et al.*, 2006; Rebbeor and Senior, 1998; von Richter *et al.*, 2009). The kinetics were fit to the Michaelis–Menten equation (equation 1) and gave values for V_{MAX} and K_m of 1344±149.8 nmol·min^{-1}·mg^{-1} and 240.4±68.1 μM respectively. This value is close to the K_m for digoxin transport in human Pgp from Caco-2 cells of 385 μM (Hansen and Nilsen, 2009). Although our K_m value was in the general range of previously determined K_m values for digoxin-induced ATPase activation of Pgp, the previously determined K_m values vary widely in the literature (Matsunaga *et al.*, 2006; Rebbeor and Senior, 1998; von Richter *et al.*, 2009). A K_m value of 1.2 μM for ATPase activation by digoxin was determined in Caco-2 membrane vesicles containing human Pgp (Matsunaga *et al.*, 2006), whereas a K_m value of 83.7 μM for ATPase activation was reported for human Pgp-enriched insect cell membranes (von Richter *et al.*, 2009). For CR1R12 cells containing Pgp, maximal activation of ATP hydrolysis was not even reached at 1000 μM digoxin (Hansen and Nilsen, 2009) implying a K_m that is considerably higher than 500 μM. This wide variation may be due to differences in membrane preparation, in lipid composition and/or in protein/lipid ratios.

2.4.2. The effect of verapamil on the affinity of digoxin to Pgp by intrinsic protein fluorescence

Quenching of intrinsic protein fluorescence was used to probe the binding affinities of verapamil and digoxin to Pgp. Unfortunately, Pgp fluorescence at ~330 nm was severely masked by inner filter effects and background fluorescence by verapamil when the protein was excited between 260 and 280 nm. Exciting the protein at 295 nm minimized these negative effects of verapamil on the protein fluorescence signal. Unlike previous studies with hamster Pgp (Romsicki and Sharom, 1999), no significant verapamil-induced quenching of $F_{corrected}$ was observed. However, this characteristic allowed us to examine the effects of verapamil on the affinity of digoxin to Pgp.

Figure 2.3 shows the effect of digoxin on the protein fluorescence of Pgp in the presence of low and high concentrations of verapamil. Pgp was most sensitive to protein fluorescence quenching by digoxin when the protein was excited at 280 nm. Figure 2.3 A shows the effect of a range of digoxin concentrations on the uncorrected normalized protein fluorescence of Pgp after exciting at 280 nm. After correcting the fluorescence with equation 3 the amplitude at 333 nm in panel A was plotted as a function of the digoxin concentration in Figure 2.3 B and shows that Pgp is quenched ~10% at saturating levels of digoxin. The titration curve appears to be monophasic with a K of 0.0100±0.0018 μM^{-1} after fitting to equation 4. To determine if the digoxin-induced quenching was due to a dynamic or a static quenching process, the titration was also performed at 37°C, which caused a decrease in the K value to 0.0030±0.0008 μM^{-1} and showed that digoxin induced static quenching of Pgp. This allowed us to calculate a dissociation constant (K_D) for digoxin binding to Pgp at 25°C of 100±18 μM (i.e. $K_A=1/K_D$). A digoxin titration of Pgp was performed in the presence of 8 μM verapamil, which caused the highest

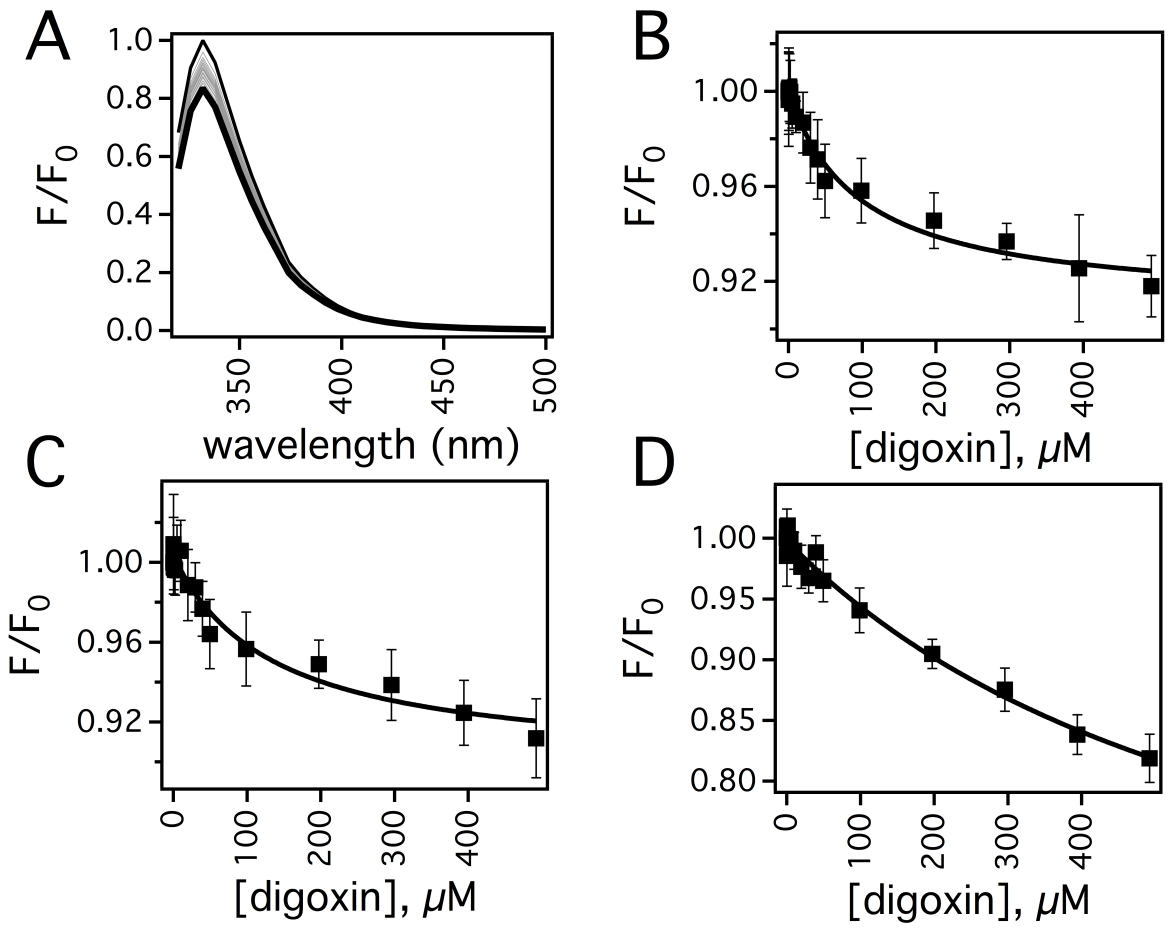

Figure 2.3. Digoxin-induced fluorescence quenching of Pgp in the presence of verapamil at 25°C. A) Pgp fluorescence spectra in the presence of a range of digoxin concentrations after exciting at 280 nm. The spectrum at 0 μM and 250 μM digoxin are shown as thin and thick lines, respectively, while intermediate concentrations of digoxin are shown as gray lines. Protein fluorescence emission at 333 nm as a function of digoxin concentration and in the presence of B) 0 μM, C) 8 μM and D) 50 μM verapamil. The average and standard deviations are represented as points and bars, respectively, and reflect at least three independent experiments.

activation of Pgp-coupled ATP-hydrolysis in Figure 2.2 (closed squares). The $F_{corrected}$ at 333 nm was plotted as a function of protein concentration and is shown in Figure 2.3 C. A K_A value of 0.0074±0.0033 μM^{-1} (K_D=135±61 μM) was extracted from fitting the curve, which was very similar to the value determined in the absence of verapamil implying that both verapamil and digoxin are bound simultaneously to Pgp. The verapamil concentration was increased to 50 μM with the $F_{corrected}$ digoxin titration shown in Figure 2.3 D. The K_A determined by fitting this fluorescence quenching curve was 0.0015±0.00057 μM^{-1} (K_D=679±261 μM). This is significantly lower than the K_A value determined at 8 μM and 0 μM verapamil. The decrease in K_A suggest that verapamil and digoxin are competitive at higher verapamil concentrations and that there is overlap in their binding sites. Digoxin titrations at higher verapamil concentrations with Pgp were attempted, but suffered from significant interference from inner filter effects by and fluorescence from verapamil (results not shown).

2.4.3. Drug-induced conformational changes of Pgp by verapamil and digoxin

Acrylamide quenching of tryptophan fluorescence in the presence of drugs was used to investigate drug-induced conformational changes of Pgp. Figure 2.4 shows Stern–Volmer plots (i.e. F_0/F compared with [acrylamide]) in the absence and presence of drugs to probe protein conformational changes and tryptophan accessibility. The slope of the Stern–Volmer plot for Pgp in the absence of drugs had a K_{SV} value of 1.55±0.04 M^{-1} (Figure 2.4 A, closed squares). The slope of the Stern–Volmer plot with NATA Figure 2.4 A, open squares) was measured to determine non-specific tryptophan interactions, and had a relatively high K_{SV} value of 15.14±0.57 M^{-1} that showed most of the tryptophans of Pgp are inaccessible to acrylamide. Figures 2.4 B and C show the Stern–Volmer plots of Pgp in the presence of low and high

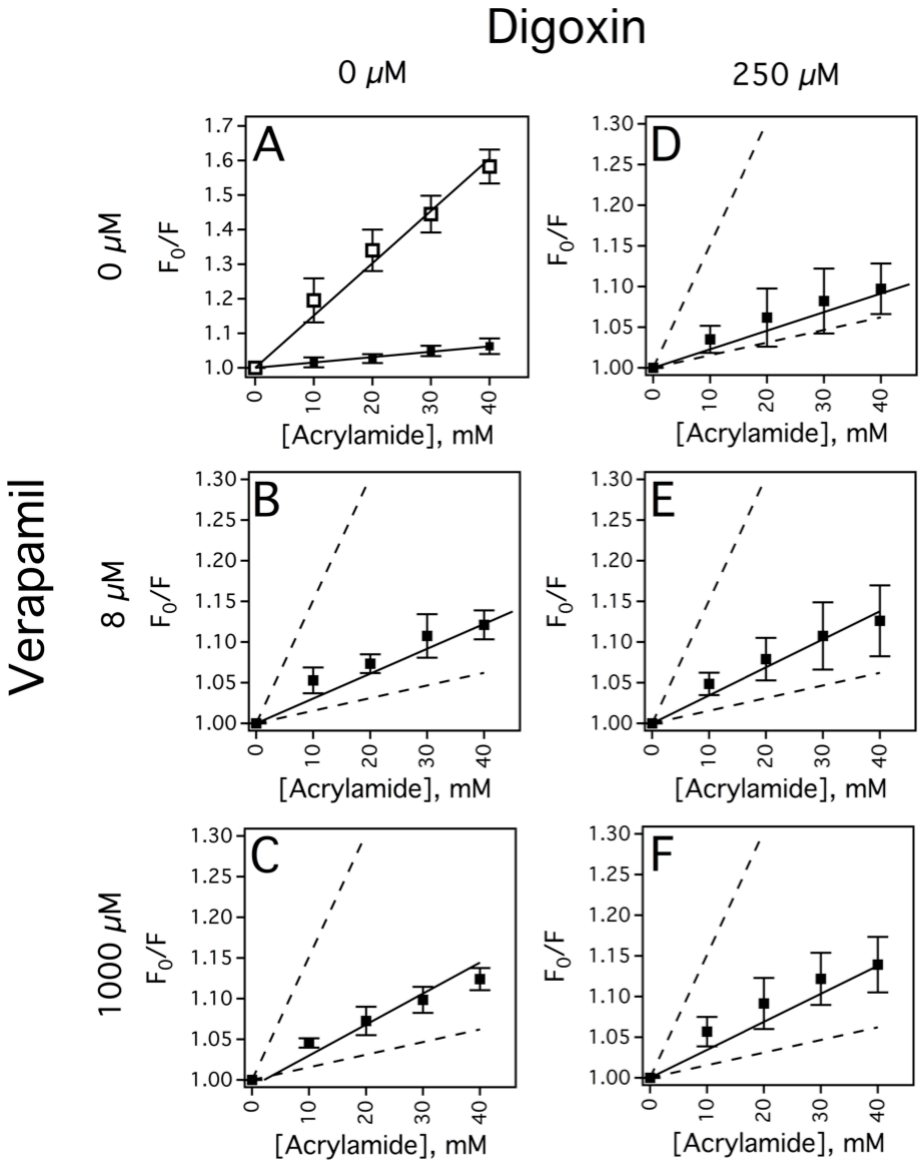

Figure 2.4. Acrylamide quenching of the Pgp transporter in the presence of verapamil and digoxin. A) The Stern-Volmer plots of NATA (open squares) and Pgp in the absence of drugs (closed squares). The Stern-Volmer plots of Pgp in the presence of B,E) 8 μM and C,F) 1000 μM verapamil. D, E, F) The Stern-Volmer plots of Pgp with 250 μM digoxin added in addition to verapamil. For comparison, the slopes in panel A are presented as dashed lines in panels B through F. The average and standard deviations are represented as points and bars, respectively, and reflect at least three independent experiments.

concentrations of verapamil. K_{SV} values of 3.06±0.21 M^{-1} and 3.81±0.26 M^{-1} were determined from the slopes of the plots with low and high concentrations of verapamil respectively. These differences show that verapamil shifts Pgp into at least two distinct conformations and the largest conformational changes occur at low concentrations of verapamil. This observation is consistent with verapamil-induced Pgp conformational changes deduced from cross-linking of (T. W. Loo *et al.*, 2003a, 2003b, 2003c), trypsin digestion of (G. Wang *et al.*, 1998) and antibody competition with Pgp (Nagy *et al.*, 2001). The slope of the Stern–Volmer plot for Pgp in the presence of 250 μM digoxin was 2.29±0.12 M^{-1} (Figure 2.4 D). When 8 μM of verapamil was added to 250 μM digoxin (Figure 2.4 E), the K_{SV} value increased to 3.44±0.19 M^{-1}. Addition of high concentrations of verapamil to Pgp in the presence of 250 μM digoxin increased the slope of the Stern–Volmer plot to 3.87±0.26 M^{-1} (Figure 2.4 F), which is similar to the K_{SV} value determined from **Figure 2.4** C without digoxin and implies that they are in a similar conformation.

2.4.4. Interactions of verapamil and digoxin with Pgp determined by STDD NMR

STDD NMR was used to probe the interactions of verapamil and digoxin with Pgp. Figure 2.5 shows the STDD NMR of verapamil and digoxin with Pgp. Figures 2.5 A and B show the STDD NMR spectrum and amplification factors, respectively, with 1 mM verapamil and 1 μM Pgp. Overall, the strongest interactions with Pgp occurred with the aromatic and methoxy groups of verapamil with an STDD amplification factor of ~15 indicating that they are the most important functional groups for molecular recognition by Pgp. STDD amplification factors that were half of these groups were observed for the methyls labelled A, A′ and Q with STDD amplification factors of ~7. There were some weak STDD signals observed from the alkyl group

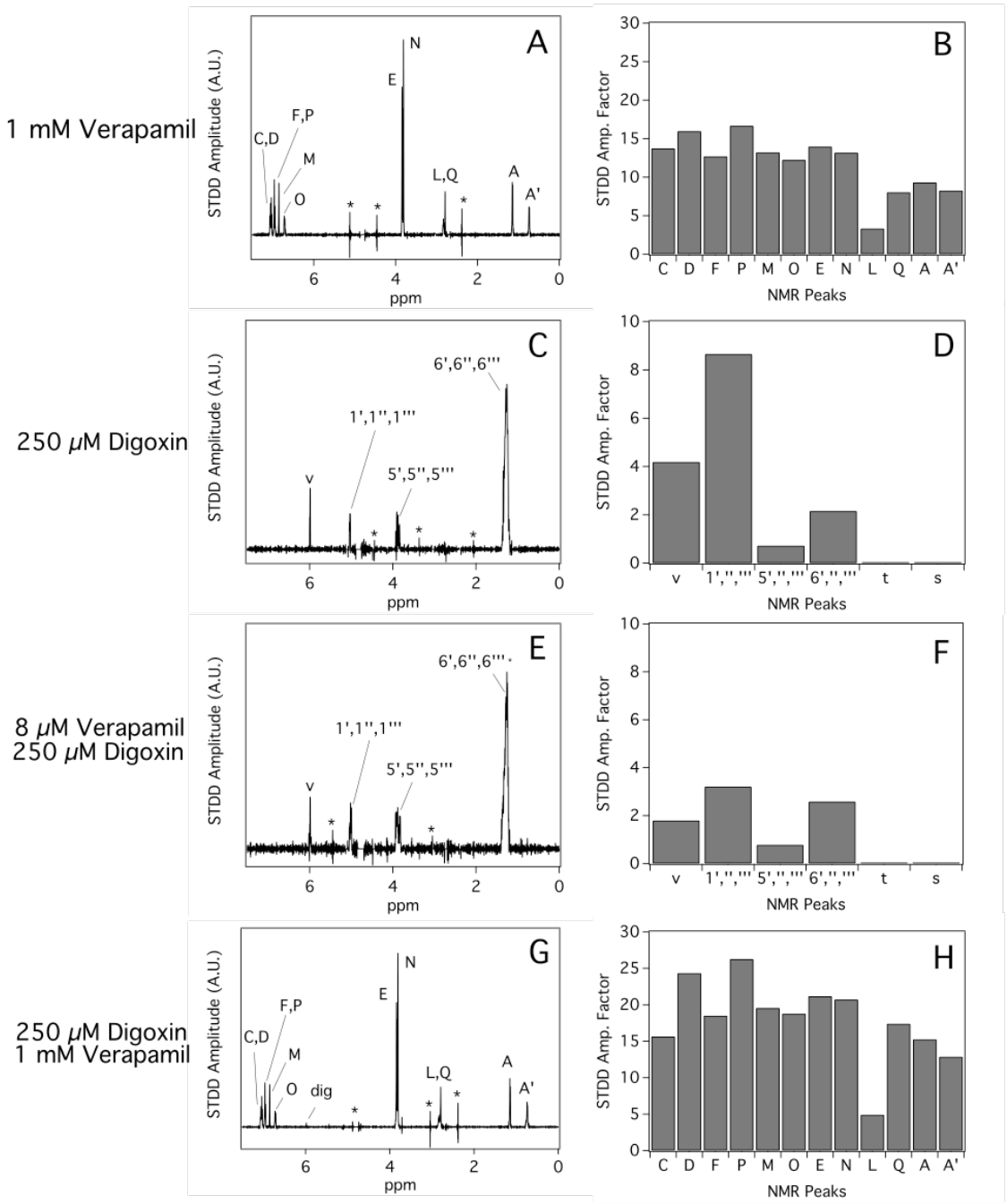

Figure 2.5. Saturation transfer double difference (STDD) NMR of verapamil and digoxin with 1 μM Pgp. The STDD amplification (amp.) factors were calculated from the STDD NMR spectra (A, C, E, and G) for verapamil (B and H) and digoxin (D and F). The concentrations of verapamil and digoxin are shown on the left side of the figure. Parameters for the NMR experiments are in the *Experimental* section.

(labelled L) of the distal phenyl group. No ^{1}H STDD NMR peaks were observed for the other protons labelled G, H, I and K.

Figures 2.5 C and D show the STDD NMR spectrum and amplification factors of 250 μM digoxin with Pgp. Significant STDD NMR peaks were observed for several protons (e.g. 1‴) emanating from the sugars and proton from the furan-2-one functional group. The highest STDD amplification factor was observed for the proton that is near the 1,4 β-linkage with an STDD amplification factor of ~8. To investigate the effect of verapamil on the interactions of digoxin with the transporter, 8 μM of verapamil was added to samples containing protein and 250 μM digoxin in Figures 2.5 E and F. Because of the low verapamil concentration, no STDD NMR peaks were observed for this drug. The relative amplitudes of the STDD NMR spectrum were quite similar to the STDD NMR spectrum taken without 8 μM verapamil. Therefore, low concentrations of verapamil did not significantly perturb digoxin's bound orientation to Pgp. However, the absolute amplitudes of the STDD NMR spectrum and amplification factors decreased ~50% in the presence of 8 μM verapamil. This decrease was attributed to a fraction of verapamil molecules competing with digoxin bound to Pgp and to small errors in measuring the drug/protein ratios. The effect of higher concentrations of verapamil on digoxin's interaction with Pgp is shown in Figures 2.5 G and H. No digoxin STDD NMR peaks were observed in the STDD NMR spectrum, which indicates complete displacement of digoxin from Pgp. The STDD amplification factors of verapamil were very similar to the ^{1}H STDD NMR spectrum without digoxin (Figure 2.5 A).

2.4.5. Modelling Pgp-coupled ATPase activity with a panel of digoxin and verapamil concentrations

Figure 2.6 shows a DDI model and Pgp-coupled ATPase activity curves with a panel of digoxin and verapamil concentrations. The model shown in Figure 2.6 A was the simplest that encompassed the results of the ATPase activity, intrinsic tryptophan fluorescence and the STDD NMR experiments. In the model, two verapamil molecules bind to Pgp, which is consistent with the biphasic ATP hydrolysis kinetics shown in Figure 2.2. The model also shows that verapamil and digoxin bind simultaneously to Pgp (i.e. the enzyme verapamil-digoxin complex (EVD)). This is supported by the fact that the digoxin K_D is not significantly perturbed at low concentrations of verapamil and is also consistent with non-competitive inhibition for digoxin transport by verapamil (Ito *et al.*, 1993; Verschraagen *et al.*, 1999). In the model, higher concentrations of verapamil competitively displaces digoxin from its binding site on Pgp. Competitive displacement of digoxin by verapamil was observed at 50 μM verapamil in the intrinsic tryptophan measurements of Pgp (Figure 2.3 D). It was also demonstrated in the STDD NMR spectrum in Figure 2.5 G by a lack of ^{1}H digoxin STDD NMR peaks.

Figures 6B and 6C shows the Pgp ATPase activity with a range of digoxin and verapamil concentrations. Because of the complexity of the model shown in Figure 2.6 A, the kinetics curves in Figures 2.6 B and C were fit using the COPASI software package. A complete list of kinetic and thermodynamic parameters used to fit the curves in the figures is presented in Supplementary Table S1 of the Supplementary Information. The fits to the ATPase activity kinetic curves had correlations (R) that were 0.9 or greater with one exception, which had a low χ^2. The average basal ATP hydrolysis activity (V_{MAX0}) determined from the fits was 538±64 nmol·min^{-1}·mg^{-1}.

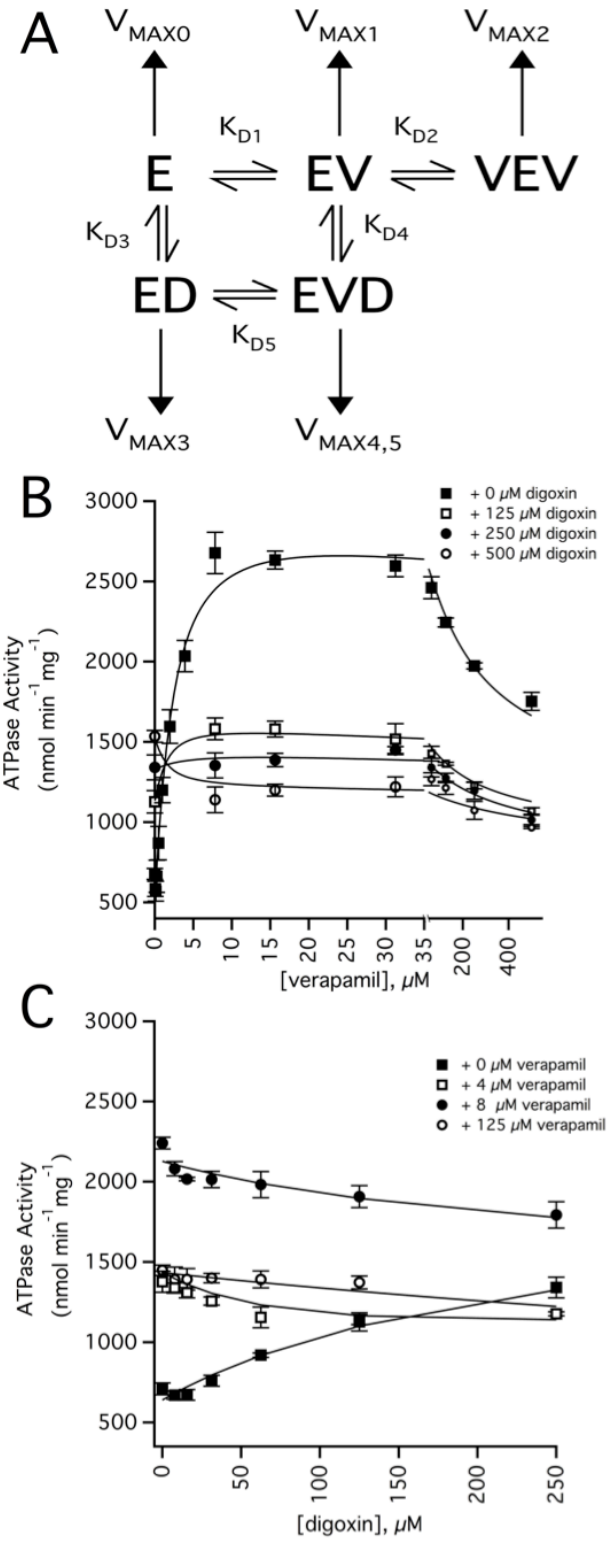

Figure 2.6. DDI effects of verapamil and digoxin on the ATPase activity of Pgp. A) DDI model used to fit the ATPase activity curves. Horizontal and vertical arrows denote the equilibria

between bound states and the ATPase activity from the bound states, respectively. E, V and D correspond to Pgp, verapamil and digoxin, respectively. B) Verapamil-induced activation of ATPase activity in the presence of 0 μM (closed squares), 125 μM (open squares), 250 μM (closed circles) and 500 μM digoxin (open circles). C) Digoxin-induced activation of ATPase activity in the presence of 0 μM (closed squares), 4 μM (open squares), 8 μM (closed circles) and 125 μM verapamil (open circles). The fits are shown as lines, the error bars represent the standard deviation and the points represent an average of at least three independent experiments. The statistics and the values used to fit the curves are shown in Table S1 of the *Supplementary Information*.

Figure 2.6 B shows the effect of digoxin on the ATPase activity with a range of verapamil concentrations. In the absence of digoxin, K_{D1}, K_{D2}, V_{MAX1} and V_{MAX2} values of 1.83 μM, 211 μM, 3000 nmol·min^{-1}·mg^{-1} and 1100 nmol·min^{-1}·mg^{-1}, respectively, for verapamil-induced activation of Pgp-coupled ATP hydrolysis were extracted from the fits. These dissociation constants were very similar to those obtained by fitting the ATPase activity kinetics curve in Figure 2.2 (open squares). Fitting all of the curves gave an average K_{D1}, K_{D2}, V_{MAX1} and V_{MAX2} for verapamil-induced activation of Pgp-coupled ATP hydrolysis of 1.95±0.89 μM, 187±41 μM, 2757±313 nmol·min^{-1}·mg^{-1} and 896±132 nmol·min^{-1}·mg^{-1} respectively.

Figure 2.6 C shows the effect of verapamil on the ATPase activity with a range of digoxin concentrations. In the absence of verapamil, the ATPase activity kinetics with digoxin was monophasic and fits well to the model in Figure 6A with a K_{D3} and V_{MAX3} of 239 μM and 1983 nmol·min^{-1}·mg^{-1}, which is similar to the K_D and V_{MAX} values obtained from fitting Figure 2.2 (open circles). The average K_{D3} and V_{MAX3} values for digoxin-induced ATPase activation determined from fitting all the curves with COPASI were 206±53 μM and 1981±207 nmol·min^{-1}·mg^{-1}.

The remaining parameters were estimated indirectly by fitting with COPASI. The affinity of digoxin to Pgp in the presence of verapamil (K_{D4}) was 292±89 μM. This is very similar to the K_{D2} determined in the absence of verapamil. The affinity of verapamil to Pgp in the presence of digoxin (K_{D5}) was 3.41±1.91 μM, which is relatively close to K_{D1}. These results suggest that verapamil and digoxin were essentially not cooperative with respect to binding to Pgp. The $V_{MAX4,5}$ for drug-induced ATPase activation from simultaneous binding of digoxin and verapamil was 121±139 nmol·min^{-1}·mg^{-1} and reflects an almost complete inhibition of ATP hydrolysis in the presence of both drugs. In this case, verapamil and digoxin are negatively cooperative with

respect to Pgp-coupled ATP hydrolysis. This also correlates well with non-competitive inhibition of digoxin transport by Pgp in the presence of verapamil (Ito *et al.*, 1993; Verschraagen *et al.*, 1999).

2.5. DISCUSSION

In Figure 2.7, we propose a DDI transport model with Pgp based on our results with verapamil and digoxin, and the conformational changes that Pgp is known to undergo with nucleotide cofactors and drugs (T. W. Loo *et al.*, 2003a, 2003b; Ritchie *et al.*, 2011; Verhalen *et al.*, 2012). For simplicity, we have represented Pgp in our model by three conformations: 'open', 'closed' and 'intermediate'. In reality, these conformations represent an ensemble average between a range of conformations. In the 'open' conformation, the NBDs are relatively far apart and the cytosolic side is exposed to the bulk solvent. In the 'closed' conformation, the NBDs are in contact with each other and the extracellular side is exposed to the bulk solvent. The 'intermediate' conformation is between the 'open' and 'closed' conformations. In this conformation, both the cytosolic and extracellular sides of Pgp are exposed to the bulk solvent.

Drug-induced changes in tryptophan accessibility deduced from the acrylamide quenching experiments implied that Pgp occupies distinct conformations at each of the digoxin and verapamil concentrations. Unfortunately, this information cannot be used to assign specific drug-bound Pgp conformations. Instead, the assignment was based on drug-induced activation of the Pgp-coupled ATP hydrolysis rate. Our rational was based on the fact that site-directed mutagenesis and cross-linking studies of Pgp in addition to structural studies of the bacterial transporters with nucleotide analogues have demonstrated that the interaction of the Pgp

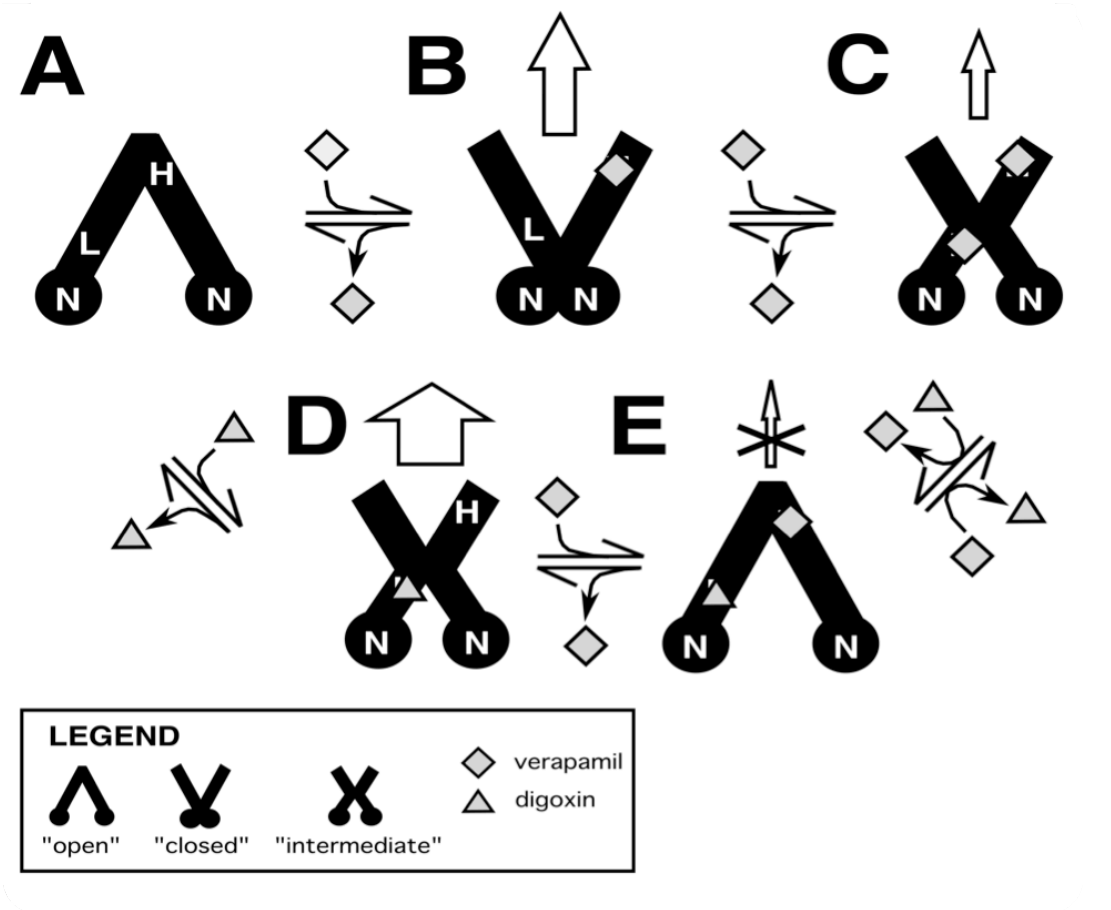

Figure 2.7. DDI transport model of verapamil and digoxin with Pgp. Pgp is shown as a cartoon representation of three conformational states: "open," "closed" and "intermediate." Verapamil and digoxin are represented as diamonds and triangles, respectively. The panels show Pgp A) in the absence of drugs, B) with 1 bound verapamil molecule, C) with 2 bound verapamil molecules, D) with 1 digoxin molecule bound and E) with 1 bound verapamil and 1 bound digoxin. The top and the bottom of the Pgp representations are the extracellular and cytosolic sides, respectively. The vertical arrows denote transport and the size of the arrows reflect their relative transport rates, while X denotes transport inhibition. H, L and N are the high affinity binding site, low affinity binding site and the nucleotide binding domains, respectively.

nucleotide domains with each other is essential for ATP hydrolysis (Beaudet and Gros, 1995; Hrycyna *et al.*, 1999; Lawson *et al.*, 2008; T. W. Loo *et al.*, 2002, 2003a; T. W. Loo *et al.*, 2012; Urbatsch *et al.*, 1995). Therefore, the average distance between the NBDs of Pgp was correlated to the ATP hydrolysis rate in our model. In other words, drugs that induce a relatively low and high ATPase rates will shift Pgp into 'open' and 'closed' conformations respectively.

The locations of the verapamil-binding sites are currently unknown. The biphasic verapamil ATPase activation kinetics that are shown in Figures 2 and and66 suggest a high- and a low-affinity verapamil-binding site on Pgp. Several studies have identified residues clustered near the extracellular side of Pgp (Hafkemeyer *et al.*, 1998; T. W. Loo *et al.*, 2003b; Welker *et al.*, 1995) and G185 (Omote *et al.*, 2004; Rao, 1995), which lies in the transmembrane region of Pgp, that have marked effects on verapamil-induced activation of ATP hydrolysis and transport. Deletion of residues between 78 and 97 near the extracellular side of human Pgp caused a dramatic increase in the K_m for ATPase activation by verapamil (Welker *et al.*, 1995). Multiple mutations near the extracellular side of human Pgp decreased activity towards verapamil transport (Hafkemeyer *et al.*, 1998). Permanent ATPase activation of human Pgp was observed in cysteineless human Pgp with an I306C mutation labelled with a thiol-reactive verapamil analogue (T. W. Loo *et al.*, 2003b). Mutating the G185 residue had very strong effects on the V_{MAX} of verapamil-induced ATPase activation (Omote *et al.*, 2004; Rao, 1995). The mutation also had significant effects on the K_i for substrate inhibition for verapamil, but negligible effects on verapamil's K_m (Omote *et al.*, 2004). By affecting the K_i and not the K_m suggested to us that the mutation is affecting an alternate verapamil-binding site. With this information, the high-affinity (H) drug-binding site is placed roughly near the extracellular side of Pgp, whereas the

low-affinity (L) drug-binding site is closer to the NBDs within the transmembrane region of the transporter in Figure 2.7 A.

Figure 2.7 A shows Pgp in the absence of ligands. Because the ATPase hydrolysis rate in the absence of ligands is relatively low at ~500 nmol·min^{-1}·mg^{-1}, Pgp will be in an 'open' conformation with the NBDs (N) separated in our model.

At low verapamil concentrations, the drug binds to the H site in Figure 7B. Fitting the Pgp-coupled ATPase activity kinetics of Figure 2.6 B gave a V_{MAX} of ~3000 nmol·min^{-1}·mg^{-1}. This is the highest ATPase activation observed for either drug. Therefore, Pgp is proposed to be in the 'closed' conformation under these conditions.

At higher verapamil concentrations, the drug will occupy the L site on Pgp in Figure 2.7 B. The degree of ATPase activation is less than half the Pgp-coupled ATPase activation at lower verapamil concentrations, but is significantly higher than basal Pgp-coupled ATPase activity. Therefore, Pgp is proposed to be in an intermediate conformation. Consistent with the concentration-dependence observed for ATPase activation by verapamil, the drug transport rate is also concentration-dependent. In Caco-2 cells containing human Pgp, verapamil had a higher permeability ratio with Pgp at low opposed to higher verapamil concentrations (Faassen *et al.*, 2003). Also, human Pgp overexpressed in LLC-PK1 cells had higher efflux ratios at 350 nM than 5 μM verapamil (Pauli-Magnus *et al.*, 2000; Schwab *et al.*, 2003). Therefore, we propose that verapamil occupancy at the H site alone (Figure 2.7 B) will lead to higher verapamil transport rates than occupancy at both drug-binding sites (Figure 2.7 C).

Addition of digoxin leads to formation of Pgp complex shown in Figure 2.7 D. The affinities deduced from the intrinsic protein fluorescence (Figure 2.3) and from fitting the ATPase activity kinetics curves (Figures 2.2 and 2.6) posits the drug in the L site. The degree of

Pgp-coupled ATPase activation by digoxin was similar to the Pgp-coupled ATPase activation in the presence of high concentrations of verapamil. The relative tryptophan accessibility determined from the slopes of the Stern–Volmer plots was similar under both of these conditions (cf. Figures 2.4 E and C). Therefore, Pgp will be in an intermediate conformation in our model. The permeability/efflux ratios of digoxin with Pgp in several cell lines ranged between 4 and 35 (Haslam *et al.*, 2008; Schwab *et al.*, 2003; Taub *et al.*, 2005; Q. Wang *et al.*, 2005). This contrasts with the permeability/efflux ratios for Pgp at low verapamil concentrations, which were generally lower and ranged from ~1 to 6 (Faassen *et al.*, 2003; Haslam *et al.*, 2008; Schwab *et al.*, 2003). These results suggest that the coupling between ATP hydrolysis and transport for drugs may be ligand dependent.

When low verapamil concentrations are added to the digoxin–Pgp complex, verapamil will occupy the H site and form the complex shown in Figure 2.7 E. Several lines of evidence support the simultaneous binding of verapamil and digoxin to Pgp. First, verapamil non-competitively inhibits digoxin transport by Pgp (Ito *et al.*, 1993; Verschraagen *et al.*, 1999). Second, the K_Ds determined from fitting the intrinsic protein fluorescence quenching curves in Figure 3 showed that addition of low concentrations of verapamil does not significantly change the K_D of digoxin to Pgp. Third, there are significant ^{1}H STDD NMR peaks for digoxin at 8 μM verapamil (Figure 2.5 E), which is a high enough verapamil concentration to saturate the H site. Fitting the Pgp-coupled ATPase activity curves in Figure 2.6 revealed that binding of both drugs will inhibit ATP hydrolysis. Therefore, Pgp will be in the ‘open’ conformation.

Higher concentrations of verapamil will completely displace digoxin from the L site forming the double bound complex in Figure 2.7 C. This configuration is supported by our results that showed the affinity decreased significantly at verapamil concentrations above 8 μM

(Figure 2.3). This is also supported by the complete loss of ^{1}H STDD NMR signals from digoxin in the presence of 1 mM verapamil (Figure 2.5 G) and implied by the similarity of the Stern–Volmer plots of Pgp with 1 mM verapamil in the absence and presence of 250 μM digoxin (cf. Figures 2.4 C and F).

2.6. SUPPLEMENTARY INFORMATION

Supplementary Figures 2.8 A and B show the ^{1}H NMR peak assignments for verapamil and digoxin, respectively. The verapamil and digoxin ^{1}H NMR peak assignments from this study were virtually identical to previous assignments (Aulabaugh *et al.*, 1992; Maccotta *et al.*, 1991a; Tetreault and Ananthanarayanan, 1993). Hydroxyl protons of digoxin were not visible in the ^{1}H proton NMR spectrum because of exchange broadening.

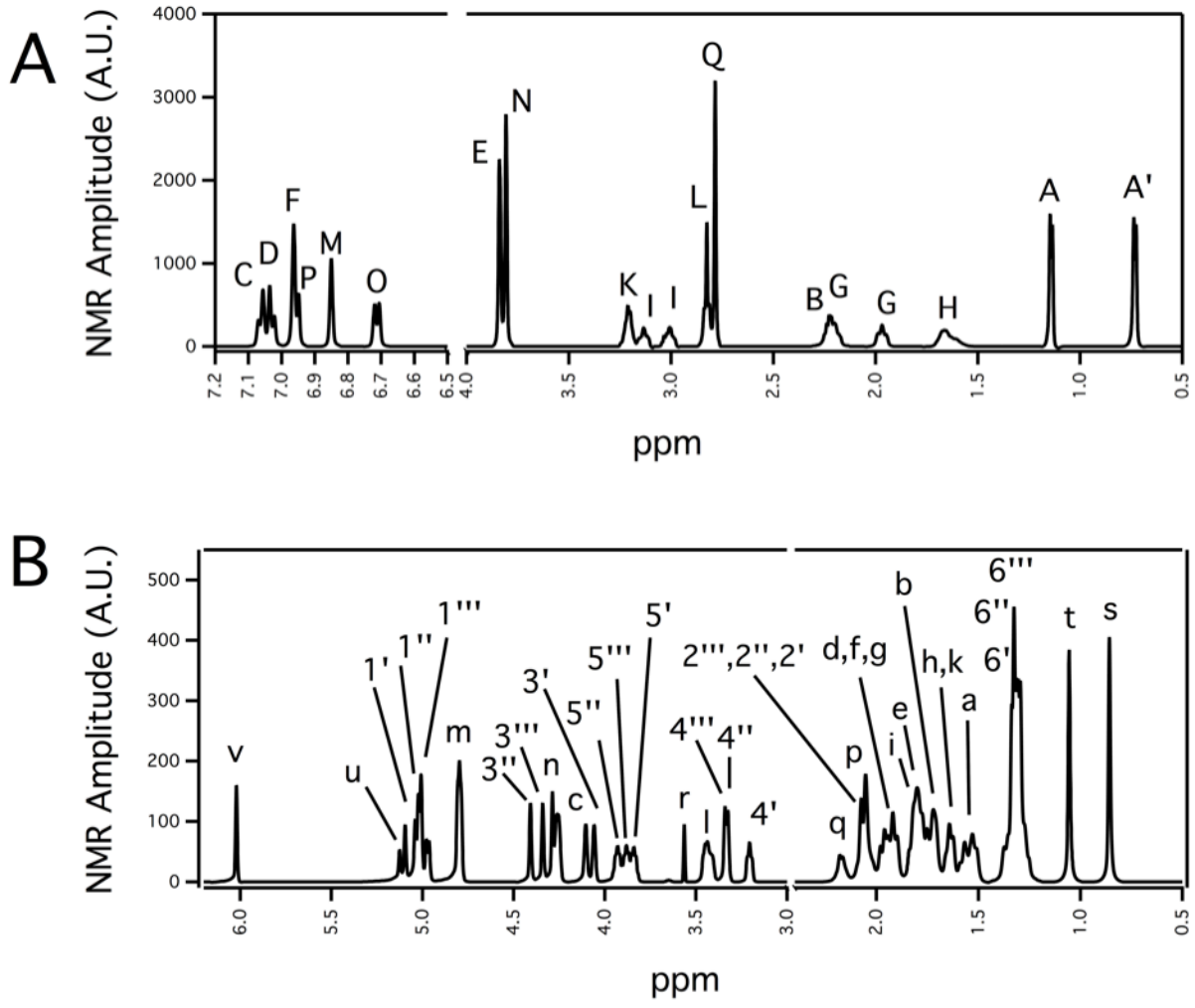

Supplementary Figure 2.8. ^{1}H proton NMR assignments for 1 mM verapamil in 100 mM KPi, pD 7.4 and 200 mM digoxin in d^{6}-DMSO.

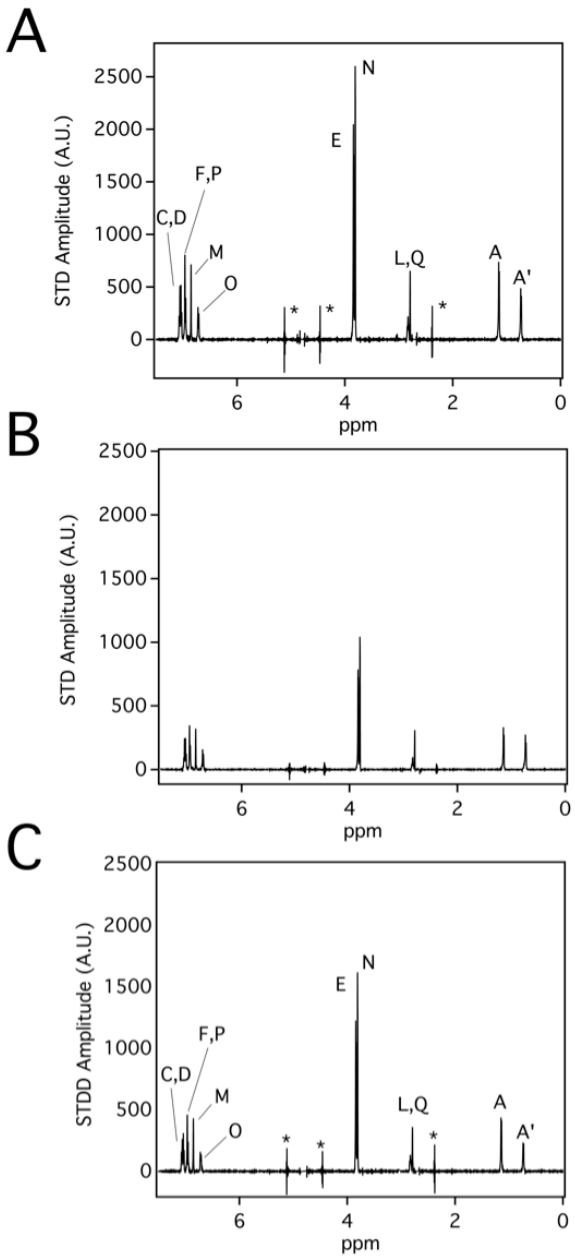

Supplementary Figure 2.9. Subtraction of background STD contributions from the saturation transfer between liposomes and verapamil. A) STD NMR spectrum of 1 mM verapamil with 1 μM of the mouse Pgp transporter in proteoliposomes. B) STD NMR of 1 mM verapamil and liposomes in the absence of Pgp. C) STDD NMR of 1mM verapamil with with1 μM of the mouse Pgp transporter in proteoliposomes. The peaks denoted with an * are subtraction artifacts.

Supplementary Table 2.1. Fitting parameters and their averages used for fitting the ATPase activity curves with verapamil and digoxin.

verapamil, μM	0 – 500				0	4	8	125	
digoxin, μM	0	125	250	500	0 - 250				Average
V_{MAX0}[b]	526	506	543	560	641	451	605	470	538 ± 64
K_{D1}[a] V_{MAX1}[b]	1.83 3000	1.00 2500	3.00 3100	1.00 3164	- -	1.72 2500	1.85 2536	3.27 2500	1.95 ± 0.89 2757 ± 313
K_{D2}[a] V_{MAX2}[b]	211 1100	150 900	150 800	221 800	- -	250 808	175 1062	150 800	187 ± 41 896 ± 132
K_{D3}[a] V_{MAX3}[b]	- -	171 1993	120 1708	288 2077	239 1983	220 1703	207 2200	200 2200	206 ± 53 1981 ± 207
K_{D4}[a]	-	231	207	309	-	208	394	400	292 ± 89
K_{D5}[a]	-	1.00	5.00	1.00	-	4.52	3.92	5.00	3.41 ± 1.91
$V_{MAX4,5}$[b]		0.00	84.5	5.85		43.9	292	300	121 ± 139
R- Correlation	0.994	0.992	0.968	0.921	0.994	0.986	0.909	0.704[c]	

[a] In units of μM

[b] In units of nmol min^{-1} mg^{-1}

[c] $X^2 = 2.05$

CHAPTER 3

COOPERATIVITY BETWEEN VERAPAMIL AND ATP BOUND TO THE EFFLUX TRANSPORTER P-GLYCOPROTEIN[3]

[3] Ledwitch, K. V., Gibbs, M. E., Barnes, R. W. and A. G. Roberts. (2016). *Biochemical Pharmacology.* 18, 96-108. Reprinted here with permission of publisher.

3.1. ABSTRACT

The P-glycoprotein (Pgp) transporter plays a central role in drug disposition by effluxing a chemically diverse range of drugs from cells through conformational changes and ATP hydrolysis. A number of drugs are known to activate ATP hydrolysis of Pgp, but coupling between ATP and drug binding is not well understood. The cardiovascular drug verapamil is one of the most widely studied Pgp substrates and therefore, represents an ideal drug to investigate the drug-induced ATPase activation of Pgp. As previously noted, verapamil-induced Pgp-mediated ATP hydrolysis kinetics was biphasic at saturating ATP concentrations. However, at subsaturating ATP concentrations, verapamil-induced ATPase activation kinetics became monophasic. To further understand this switch in kinetic behavior, the Pgp-coupled ATPase activity kinetics was checked with a panel of verapamil and ATP concentrations and fit with the substrate inhibition equation and the kinetic fitting software COPASI. The fits suggested that cooperativity between ATP and verapamil switched between low and high verapamil concentration. Fluorescence spectroscopy of Pgp revealed that cooperativity between verapamil and a non-hydrolyzable ATP analog leads to distinct global conformational changes of Pgp. NMR of Pgp reconstituted in liposomes showed that cooperativity between verapamil and the non-hydrolyzable ATP analog modulate each other's interactions. This information was used to produce a conformationally-gated model of drug-induced activation of Pgp-mediated ATP hydrolysis.

3.2. INTRODUCTION

P-glycoprotein (Pgp) is an ATP hydrolysis-driven efflux transporter that is part of the ATP-binding cassette (ABC) superfamily of proteins (Boumendjel *et al.*, 2009; S. F. Zhou,

2008). The transporter effluxes a chemically and structurally diverse range of molecules, including anticancer drugs, neurotherapeutics and cardiovascular drugs, from the cytosol to the extracellular space across cell membranes (Boumendjel *et al.*, 2009; S. F. Zhou, 2008). The transporter is expressed at relatively high concentrations in the brain, intestines, liver, placenta, and the kidneys (Ceckova-Novotna *et al.*, 2006; Lum and Gosland, 1995). Pgp expression level is also influenced by genetic polymorphisms and disease (Cascorbi *et al.*, 2004; Meissner *et al.*, 2002). The transporter functions to protect tissues from chemical toxicity, but also leads to drug resistance and can significantly affect drug disposition (Boumendjel *et al.*, 2009; S. F. Zhou, 2008). For example, the transporter protects the brain from chemical insults by effluxing drugs across the blood–brain barrier (BBB) (Ramakrishnan, 2003), but also makes cancerous tumors overexpressing the protein resistant to anticancer drugs (Owens, 2005). As a result, there has been keen interest in unraveling the molecular and structural basis of transport with Pgp. This knowledge is critical for the development of novel transport inhibitors, drugs with desirable transport properties and improving predictions of *in vivo* drug disposition from *in vitro* measurements.

Most of our structural understanding of the transporter comes from X-ray crystallography of mouse Pgp (Abcb1a), *Caenorhabditis* (*C.*) *elegans* Pgp and bacterial transporters (Aller *et al.*, 2009; Dawson *et al.*, 2007; Jin *et al.*, 2012; A. Ward *et al.*, 2007). The X-ray crystal structure of mouse Pgp revealed a 170 kD pseudosymmetric monomer, consisting of two nucleotide-binding domains (NBDs) and 12 transmembrane (TM) helices [10]. The bacterial transporter X-ray crystal structures of MsbA and SAV1866 have only 6 TM helices, but as dimers these proteins resemble the 3-dimensional fold of mammalian Pgps (Dawson *et al.*, 2007; A. Ward *et al.*, 2007). The bacterial transporter X-ray crystal structures have also been found in different

conformations with nucleotide cofactors suggesting that conformational changes play a role in transport (Dawson *et al.*, 2007; Hohl *et al.*, 2014; A. Ward *et al.*, 2007). Since both bacterial and mouse Pgp have conserved motifs within the NBDs, including Walker A, Walker B and ABC signature motifs (e.g. Becker *et al.*, 2009), they are considered to have similar transport mechanisms. From these bacterial transporter structures, a conformationally gated transport model was proposed (Dawson *et al.*, 2007; A. Ward *et al.*, 2007).

Despite the availability of X-ray crystal structures, our understanding of the coupling between drug binding, ATP hydrolysis and transport remains limited. Cross-linking studies of Pgp in human embryonic kidney (HEK) 293 cell membranes suggest that drug-induced conformational changes can occur with the NBDs or the transmembrane region (T. W. Loo *et al.*, 2003a, 2003b). A study on human Pgp in nanodiscs with antibodies showed that there are ligand and cofactor-dependent conformational changes (Ritchie *et al.*, 2011). A fluorescence study with mouse Pgp found differences in fluorescence resonance energy transfer (FRET) with drugs, nucleotide cofactors and their analogs suggesting conformational changes (Verhalen *et al.*, 2012).

In addition to being substrates for the transporter, a number of drugs are known to activate ATP hydrolysis of Pgp, but little is known of the molecular mechanism or its relationship to transport. One of the most studied drugs is the cardiovascular drug verapamil (Fig. 1A), which is used to treat hypertension, chest pain and arrhythmia (Fleckenstein, 1977; Gould *et al.*, 1982; G. R. Lewis *et al.*, 1978; G. R. Lewis *et al.*, 1979; Neugebauer, 1978), and can function as both a substrate and an inhibitor of the transporter (Wessler *et al.*, 2013). The drug is known to activate Pgp-coupled ATP hydrolysis from a number of *in vitro* studies (e.g. Aanismaa and Seelig, 2007; Litman, Zeuthen*, et al.*, 1997b). The kinetics of verapamil-induced

Pgp-coupled ATP hydrolysis is biphasic (Aanismaa and Seelig, 2007; Borgnia *et al.*, 1996; Litman, Nielsen*, et al.*, 1997; Litman, Zeuthen*, et al.*, 1997b; Orlowski *et al.*, 1996; Sharom *et al.*, 1995), suggesting at least two verapamil binding sites. Biphasic drug-induced ATPase activation kinetics has been observed with a chemically diverse range of substrates from amitriptyline to vinblastine (e.g. Aanismaa and Seelig, 2007; Borgnia *et al.*, 1996; Litman, Nielsen*, et al.*, 1997) implying a common mechanism between these types of substrates and Pgp. Despite the large number of studies, the molecular basis for drug-induced ATPase activation of Pgp and the underlying interactions between drugs, ATP and Pgp are not well understood.

In the proposed studies, the interactions of verapamil and ATP were investigated with Pgp reconstituted into liposomes. To investigate the coupling between verapamil and ATP, verapamil-induced activation of ATPase activity was examined with a range of verapamil and ATP concentrations. Acrylamide quenching of intrinsic tryptophan fluorescence spectroscopy was used to investigate drug and nucleotide-induced conformational changes of Pgp. The interactions between verapamil and a non-hydrolyzable ATP analog were investigated by the saturation transfer double difference (STDD) NMR technique. These results were used to build a model of verapamil-induced ATPase activation of verapamil efflux by the transporter. Since similar biphasic drug-induced ATPase activation is observed for several Pgp substrates, this mechanism will likely be generalizable (e.g. Aanismaa and Seelig, 2007; Borgnia *et al.*, 1996; Litman, Nielsen*, et al.*, 1997).

3.3. MATERIALS AND METHODS

3.3.1 Materials

Adenosine 5′-(β,γ-imido)triphosphate lithium salt (AMPPNP) was purchased from Sigma Aldrich (Milwaukee, WI) and verapamil hydrochloride was purchased from Fagron (St. Paul, MN). The detergent *n*-dodecyl-*β*-*d*-maltoside (DDM), which is used in protein purification, was purchased from EMD Millipore Corporation (San Diego, CA). *Escherichia coli* (*E. coli*) total lipid extract powder was purchased from Avanti Polar Lipids Inc. (Alabaster, AL) and cholesterol was purchased from Amresco (Solon, OH) for liposome preparations. Disodium ATP (Na_2ATP) was purchased from Amresco (Solon, OH) and sodium orthovanadate (Na_3VO_4) was purchased from Enzo Life Sciences (Farmingdale, NY) for the ATPase activity assays. Acrylamide was purchased from Calbiochem (San Diego, CA) for the acrylamide quenching experiments. Deuterium oxide (D_2O) was purchased from Cambridge Isotope Laboratories (Tewksbury, MA) and deuterated (d_{10}) DTT was purchased from CDN Isotopes (Quebec, Canada) for NMR experiments. Dithiothreitol (DTT) was purchased from Gold Biotechnology (St. Louis, MO). HEPES was purchased from Calbiochem (San Diego, CA). Tris-HCl was purchased from Amresco (Solon, OH). $MgCl_2$ and NaCl were purchased from J.T. Baker (Center Valley, PA). NH_4Cl was purchased from Sigma Aldrich (Milwaukee, WI). $MgSO_4$, NaN_3, and potassium phosphate were all purchased from Thermo Fisher Scientific (Waltham, MA).

3.3.2. Pgp purification and reconstitution

The wild-type his-tagged mouse Pgp transporter was purified from *Pichia* (*P.*) *pastoris* and reconstituted into liposomes as described previously (Bai *et al.*, 2011; Ledwitch, Barnes*, et al.*, 2016; Lerner-Marmarosh *et al.*, 1999). Briefly, detergent solubilized Pgp was reconstituted

into liposomes composed of 80% w/v Avanti *Escherichia* (*E.*) *coli* Total Lipid Extract (Avanti Polar Lipids, Alabaster, AL) and 20% w/v cholesterol. The final lipid to protein ratio was 0.16 mg ml^{-1} liposomes per μM^{-1} Pgp. Proteoliposomes were stored in aliquots at −80 °C in HEPES buffer (20 mM HEPES, 100 mM NaCl, 5 mM $MgCl_2$, 2 mM DTT, pH 7.4). Protein concentration was determined using the extinction coefficient of 1.28 ml mg^{-1} cm^{-1} (0.181 μM^{-1} cm^{-1}) (Bai *et al.*, 2011) or the DC Protein Assay Kit II (Bio-Rad, Hercules, CA).

3.3.3. ATPase activity measurements

The specific ATPase activity of the Pgp transporter was measured using the Chifflet colorimetric assay as described previously (Chifflet *et al.*, 1988). The rate of ATP hydrolysis was determined by measuring the amount of free inorganic phosphate (P_i) through the formation of *Pi* and ammonium molybdate. This *Pi*-molybdenum complex produces a strong absorbance signal at 850 nm and was measured on a 96-well plate in a FlexStation 3 spectrometer (Molecular Devices, Sunnyvale, CA). The ATPase activity with verapamil and ATP was measured with 50 nM liposome reconstituted Pgp in Chifflet buffer (150 mM NH_4Cl, 5 mM $MgSO_4$, 0.02% w/v NaN_3, 50 mM Tris-HCl, 2 mM DTT, pH 7.4). As a control, 200 μM Na_3VO_4 was added to the ATP titration to show Pgp-mediated ATPase activity inhibition.

Linear transformations such as the Hans-Woolf, Lineweaver-Burk (double reciprocal) or Eadie-Hofstee plots are classical approaches used to fit enzyme kinetics in the absence of computers (Cook and Cleland, 2007; Segel, 1975a). These types of plots suffer from a lack of variable independence across the axes and biasing of the error and the data points (Leatherbarrow, 1990; Martin, 1997; Ranaldi *et al.*, 1999). These methods have generally been superseded by non-linear regression methods that are significantly more accurate and no longer

computationally inaccessible (Leatherbarrow, 1990). For monophasic ATP hydrolysis kinetics, the ATP hydrolysis rate (v), the maximum ATP hydrolysis rate (V_{MAX}), the basal ATPase hydrolysis rate (v_{basal}) and the Michaelis-Menten constant (K_m) was estimated with the Michaelis-Menten equation (equation 1) (A. G. Roberts *et al.*, 2011; Segel, 1975a).

$$v = \frac{V_{MAX}\,[L]}{K_m + [L]} + v_{basal} \qquad (1)$$

In cases where the ATP hydrolysis kinetics was biphasic, the V_{MAX}, K_m and the inhibitory constant (K_i) were estimated with the substrate inhibition equation (equation 2) (A. G. Roberts *et al.*, 2011; Segel, 1975a).

$$v = \frac{V_{MAX}}{1 + \frac{K_m}{[L]} + \frac{[L]}{K_i}} + v_{basal} \qquad (2)$$

For more complicated kinetics, fitting equations have been developed in some cases, but often require specialized numerical methods that result in multiple solutions e.g. (Davydov *et al.*, 2005).

To overcome these challenges, a variety of advanced software modeling packages have been developed to fit arbitrary kinetic models including the free Complex Pathway Simulator (COPASI) and the proprietary Berkeley Madonna (University of California, Berkeley, CA). To estimate the discrete V_{MAX}*s* and K_D*s*, the ATP hydrolysis kinetics in this study were fit to kinetic models using the evolutionary algorithm in the COPASI software (Hoops *et al.*, 2006).

3.3.4. Saturation transfer double difference (STDD) NMR

The STDD NMR technique is a method for characterizing ligand interactions with membrane proteins in the presence of lipids e.g. (Claasen *et al.*, 2005a; Ledwitch, Barnes*, et al.*, 2016; R. P. Venkitakrishnan *et al.*, 2012). With this technique, the protein is selectively excited with a radio frequency (RF) outside of the frequency of ligand proton NMR peaks, which

disperses the RF throughout the protein by spin diffusion. This RF saturation is transferred from the protein to protons on the bound ligand, ligand is exchanged with the bulk solvent and the ^{1}H STD NMR signal is observed (Mayer and Meyer, 2001b). In the presence of lipids such as Pgp reconstituted in liposomes, there will be significant RF saturation transfer interference from non-specific interactions between the ligand and the liposomes. Utilizing the STDD NMR technique allows the saturation transfer between the lipid and the ligand to be subtracted from the ^{1}H STD NMR signal (Claasen *et al.*, 2005a; Haselhorst *et al.*, 2007).

The STDD NMR procedure for membrane proteins was performed as described previously (Ledwitch, Barnes*, et al.*, 2016; R. P. Venkitakrishnan *et al.*, 2012). All the STDD NMR samples contained 1 μM Pgp reconstituted into liposomes in 80% deuterated 100 mM KPi buffer, pD 7.4. For the STDD NMR experiments, a saturation transfer difference (STD) pulse sequence was used with a WATERGATE pulse sequence to suppress background water (M. Piotto *et al.*, 1992), with a 30 ms $T_{1\rho}$ spin lock filter to suppress background NMR signals and a train of 50 ms gaussian shaped selective pulses to excite the protein (Horie *et al.*, 2014). A total of 512 off-resonance spectra were subtracted from on-resonance spectra within the pulse program with a 2 s saturation pulse by phase cycling at 40 and −1.5 ppm, respectively. To produce the STDD NMR spectrum, control samples were performed under identical conditions with the liposomes and the ligands. The ^{1}H STD NMR spectrum with liposomes and ligands was subtracted from the ^{1}H STD NMR spectrum of Pgp reconstituted in liposomes with ligands (ΔI) to isolate specific interactions between the ligand and Pgp. The STDD amplification factor was calculated using the following equation (equation 3) (Ledwitch, Barnes*, et al.*, 2016; Mayer and Meyer, 2001b):

$$STDD\ Amplification\ Factor = \frac{[L]}{[P]}\frac{\Delta I}{I_0} \qquad (3)$$

where [P] is the protein concentration and I_0 is the amplitude of the ^{1}H NMR peaks in the absence of excitation pulses.

All NMR experiments were performed on an 800 MHz Varian INOVA spectrometer at 25 °C equipped with a 5 mm z-gradient ^{1}H{^{13}C/^{15}N} cryoprobe. The ^{1}H NMR peaks for verapamil and AMPPNP were assigned using standard ^{1}H 1D and 2D NMR techniques. NMR spectra were processed using the iNMR software package (http://www.inmr.net) and analyzed using Igor Pro 6.2 (Wavemetrics, Tigard, OR). The molecular structure of verapamil and AMPPNP with the nuclei labeled are shown in Fig. 5A and E.^{1}H NMR peak assignments for verapamil and AMPPNP are shown in Fig. 5B and F, respectively, and were essentially identical to previous ^{1}H NMR assignments (Maccotta *et al.*, 1991b; Tetreault and Ananthanarayanan, 1993; Ulrich *et al.*, 2008).

3.3.5. Intrinsic tryptophan fluorescence

Fluorescent quenching of tryptophan residues has been used to measure the binding affinity of drugs and nucleotides to Pgp (Ledwitch, Barnes*, et al.*, 2016; Liu *et al.*, 2000; Sharom *et al.*, 2003). The quenching of protein fluorescence with the nucleotide AMPPNP and 1 μM Pgp reconstituted in liposomes was performed as described (Ledwitch, Barnes*, et al.*, 2016) in Chifflet buffer at pH 7.4. Pgp tryptophan residues were excited at 295 nm and the fluorescence emission maximum was measured at 333 nm on an Olis DM 45 spectrofluorimeter. The fluorescence was measured with an integration time of 0.8 s that produced an average maximum fluorescence signal at 333 nm of ~200,000. AMPPNP-induced fluorescent quenching was corrected ($F_{corrected}$) for background fluorescence, dilution and inner filter effects with the following equation (equation 4) (Lakowicz, 1999):

$$F_{corrected} = (F - B)10^{\frac{(\varepsilon_{ex}\, b_{ex} + \varepsilon_{em} b_{em})[Q]}{2}} \qquad (4)$$

where F is the measured protein fluorescence, B is the background and $[Q]$ is the quenching ligand concentration. The extinction coefficients (ε) for excitation and emission are ε_{ex} and ε_{em}, respectively. AMPPNP was essentially transparent above 300 nm and had a ε_{295} of 0.03 mM^{-1} cm^{-1} at 295 nm. The pathlength (b) along the excitation and emission axes are b_{ex} and b_{em}, respectively.

Ligand-induced quenching of protein fluorescence can either have a static or a dynamic quenching mechanism. Fluorescence quenching caused by complexation of a ligand to a protein and related to a ligand's affinity is known as a static quenching (Lakowicz, 1983). Alternatively, there are instances where random collisions between the ligand and the protein will induce fluorescence quenching by a mechanism known as dynamic quenching (Lakowicz, 1999). Regardless of the nature of the quenching, monophasic fluorescent quenching curves were fit to equation 5 (Lakowicz, 1999):

$$F_{corrected} = \frac{F_{corrected,0}}{1+K[Q]} + F_{unquenched} \qquad (5)$$

where $F_{corrected,0}$ is the protein fluorescence in the absence of a quenching ligand and K is the association constant (K_A) or the Stern-Volmer quenching constant (K_{SV}) in the case of a static and dynamic quenching processes, respectively. Curves that were biphasic were fit with equation 6 (Doppenschmitt *et al.*, 1998):

$$F_{corrected} = \frac{F_{0,L}}{1+ K_L[Q]} + \frac{F_{0,H}}{1+K_H[Q]} + F_{unquenched} \qquad (6)$$

where $F_{0,L}$ and $F_{0,H}$ are the fluorescence amplitudes and K_H and K_L are the apparent equilibrium constants at low and high concentrations, respectively. The two different quenching mechanisms were differentiated by performing the fluorescence titration experiments at two different temperatures (Lakowicz, 1999). In the case of a dynamic quenching mechanism, the apparent K

value will increase with increasing temperature as a result of increases in collisional frequency. For a static quenching process, the *K* value will decrease with increasing temperature as a result of decreases in the residence time of the ligand.

3.3.6. Acrylamide quenching

Changes in the accessibility of tryptophan residues in proteins can be used as a tool to assess conformational changes upon ligand binding using the collisional quencher acrylamide (Liu *et al.*, 2000; Sonveaux *et al.*, 1999). Acrylamide quenches intrinsic tryptophan fluorescence in a dynamic fashion and has been used to probe conformational changes of Pgp (Liu *et al.*, 2000; Russell and Sharom, 2006; Sonveaux *et al.*, 1999). For these experiments, fluorescence emission with 1 μM Pgp reconstituted in liposomes was measured at 333 nm following excitation at 295 nm. Fluorescence intensities were corrected for with equation 4 (Lakowicz, 1999). The $F_{corrected,0}/F_{corrected}$ was plotted as a function of acrylamide concentration to produce the Stern-Volmer plots. The extent of dynamic tryptophan quenching was estimated from the slopes of the Stern-Volmer curves, which is related to K_{SV} by $F_{corrected,0}/F_{corrected} = 1 + K_{SV}[Q]$ (Lakowicz, 1999).

3.4. RESULTS

3.4.1. The effects of saturating and subsaturating ATP on verapamil-induced Pgp-coupled ATPase activity

Drug-stimulated ATPase activity of Pgp is typically evaluated at saturating ATP concentrations e.g. (Aanismaa and Seelig, 2007; Hafkemeyer *et al.*, 1998; Kerr *et al.*, 2001; Tip W. Loo and Clarke, 1997; Shapiro and Ling, 1994; Sharom, Yu*, et al.*, 1999). However, *in vivo*,

intracellular ATP concentrations can vary widely from submillimolar levels up to 10 mM (Gribble *et al.*, 2000; Kennedy *et al.*, 1999; Manfredi *et al.*, 2002; Schwiebert and Zsembery, 2003). These values vary depending on cell and tissue type (Ataullakhanov and Vitvitsky, 2002) and can fluctuate significantly in disease states (Wong *et al.*, 1992; Y. Zhou *et al.*, 2012). Intracellular ATP concentration can also affect cellular function (Gajewski *et al.*, 2003; Huang *et al.*, 2010; Leist *et al.*, 1997; Soltoff, 1986). Therefore, the effect of ATP concentration on verapamil-stimulated ATPase activity with Pgp was examined.

Figure 3.1 shows the verapamil-induced activation of Pgp ATP hydrolysis in the presence of 3.2 mM (closed squares) and 0.25 mM (open squares) ATP. Kinetics of Pgp-coupled ATP hydrolysis in the presence of saturating ATP (Figure 3.1 A, closed squares) were biphasic with substrate activation and inhibition reaching a maximum activation of 3–4-fold at 8 μM verapamil and decreasing to basal ATPase levels at saturating verapamil. Fitting the kinetics to the substrate inhibition equation (equation 2) produced values for V_{MAX}, K_m, and K_i of 1623 ± 97 nmol min^{-1} mg^{-1}, 1.9 ± 0.5 μM and 214 ± 52 μM, respectively, which are similar to previous estimates (Ledwitch, Barnes*, et al.*, 2016). As suggested previously (Ledwitch, Barnes*, et al.*, 2016), this characteristic implies a high and a low affinity verapamil binding site on Pgp. Biphasic verapamil-induced ATP hydrolysis kinetics has been observed in hamster (Borgnia *et al.*, 1996; Litman, Zeuthen*, et al.*, 1997b; Orlowski *et al.*, 1996; Sharom *et al.*, 1995), mouse (Ledwitch, Barnes*, et al.*, 2016; Litman, Nielsen*, et al.*, 1997) and human (Aanismaa and Seelig, 2007) Pgp. Biphasic drug-induced ATPase activation kinetics is also a common feature of Pgp substrates including actinomycin D, paclitaxel, valinomycin, progesterone, quinidine and dipyridamole (Gatlik-Landwojtowicz *et al.*, 2006; Jin *et al.*, 2012; Litman, Zeuthen*, et al.*, 1997b).

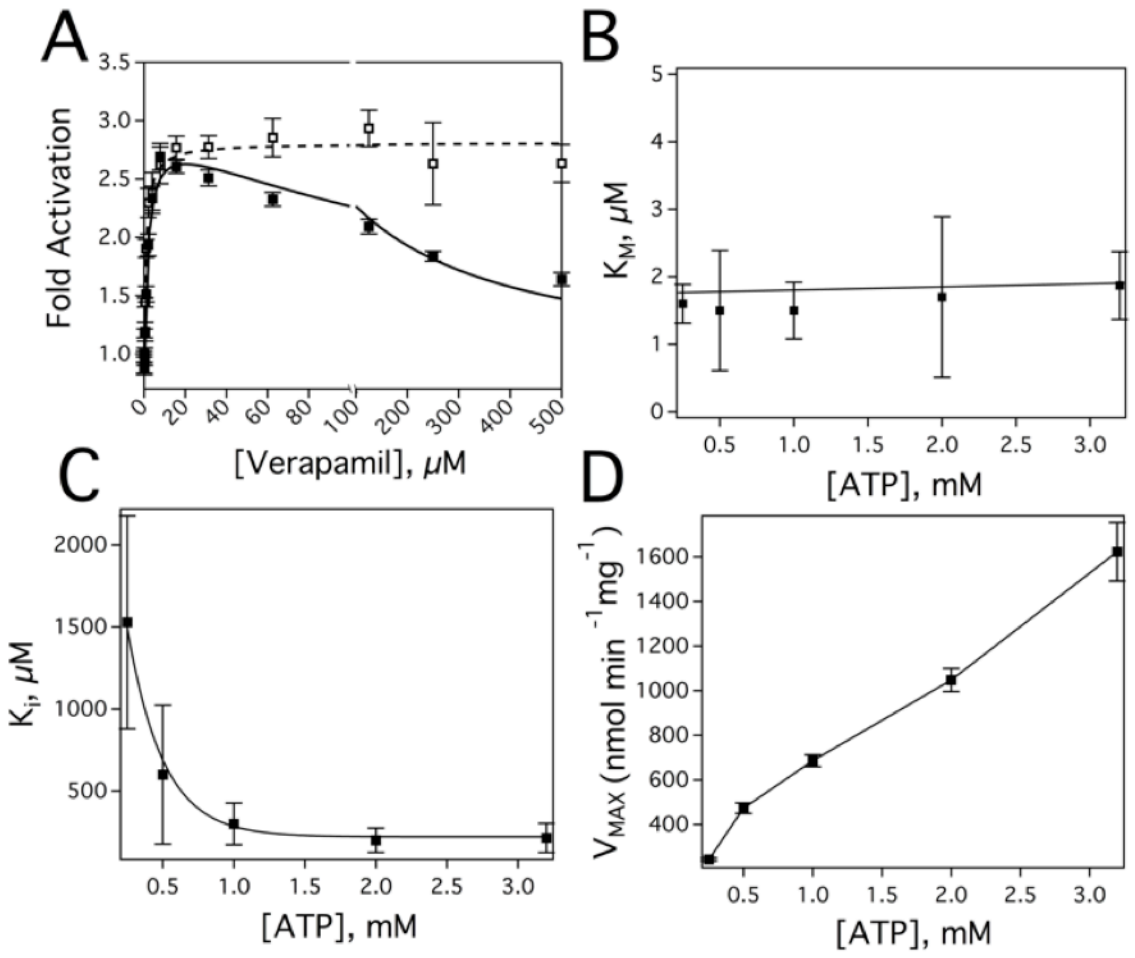

Figure 3.1. The effect of ATP on verapamil-induced ATPase activation of Pgp. A) The Pgp-coupled ATPase activity as a function of verapamil concentration in the presence of 3.2 mM (closed squares) and 0.25 mM ATP (open squares). The kinetic fits are shown as a dashed and solid line and were fit to equation 1 and 2, respectively. B) The Michaelis-Menten constant (K_m), C) the inhibition constant (K_i) and D) the V_{MAX} for verapamil-induced Pgp ATPase activity as a function of different ATP concentrations. Error bars represent the standard deviation and the points represent the average of at least three independent experiments.

Surprisingly, when the verapamil-induced ATPase activity was measured at subsaturating ATP (Figure 3.1 A, open squares) concentrations, the kinetics became almost monophasic and reached a maximum fold-activation close to that observed for Pgp at saturating ATP. Fitting the monophasic ATP hydrolysis kinetics to the Michaelis-Menten equation (equation 1) gave a V_{MAX} and K_m of 233 ± 8 nmol min^{-1} mg^{-1} and 0.94 ± 0.2 μM, respectively. The relatively low V_{MAX} is consistent with previous observations at low ATP (Ambudkar *et al.*, 1992) and the K_m at this low ATP concentration is very similar to the K_m at saturating ATP concentrations (Figure 3.1 A, closed squares).

To uncover the relationship between ATP and verapamil, the ATP hydrolysis kinetics were measured with a range of verapamil and ATP concentrations and fit to the substrate inhibition equation (equation 2). The K_m and K_i from the substrate inhibition equation were previously attributed to a high and low affinity site on the transporter (Ledwitch, Barnes*, et al.*, 2016). Figure 3.1 B and C shows the effect of ATP concentration on the K_m and K_i for verapamil stimulated Pgp ATPase activity, respectively. In Figure 3.1 B, the K_m for verapamil over a range of ATP concentrations was essentially unaffected, which suggests that verapamil at the K_m-associated binding site and ATP are not cooperative. However, the K_i for verapamil dramatically decreases with increasing ATP concentration (Figure 3.1 C). These results imply that verapamil at the K_i-associated binding site and ATP are cooperative. Figure 3.1 D shows the apparent V_{MAX} as a function of ATP concentration. As expected (Ambudkar *et al.*, 1992), the apparent V_{MAX} increased with increasing ATP concentration. Since these are only apparent kinetic parameters, further analysis is required to determine the discrete dissociation constants and the V_{MAX}s for the individual verapamil and ATP bound states.

3.4.2. Modeling Pgp-coupled ATPase activity with verapamil and a panel of ATP concentrations

Fitting the ATP hydrolysis kinetics with the substrate inhibition equation in Figure 3.1 A implied that there is a high affinity non-cooperative verapamil binding site and a low affinity cooperative verapamil binding site with ATP. To obtain the microscopic dissociation constants and V_{MAX}s, verapamil and ATP were investigated by fitting the verapamil-induced ATP hydrolysis kinetics over a range of verapamil and ATP concentrations using COPASI.

Figure 3.2 A shows the model used to fit the ATP hydrolysis kinetics and is the simplest that could fit all the data. The verapamil interactions leading to biphasic ATP hydrolysis kinetics in Figure 3.1 A (closed squares) is represented by EV and EVV for binding of one and two verapamil molecules, respectively. The affinity of verapamil to E and EV is defined by K_{D1} and K_{D2}, respectively. Nucleotide binding to Pgp is shown as E-ATP, EV-ATP and EVV-ATP with affinities of K_{D3}, K_{D4} and K_{D5}, respectively. Pgp-mediated ATP hydrolysis from these states is defined by V_{MAX0}, V_{MAX1} and V_{MAX2}.

Figure 3.2 B (closed squares) shows the effect of ATP concentration on the basal activity of Pgp in the absence of verapamil and has a hyperbolic shape; therefore, the curve was fit to the Michaelis-Menten equation (equation 1). The fit gave a V_{MAX} of 619 ± 18 nmol min^{-1} mg^{-1} and a K_m of 879 ± 69 μM. In the presence of 200 μM of the Pgp inhibitor Na_3VO_4 and a range of ATP concentrations (Figure 3.2 B, open squares), the amplitude of the hyperbolic curve was relatively weak. Fitting the ATP hydrolysis kinetics with equation 1 gives a V_{MAX} of 172 ± 24 nmol min^{-1} mg^{-1} and K_m of 906 ± 476 μM. The large decreases in V_{max}, but no significant change in K_m, demonstrates that Na_3VO_4 is a non-competitive inhibitor of Pgp-mediated ATP hydrolysis as has been previously noted (Litman, Zeuthen*, et al.*, 1997a). The

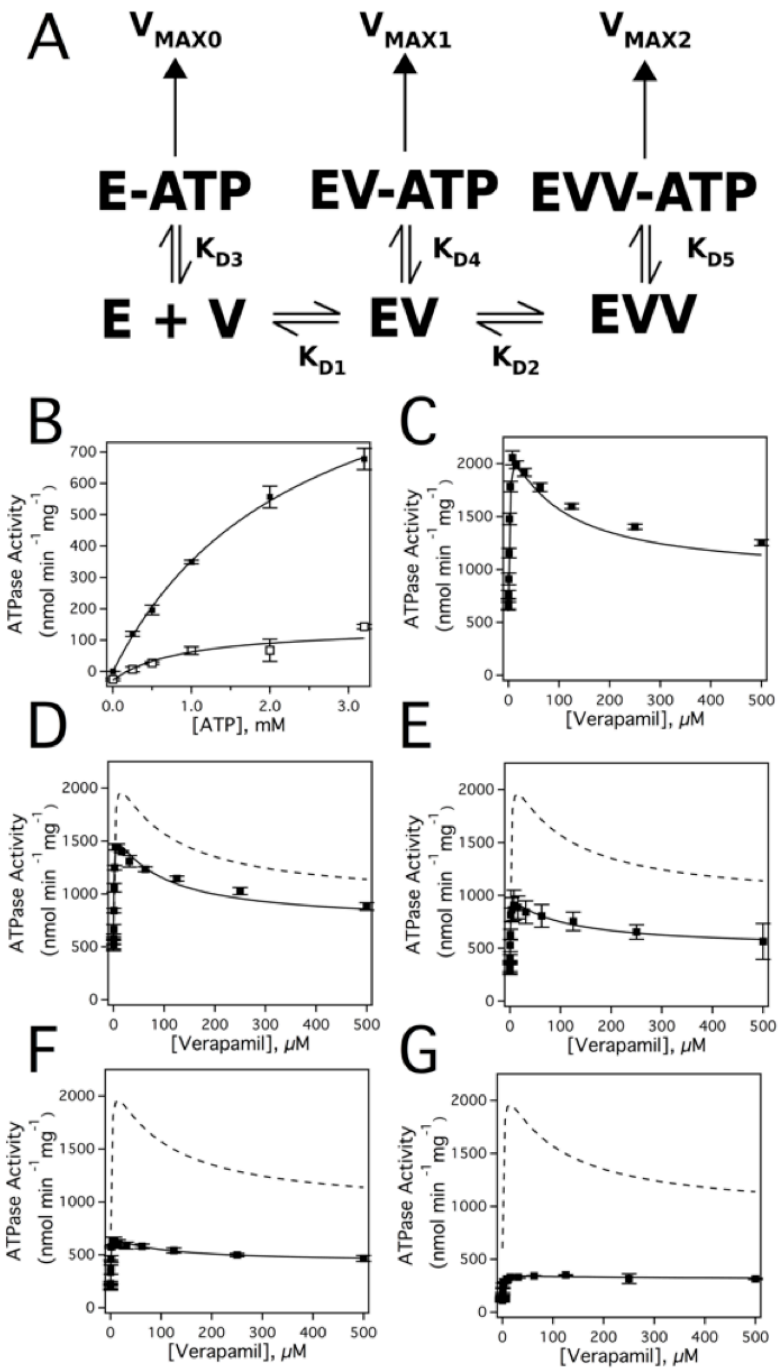

Figure 3.2. Deconvoluting the Pgp-mediated ATP hydrolysis kinetics in the presence of verapamil and ATP. A) The verapamil-nucleotide cooperativity model used to fit the ATP hydrolysis kinetics. Horizontal and vertical left/right arrows denote the equilibria between bound

states. The vertical arrows at the top of the panel represent the ATPase activity from the bound states. E and V correspond to Pgp and verapamil, respectively. B) Pgp-mediated ATP hydrolysis activity as a function of ATP concentration. Verapamil-induced activation of Pgp-mediated ATPase activity at C) 3.2, D) 2.0, E) 1.0, F) 0.5, and G) 0.25 mM ATP. For comparison, the kinetics in panel C at 3.2 mM ATP is shown as a dashed line in panels D through G. The error bars and the points represent the standard deviation and average, respectively, of three independent experiments.

differences in V_{MAX}s gives a Na_3VO_4 sensitive V_{MAX} for Pgp of 447 ± 30 nmol min^{-1} mg^{-1}. The fitted values are within range of V_{MAX} and K_ms observed in the literature of 500–2000 nmol min^{-1} mg^{-1} and 0.3–1 mM, respectively (Kerr *et al.*, 2001; Liu *et al.*, 2000; Qu *et al.*, 2003; Shapiro and Ling, 1994; Sharom *et al.*, 1995; Urbatsch and Senior, 1995).

Figure 3.2 C through G shows the verapamil-induced Pgp-coupled ATPase activity over a range of ATP concentrations starting at saturating ATP (3.2 mM) and decreasing to subsaturating ATP (0.25 mM). These kinetics were fit using the COPASI software package. The average basal ATPase activity of Pgp (i.e. V_{MAX0}) determined from fitting with COPASI was 672 ± 93 nmol min^{-1} mg^{-1} and the average K_{D3} for ATP in the absence of ligands was 1163 ± 110 μM. The average fitted K_{D1} and K_{D2} values for verapamil to E and EV were 1.11 ± 0.50 μM and 270 ± 45 μM, respectively, which were similar to previous estimates (Ledwitch, Barnes*, et al.*, 2016).

In the presence of a single bound verapamil molecule (i.e. EV), the average affinity of ATP was not significantly perturbed and had an average K_{D4} of 1242 ± 217 μM. This result suggests that verapamil and ATP are not cooperative with respect to binding within the EV-ATP complex, which is consistent with the lack of ATP concentration dependence for the verapamil K_m in Figure 3.1 B. However, Pgp mediated ATP hydrolysis was activated about 4-fold in the presence of a single bound verapamil molecule to a V_{MAX1} of 2561 ± 295 nmol min^{-1} mg^{-1}. Thus, verapamil and ATP are positively cooperative with respect to ATP hydrolysis within the EV-ATP complex. Non-competitive inhibitors have analogous effects with enzymes, except they inhibit enzyme activity (Segel, 1975a) rather than activate it. Therefore, a single verapamil molecule bound to Pgp behaves like a “non-competitive activator” of Pgp.

In the presence of two bound verapamil molecules, the average ATP affinity increased ~4-fold with a decreased K_{D5} of 257 ± 44 μM. This correlates well with the decreased K_i observed at increasing ATP concentration that is shown in Figure 3.1 C. The increased affinity of ATP shows that verapamil and ATP are cooperative with respect to binding within the EVV-ATP complex. Fitting also revealed that there was more than a twofold decrease in the maximum ATP hydrolysis rate with a V_{MAX2} of 760 ± 147 nmol min^{-1} mg^{-1}. The decreased V_{MAX} is in line with the reduced ATP hydrolysis activity that was observed at high verapamil concentration (Figure 3.1 A, closed squares). The decrease in V_{MAX} shows that ATP and verapamil are negatively cooperative with respect to ATP hydrolysis within the EVV-ATP complex. A complete list of kinetic and thermodynamic parameters used to fit the curves is shown in Table 3.1. In all cases, the *R*-correlation values for the fits were greater than 0.988.

3.4.3. The binding affinity of AMPPNP to Pgp by tryptophan fluorescence

The non-hydrolyzable ATP analog AMPPNP has been used as a surrogate for ATP to study nucleotide interactions with Pgp (Liu *et al.*, 2000; Rosenberg *et al.*, 2003; Siarheyeva *et al.*, 2010; Urbatsch *et al.*, 1994). The ATP analog is advantageous for investigating nucleotide interactions with Pgp because several analogous bacterial transporter X-ray crystal structures have been solved with it (Dawson and Locher, 2007; Hohl *et al.*, 2014; A. Ward *et al.*, 2007). In addition, AMPPNP does not undergo ATP hydrolysis like other nucleotide analogs (Resetar and Chalovich, 1995).

To ensure that saturating AMPPNP concentrations were used in this study, AMPPNP interactions were investigated by nucleotide-induced quenching of Pgp tryptophan fluorescence (Figure 3.3). Figure 3.3 A shows the effect of a range of AMPPNP concentrations on the Pgp

Verapamil, μM	0–500					
ATP, mM	3.2	2	1	0.5	0.25	Average
K_{D1}[a]	1.93	1.00	0.89	0.61	1.12	1.11 ± 0.50
K_{D2}[a]	299.7	299.7	249.8	200.0	300.0	269.8 ± 44.6
K_{D3}[a]	1129.6	1000.5	1205.7	1179.0	1299.3	1162.8 ± 109.7
V_{max0}[b]	817.5	700.0	608.6	582.6	653.1	672.4 ± 92.6
K_{D4}[a]	1000.0	1026.8	1342.1	1488.6	1352.1	1241.9 ± 216.7
V_{max1}[b]	3000.0	2494.5	2369.4	2691.7	2250.8	2561.3 ± 294.6
K_{D5}[a]	209.6	209.6	283.1	284.8	299.9	257.4 ± 44.1
V_{max2}[b]	1000.0	800.0	644.6	669.5	685.5	759.9 ± 146.8
R- Correlation	0.9885	0.9925	0.9941	0.9936	0.9949	

[a] In units of μM.
[b] In units of nmol min^{-1} mg^{-1}.

Table 3.1. Kinetic and thermodynamic parameters and the corresponding averages used for fitting the ATPase activity curves with verapamil over a range of ATP concentrations in Figure 3.3.

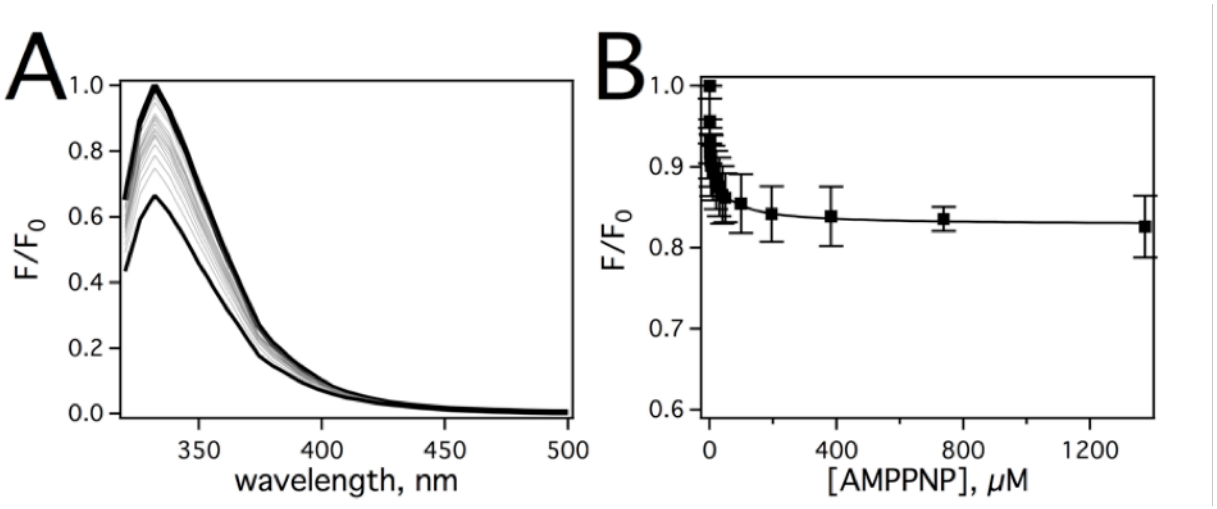

Figure 3.3. Characterization of AMPPNP binding to Pgp by tryptophan fluorescence. A) Pgp fluorescence spectra in the presence of a range of AMPPNP concentrations after exciting at 295 nm. The spectrum at 0 μM and 1.4 mM AMPPNP are shown as thick and thin lines, respectively, while intermediate concentrations of AMPPNP are shown as gray lines. B) Corrected Pgp fluorescence emission at 333 nm as a function of AMPPNP concentration. The average and standard deviations are represented as points and bars, respectively, and reflect at least three independent experiments.

tryptophan fluorescence, which decreases about 15% at saturating AMPPNP concentration. The corrected fluorescence amplitude (i.e. $F_{corrected}$) at 333 nm was plotted as a function of AMPPNP concentration in Figure 3.3 B. The quenching of tryptophan fluorescence was biphasic with a low and a high concentration phase, which was fit to equation 6 (Figure 3.3 B, solid line). The fraction quenched for the low (F_L/F_0) and high concentration (F_H/F_0) phases from the fit were 0.16 and 0.074, respectively. The K_1 and K_2 values extracted from the fit were $6.66 \pm 3.41\ \mu M^{-1}$ and $0.022 \pm 0.006\ \mu M^{-1}$, respectively. Ligand-induced quenching can occur by a static mechanism, which correlates to a ligand's affinity, or by a dynamic mechanism (Lakowicz, 1983). To determine the quenching mechanism of each phase, the AMPPNP titration with Pgp was repeated at 37 °C as described (Lakowicz, 1999; Ledwitch, Barnes*, et al.*, 2016). At this higher temperature, the K_1 associated with the low concentration phase increased to $8\ \mu M^{-1}$, while the K_2 associated with the high concentration phase decreased to $0.017\ \mu M^{-1}$ (data not shown). These results show that the low concentration-quenching phase resulted from dynamic quenching, while the high concentration-quenching phase resulted from static quenching. Therefore, the high concentration phase corresponds to a K_D of $45 \pm 13\ \mu M$ for AMPPNP. This K_D value is considerably lower than AMPPNP binding to detergent-solubilized hamster Pgp (Siarheyeva *et al.*, 2010), which likely represents differences between detergent-solubilized Pgp and Pgp reconstituted in liposomes in this study.

3.4.4. Verapamil and nucleotide-induced conformational changes of Pgp

Acrylamide quenching of tryptophan fluorescence has been successfully used to probe changes in tertiary conformation of Pgp with a wide range of ligands and nucleotide cofactors (Liu *et al.*, 2000; Russell and Sharom, 2006; Sharom, Liu*, et al.*, 1999; Siarheyeva *et al.*, 2010;

Sonveaux *et al.*, 1999). In this study, this technique was performed with Pgp in the presence of verapamil and the non-hydrolyzable ATP analog AMPPNP to determine the effect of verapamil-nucleotide cooperativity on Pgp conformation.

Figure 3.4 shows acrylamide quenching of Pgp with verapamil and AMPPNP represented as Stern-Volmer plots with the slopes reflecting the degree of tryptophan quenching. The Stern-Volmer plot for Pgp without ligands had a K_{SV} value of $1.55 \pm 0.04\ M^{-1}$ (Figure 3.4 A, closed squares), which is similar to the K_{SV} value for mouse (Ledwitch, Barnes*, et al.*, 2016) and hamster Pgp (Siarheyeva *et al.*, 2010). Significant verapamil-induced changes in the K_{SV} values of Pgp in the absence of nucleotides were observed in the Stern-Volmer plots. In Figure 3.4 B, the addition of 8 μM verapamil increases the K_{SV} value to $3.06 \pm 0.21\ M^{-1}$, while saturating verapamil concentrations (1 mM) increased the K_{SV} value further to $3.81 \pm 0.26\ M^{-1}$ (Figure 3.4 C). The similarities in the K_{SV} values suggest that their verapamil-bound Pgp conformations are similar, and that the largest conformational shift occurs at low verapamil concentration. This observation is consistent with verapamil-induced Pgp conformational changes deduced from crosslinking of (T. W. Loo *et al.*, 2003a, 2003b, 2003c), trypsin digestion of (G. Wang *et al.*, 1998), and antibody competition with Pgp (Nagy *et al.*, 2001).

In the presence of 250 μM AMPPNP (Figure 3.4 D), the K_{SV} value from the slope of the Stern-Volmer plot for Pgp decreased from $1.55\ M^{-1}$ to $0.84 \pm 0.07\ M^{-1}$, suggesting that the tryptophans became less accessible in the presence of the nucleotide analog and this is similar to the K_{SV} value determined for hamster Pgp with a nucleotide analog (Sonveaux *et al.*, 1999). The AMPPNP-induced changes in the K_{SV} value in the presence of 8 μM verapamil were more dramatic in Figure 3.4 E. The K_{SV} value decreased more than 4-fold from $3.81\ M^{-1}$ to

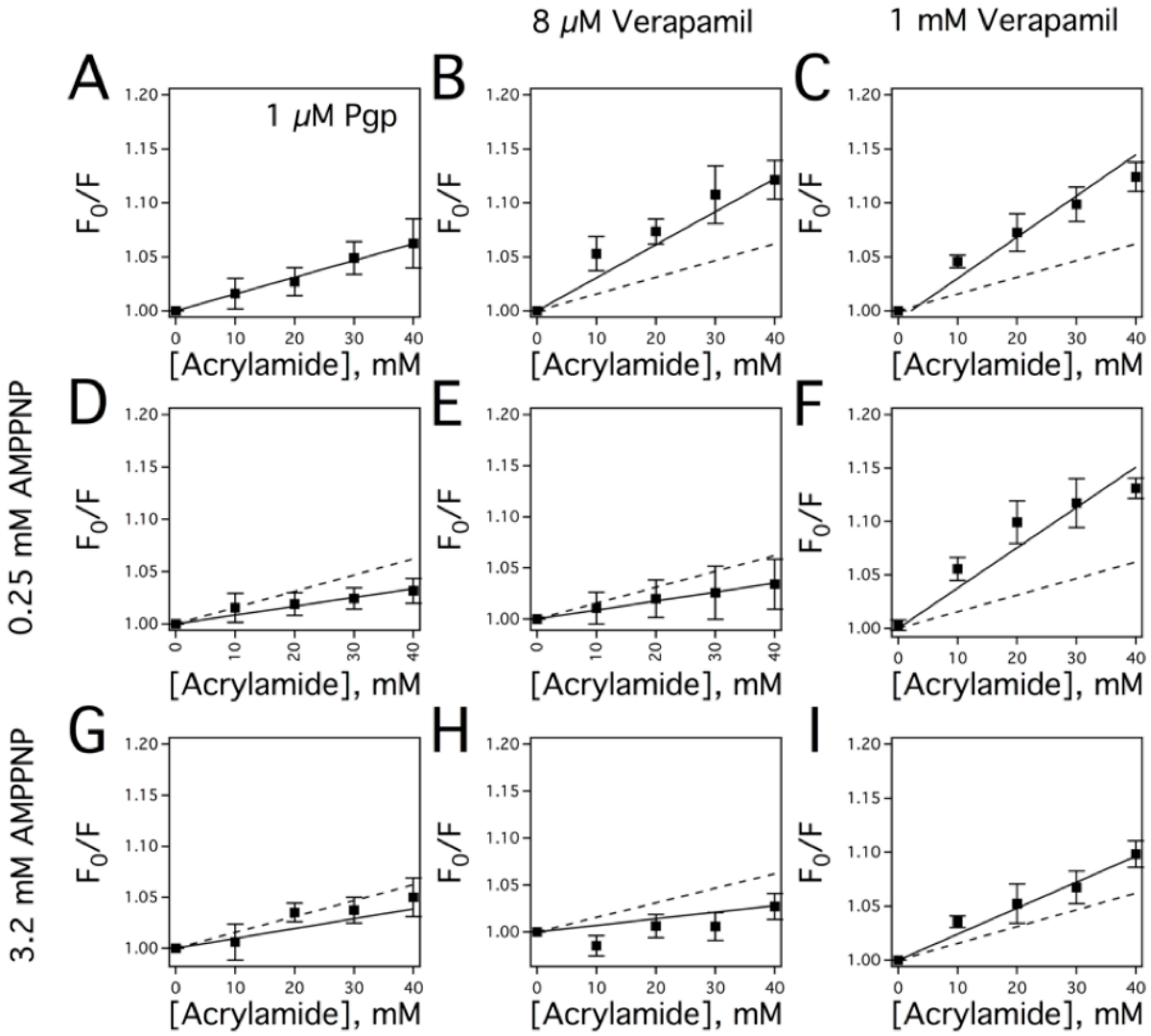

Figure 3.4. Conformational changes of Pgp in the presence of AMPPNP and verapamil characterized by acrylamide quenching of Pgp tryptophan fluorescence. A) The Stern-Volmer plot of Pgp in the absence of drugs. The Stern-Volmer plots of Pgp in the presence of B) 8 μM and C) 1000 μM verapamil. D) Stern-Volmer plot of Pgp in the presence of 0.25 mM AMPPNP. The Stern-Volmer plots of Pgp in the presence of 3.2 mM AMPPNP and E) 8 μM and F) 1000 μM verapamil. G) Stern-Volmer plot of Pgp in the presence of 3.2 mM AMPPNP. The Stern-Volmer plots of Pgp in the presence of 3.2 mM AMPPNP and E) 8 μM and F) 1000 μM verapamil. For comparison, the slope in panel A is presented as a dashed line in panels B through

F. The error bars and the points reflect the standard deviation and average, respectively, of at least three independent experiments.

$0.88 \pm 0.03\ M^{-1}$. In contrast, the K_{SV} value remained relatively constant in the presence of 1 mM verapamil and 250 μM AMPPNP (Figure 3.4 F) at $3.77 \pm 0.33\ M^{-1}$.

In the presence of saturating (3.2 mM) AMPPNP (Figure 3.4 G), the slope of the Stern-Volmer plot for Pgp remained relatively constant at $0.97 \pm 0.16\ M^{-1}$, when compared to the Stern-Volmer plot for Pgp with 250 μM AMPPNP in Figure 3.4 D. The slope of the Stern-Volmer plot also remained relatively constant with the addition of 8 μM verapamil with a K_{SV} value of $0.70 \pm 0.11\ M^{-1}$ (Figure 3.4 H). In contrast, the K_{SV} value decreased from $3.77\ M^{-1}$ to $2.28 \pm 0.21\ M^{-1}$ in the presence of 1 mM verapamil and saturating AMPPNP (Figure 3.4 I). The relatively modest AMPPNP-induced shift in K_{SV} values in the presence of 1 mM verapamil, when compared to K_{SV} value shifts with 8 μM verapamil, implies stabilization of the ligand-bound Pgp conformation.

3.4.4. Verapamil and AMPPNP interactions with Pgp probed by STDD NMR

The STDD NMR technique was used previously to deconvolute the interactions of verapamil and digoxin with Pgp and showed that verapamil competitively displaces digoxin (Ledwitch, Barnes*, et al.*, 2016). In Figure 3.5, the technique was used to investigate the cooperative molecular interactions of AMPPNP and verapamil with Pgp. To probe the high and low affinity verapamil sites on Pgp, we used 8 μM and 1 mM verapamil, respectively.

Figure 3.5 A shows the molecular structures of verapamil with the nuclei labeled. Structurally, verapamil has two dimethoxyphenyl groups that are connected together by an alkyl chain. The ^{1}H STDD NMR spectrum of verapamil is shown with the ^{1}H NMR peaks labeled in Figure 3.5 B. The STDD amplification factors for verapamil were also significantly larger than previously observed (Ledwitch, Barnes*, et al.*, 2016) as a result of using a higher frequency

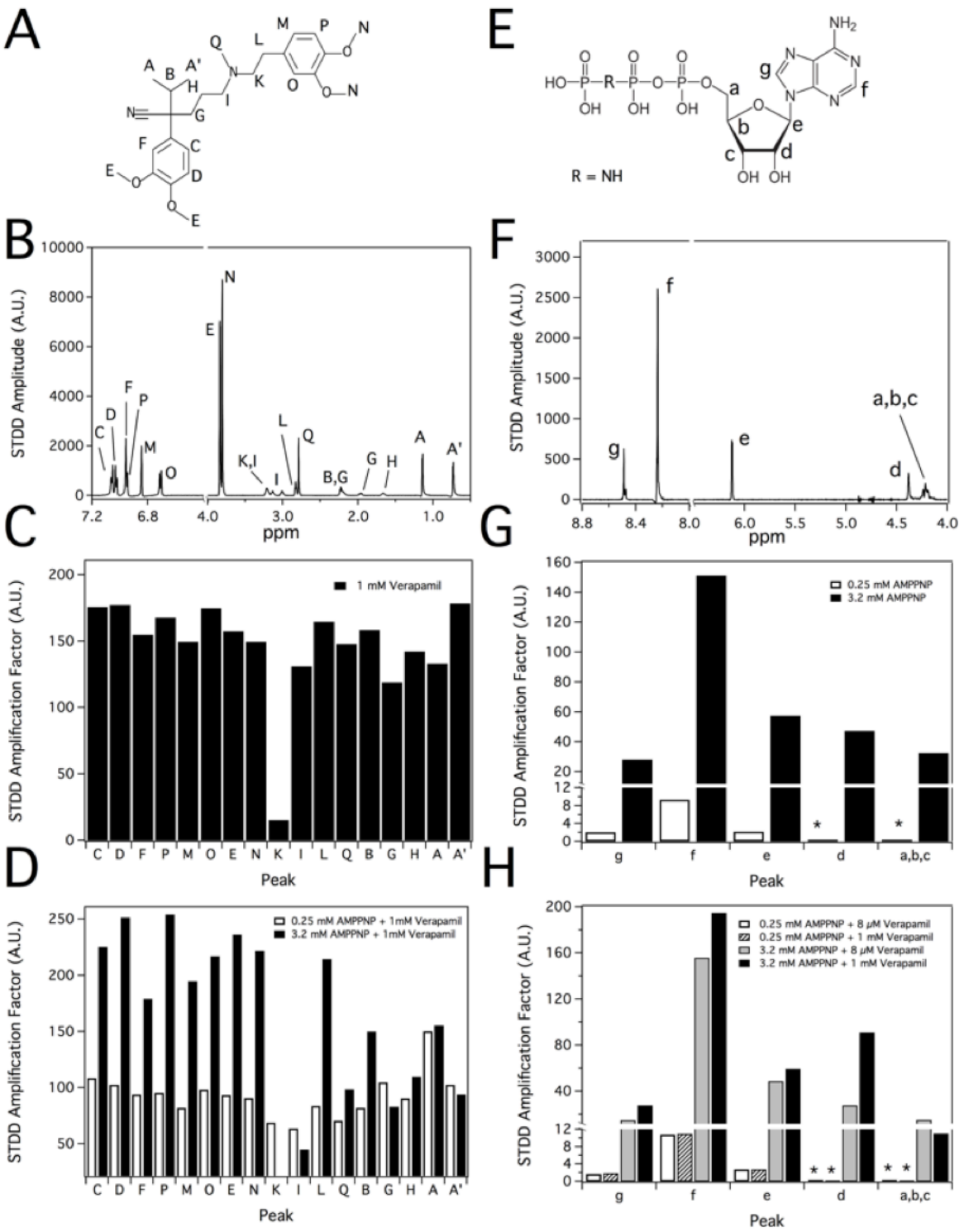

Figure 3.5. Molecular interactions of verapamil and AMPPNP with Pgp probed by saturation transfer double difference (STDD) NMR. Molecular structures of A) verapamil and E) AMPPNP

with the nuclei labeled. A representative ^{1}H STDD NMR spectra with B) 1 mM verapamil and F) 3.2 mM AMPPNP with 1 μM Pgp. The ^{1}H STDD NMR amplification factors for C) 1 mM verapamil in the absence of AMPPNP with 1 μM Pgp. D) The STDD amplification factors for 1 mM verapamil in the presence of 0.25 mM (open columns) and 3.2 mM (solid columns) AMPPNP with 1 μM Pgp. E) Molecular structure of AMPPNP with the nuclei labeled F) A representative ^{1}H proton STDD NMR spectrum of 3.2 mM AMMPNP with 1 μM Pgp. G) The STDD amplification factors of 0.25 mM (open columns) and 3.2 mM (solid columns) with 1 μM Pgp. H) The STDD amplification factors for 0.25 mM AMPPNP in the presence of 8 μM (open columns) and 1 mM verapamil (hashed columns) and 3.2 mM AMPPNP in the presence of 8 μM (gray columns) and 1 mM verapamil (solid columns) with 1 μM Pgp. STDD amplitudes in the figure with an asterisk were too small to be accurately measured.

NMR spectrometer, which allowed us to investigate several weaker verapamil ^{1}H NMR peaks labeled K, I, B, G and H (Figure 3.5 B). In the NMR spectrum, ^{1}H NMR peaks emanating from the dimethoxyphenyl groups are located downfield above 3.5 ppm, while ^{1}H NMR peaks associated with the connecting alkyl chain are found up field below 3.5 ppm. Protons in the dimethoxyphenyl group closest to the tertiary amine group are labeled M, N, O, and P and those farthest from the tertiary amine are labeled C, D, E, and F. The connecting alkyl chain between the dimethoxyphenyl functional groups consists of ^{1}H NMR proton peaks labeled G, H, I, K, L and Q and a propyl group with protons labeled A', A, and B.

Figure 3.5 C shows the Pgp specific ^{1}H STDD amplification factors for 1 mM verapamil in the absence of AMPPNP after subtracting STD NMR contributions from the liposomes. Previously, we showed by STDD NMR that dimethoxyphenyl groups of verapamil were involved in direct interactions with Pgp (Ledwitch, Barnes*, et al.*, 2016). The average STDD amplification factor for the dimethoxyphenyl functional groups of verapamil was 163 ± 12. The relative amplitudes of these STDD amplification factors were similar suggesting that all the protons of this functional group have similar interactions with Pgp. STDD NMR of Pgp and 8 μM verapamil was attempted to probe the high affinity verapamil binding site, but no verapamil ^{1}H STDD NMR peaks were observed because of the low concentration and broadening of the verapamil ^{1}H NMR peaks (data not shown). Therefore, the ^{1}H STDD NMR amplitudes and amplification factors of 1 mM verapamil primarily reflect interaction with the low affinity verapamil binding site of Pgp.

Figure 3.5 D shows the effect of low (open columns) and high (closed columns) concentrations of AMPPNP on the ^{1}H STDD amplification factors of 1 mM verapamil. At low AMPPNP concentration (Figure 3.5 D), the ^{1}H STDD NMR amplification factors of the

dimethoxyphenyl functional group decreased ~43% from the amplification factors in the absence of AMPPNP (cf. Figures 3.5 C and D, open columns). There were also significant changes in ^{1}H STDD amplification factors for the protons labeled A and A'. The ^{1}H STDD amplification factor for the proton labeled A increased 13%, and the ^{1}H STDD amplification factor for the proton labeled A' decreased more than 40%. In the presence of saturating AMPPNP (Figure 3.5 D, closed columns), the ^{1}H STDD amplification factors for the protons labeled A and A' were not significantly different from the amplification factors at low AMPPNP concentration. However, the average STDD amplification factor of the dimethoxyphenyl functional group increased more than 2-fold (Figure 3.5 D, closed columns). There were also large increases in the ^{1}H STDD amplification factors of alkyl protons labeled L and B. These differences in amplification factors between low and high AMPPNP concentration likely reflect differences in AMPPNP occupancy of Pgp. Overall, these AMPPNP-induced changes in the ^{1}H STDD NMR amplification factors of verapamil suggest that nucleotides modulate verapamil interactions when verapamil occupies the low affinity binding site.

Figure 3.5 E shows the molecular structure of AMPPNP with the nuclei labeled, which is comprised of a ribose and a purine functional group. Figure 3.5 F shows the ^{1}H STDD NMR spectrum of 3.2 mM with ^{1}H NMR peaks labeled with significant ^{1}H STDD NMR peaks for ribose and purine ring protons. Protons from the aromatic purine functional group are downfield from 6.0 ppm and are labeled g, f and e. The protons emanating from the ribose are upfield from 6.0 ppm and are labeled a, b, c and d.

Figure 3.5 G shows the ^{1}H STDD NMR amplification factors for 250 μM and 3.2 mM AMPPNP concentration with 1 μM Pgp. At low AMPPNP concentration (open columns), we were not able to reliably estimate ^{1}H STDD NMR amplification factors for the ribose protons

(labeled a–d) because the ^{1}H NMR amplitudes were very weak (data not shown). The ^{1}H STDD NMR amplification factors for the aromatic purine protons were considerably stronger with proton f producing the strongest ^{1}H STDD amplification factor. At high AMPPNP concentration (solid columns), the average STDD amplification factor for AMPPNP was 63 ± 51 (Figure 3.5 D, closed columns). The average STDD amplification factor for the purine base was 79 ± 64 with proton f exhibiting the strongest STDD amplification factor. In contrast, the STDD amplification factors were considerably weaker for the ribose sugar. The average STDD amplification factor for this group was 40 ± 11. These results suggest on average that stronger interactions occur between the purine base and Pgp than the ribose functional group. This is consistent with AMPPNP interactions observed for AMPPNP bound in the X-ray crystal structure of the analogous bacterial transporter SAV1866 (Dawson and Locher, 2007) (PDB ID: 2ONJ). In the bacterial transporter structure, the purine ring of AMPPNP was sequestered by four residues (i.e. V476, K477, Y359 and Y391), while the ribose functional group interacted with a single I356.

In Figure 3.5 H, the STDD amplification factors for 250 μM and 3.2 mM AMPPNP concentration are shown in the presence of 8 μM or 1 mM concentrations of verapamil. Because of the weak ^{1}H NMR amplitudes for ribose at low AMPPNP concentration (open and hashed columns), only ^{1}H STDD NMR amplification factors were measured for the purine base. The relative amplitudes of the amplification factors were similar to the amplification factors of 250 μM AMPPNP shown in Figure 3.5 G (open columns) with the strongest amplification factors emanating from proton f. At high AMPPNP concentration and 8 μM verapamil (gray columns), the average STDD amplification factor decreased 15%. The relative amplitudes of the STDD amplification factors remained relatively unperturbed with respect to the STDD

amplification factors in the absence of verapamil (cf. Figure 3.5 G, closed columns and Figure 3.5 H, gray columns), which is consistent with the lack of verapamil-induced effects on the K_m (Figure 3.1 B) and the K_D (Table 3.1). In the presence of saturating 1 mM verapamil (closed columns), the average ^{1}H STDD amplification factors of AMPPNP increased more than 20%. As observed under other conditions in this study, the purine protons had larger STDD amplification factors on average than the ribose protons. A notable difference in the ^{1}H STDD amplification factors of AMPPNP with saturating 1 mM verapamil is that the AMPPNP ribose proton labeled d was more than double the other STDD amplification factors observed under the other conditions. This implies that the Pgp-bound orientation of the ribose functional group of AMPPNP is perturbed in the presence of 1 mM verapamil and might be a contributing factor to the decreased Pgp-mediated ATP hydrolysis at high verapamil concentrations. Interestingly, of the non-exchangeable protons in AMPPNP, this proton is positioned closest to I356 in the AMPPNP-bound X-ray crystal structure of SAV1866 (PDB ID: 2ONJ) (Dawson and Locher, 2007) that sequesters the ribose.

3.5. DISCUSSION

A conformationally-gated model of cooperativity between verapamil and nucleotides is presented in Figure 3.6. The model is based on our results and the conformational changes that Pgp is known to undergo in the presence of nucleotides and drugs (Dawson and Locher, 2007; T. W. Loo *et al.*, 2003a, 2003b; Verhalen *et al.*, 2012; A. Ward *et al.*, 2007). The model is simply presented by three conformations: “open”, “closed” and “intermediate” as described previously (Ledwitch, Barnes*, et al.*, 2016). In reality, the model represents a structural ensemble of Pgp conformations. When the nucleotide binding domains (NBDs) are relatively far apart, Pgp is in

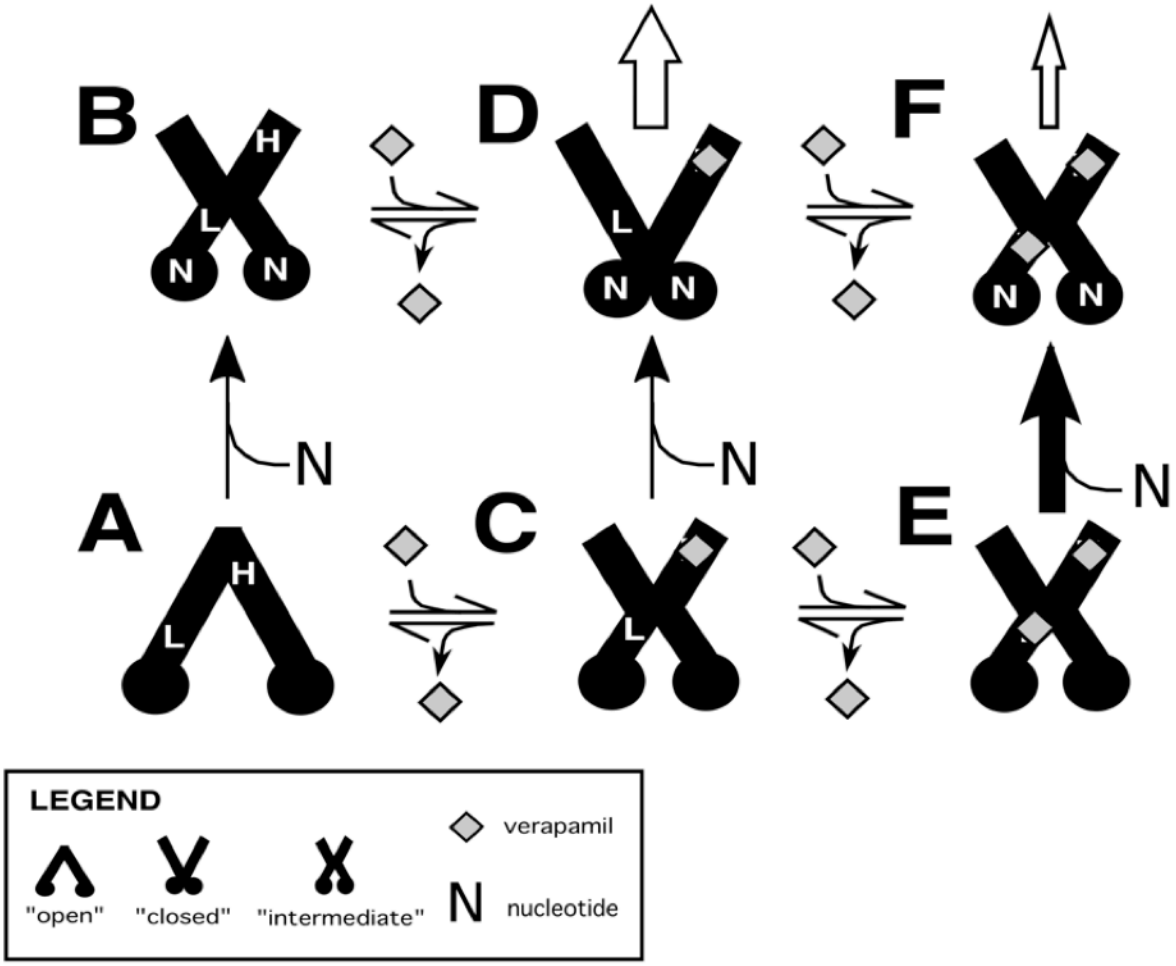

Figure 3.6. Model of drug-nucleotide cooperativity for verapamil-induced activation of Pgp-mediated ATP hydrolysis. The figure shows cartoons of Pgp in the "open", "closed" and "intermediate" conformations in the A,C,E) absence and B,D,F) presence of ATP, and in the presence of C,D) one and E,F) two verapamil molecules. Verapamil molecules are shown as gray diamonds and N represents ATP. The proposed high and low affinity verapamil binding sites of Pgp are shown as H and L, respectively. The horizontal arrows reflect equilibria between the verapamil-bound conformational states of Pgp. The middle vertical arrows reflect the degree of ATP binding to Pgp, while the arrows at the top of the figure and their size represent the degree of verapamil transport.

the “open” conformation where the cytosolic side is exposed to the bulk solvent. When the NBDs come together, Pgp is in the “closed” conformation and the extracellular side is exposed to the bulk solvent. Instances where the extracellular and cytosolic sides are equally exposed to bulk solvent is the “intermediate” Pgp conformation, which is in-between the “open” and “closed” states.

Ligand-induced changes in tryptophan accessibility deduced from the acrylamide quenching experiments of Pgp with verapamil and the non-hydrolyzable ATP analog AMPPNP in Fig. 4 suggest that their interactions significantly affect the tertiary conformation of Pgp. Ligand-induced decreases in K_{SV} values of Pgp reflect decreases in tryptophan accessibility and imply shifts toward a “closed” Pgp conformation. The similarity of K_{SV} values of Pgp in the presence of low and high verapamil concentration suggests that the verapamil-bound conformations are similar. This information should be used cautiously to assign a specific drug- or nucleotide-bound Pgp conformations, since the fluorescence quenching studies were done with a non-hydrolyzable ATP analog rather than ATP. Therefore, the conformational assignment was additionally weighted on the rates of Pgp-mediated ATP hydrolysis. Our rationale was based on the fact that cross-linking studies with Pgp, site-directed mutagenesis of Pgp, cryo-electron microscopy studies with Pgp and structural studies with bacterial transporters with nucleotide analogs have shown that the interaction of the Pgp nucleotide domains with each other is essential for ATP hydrolysis (Beaudet and Gros, 1995; Frank *et al.*, 2016; Hrycyna *et al.*, 1999; Lawson *et al.*, 2008; T. W. Loo *et al.*, 2012; Urbatsch *et al.*, 1995). In our model, the average distance between the Pgp NBDs was correlated to the ATP hydrolysis rate. For example, Pgp that has relatively high and low ATP hydrolysis rates is assumed to be in “closed” and “open” conformations, respectively. The ligand-induced changes in tryptophan accessibility of Pgp

deduced from acrylamide quenching of tryptophan fluorescence were used to gauge the degree of conformational shift.

The locations of the verapamil binding sites on Pgp have not yet been resolved. Verapamil ATP hydrolysis kinetics is biphasic, which suggests a high and low affinity verapamil-binding site on Pgp as previously reported (Ledwitch, Barnes*, et al.*, 2016) and shown in Figure 3.1 and Figure 3.2. Several studies of residues within the extracellular side of Pgp (Hafkemeyer *et al.*, 1998; T. W. Loo *et al.*, 2003b; T. W. Loo and Clarke, 1996; Welker *et al.*, 1995) and G185 (G181 for Pgp in this study) within the transmembrane region of Pgp (Omote *et al.*, 2004; Ramachandra *et al.*, 1996; Rao, 1995) had significant effects on verapamil-induced ATPase kinetics and Pgp-mediated transport of verapamil. Several mutations of residues on the extracellular side of Pgp caused marked decreases in transport of a fluorescent verapamil analog (Hafkemeyer *et al.*, 1998). Dramatic decreases in the K_m for ATPase activation of Pgp by verapamil were observed when residues between 78 and 97 were deleted (Welker *et al.*, 1995). Labeling an I306C mutant, which is located on the extracellular side of Pgp, with a thiol-reactive verapamil analog lead to permanent verapamil-induced activation of Pgp (T. W. Loo *et al.*, 2003b). Verapamil also inhibited crosslinking between residues C332 and C975 within the extracellular side of Pgp (T. W. Loo and Clarke, 1996). Mutating the G181 residue to valine within the transmembrane region of Pgp had strong effects on the V_{MAX} of verapamil-induced ATPase activation (Omote *et al.*, 2004; Ramachandra *et al.*, 1996; Rao, 1995). The G181V mutation had little effect on the K_m of verapamil-induced ATPase activation (Omote *et al.*, 2004; Ramachandra *et al.*, 1996), but a recent study showed that it had significant effects on the K_i for substrate inhibition of Pgp (Omote *et al.*, 2004). By affecting the K_i from substrate inhibition and not the K_m implies that G181 is near an alternate verapamil-binding site. Therefore, we placed

the low-affinity (L) verapamil-binding site near G181 in the transmembrane region of Pgp and the high-affinity (H) verapamil-binding site near the extracellular side of Pgp.

The conformation of Pgp in the absence of ligands is known from the X-ray crystal structure to be in the "open" conformation (Aller *et al.*, 2009) as shown in Figure 3.6 A. Acrylamide quenching experiments in Figure 3.4 showed that nucleotides reduced tryptophan accessibility of Pgp implying a shift toward the "closed" conformation. However, the V_{MAX} deduced from fitting the Pgp-coupled ATPase activation kinetics was inefficient at 500–700 nmol min^{-1} mg^{-1}. Therefore, we propose that ATP shifts Pgp to an "intermediate" conformation in Figure 3.6 B, which keeps the NBDs apart and presents an energetic barrier for ATP hydrolysis.

At low verapamil concentrations, the drug binds near the extracellular side of Pgp in our model (Figure 3.6 C and D) at the H-site. Because the rate of Pgp-mediated ATP hydrolysis was very high at ~3000 nmol min^{-1} mg^{-1}, we propose that verapamil-bound Pgp is in the "closed" conformation in the presence of ATP in Figure 3.6 D. In the absence of nucleotides, the acrylamide quenching experiments in Figure 3.4 suggested that low concentrations of verapamil induce significant changes in the tertiary conformation of Pgp. There were also significant differences in tryptophan accessibility in the absence (Figure 3.4 B) and presence (Figure 3.4 E and H) of AMPPNP at low verapamil concentration suggesting that they are in very distinct conformations. Therefore, we propose that verapamil bound at the H-site of Pgp, but in the absence of ATP, is in an "intermediate" conformation. By shifting to an "intermediate" conformation, the verapamil molecule reduces the energetic barrier for the NBDs to come together and the subsequent Pgp-mediated ATP hydrolysis and transport that follows. By reducing the ATP energetic barrier for hydrolysis, this single bound verapamil molecule is

positively cooperative with respect to ATP hydrolysis. With respect to binding, verapamil and ATP are essentially not cooperative as deduced by fitting of the verapamil-induced ATPase activation kinetics in Figures 3.1 and 3.2. The lack of binding cooperativity is consistent with the H-site being far from the NBDs.

At saturating verapamil concentrations, the drug will bind near the L-site that we hypothesize lies within the transmembrane region near G185 (G181 for the Pgp in this study). The activation of Pgp-mediated ATP hydrolysis decreased to about ~700 nmol min^{-1} mg^{-1}, which was a little bit higher than basal ATPase activity. As deduced from the slopes of the Stern-Volmer plots in Figures 3.4 B and C, tryptophan accessibility of Pgp in the absence of an ATP analog was just slightly higher at saturating verapamil concentration than low verapamil concentration implying that they have relatively similar conformations. Therefore, Pgp is shown in an "intermediate" conformation in the absence of ATP at low and saturating verapamil concentrations (Figures 3.6 C and E). Fitting of the ATP hydrolysis kinetics in Figure 3.2 revealed that the ATP affinity to Pgp increased 4-fold in the presence of saturating verapamil and that ATP and verapamil binding to Pgp is positively cooperative at saturating verapamil concentrations. Also, addition of an ATP analog only induced a relatively small decrease in tryptophan accessibility in the presence of saturating verapamil (cf. Figures 3.4 C and I) implying that Pgp's tertiary conformation was not significantly shifted by the ATP analog, when compared to the nucleotide-induced conformational change of Pgp in the presence of low concentrations of verapamil (cf. Figures 3.4 B and I). Therefore, we hypothesize that binding cooperativity between verapamil and ATP stabilizes Pgp in an "intermediate" conformation shown in Figures 3.6 E and F. With the NBDs relatively separated in the "intermediate" conformation compared to the "closed" conformation explains why ATP hydrolysis is lower at

high verapamil concentration and is similar to the basal ATP hydrolysis rate. In other words, two Pgp-bound verapamil molecules are negatively cooperative with respect to ATP hydrolysis.

In Figures 3.6 D and F of the model, verapamil transport rates are shown to correlate to verapamil occupancy of Pgp and verapamil-stimulated ATP hydrolysis rates. This relationship is supported by a study with spin-labeled verapamil and Pgp that found similar K_m and K_i values for verapamil transport and verapamil-stimulated ATPase activity (Omote and Al-Shawi, 2002). This correlation is also supported by several independent studies that have shown that Pgp-mediated transport of verapamil (Elsby *et al.*, 2008; Faassen *et al.*, 2003; Pauli-Magnus *et al.*, 2000; Schwab *et al.*, 2003) and verapamil-simulated ATP hydrolysis decreased at higher verapamil concentrations (Aanismaa and Seelig, 2007; Borgnia *et al.*, 1996; Ledwitch, Barnes*, et al.*, 2016; Litman, Nielsen*, et al.*, 1997).

In summary, Figure 3.6 shows a model for Pgp-mediated verapamil transport involving conformational changes and cooperativity between verapamil and ATP. In the absence of verapamil, Pgp is in an "open" conformation (Figure 3.6 A), and is shifted to an "intermediate" conformation by ATP (Figure 3.6 B). In this conformation, the ATPase activity will be low because the separation in NBDs represents an energetic barrier for ATP hydrolysis. At low concentrations, verapamil will occupy the H-site on Pgp and will shift the transporter into an "intermediate" conformation in Figure 3.6 C. Since the H-site is within the extracellular domain far from the NBDs, verapamil occupancy at the H-site will not significantly affect the binding affinity of ATP. In other words, verapamil and ATP are not cooperative with respect to binding. However, because Pgp is in an "intermediate" rather than an "open" conformation, verapamil reduces the energetic barrier for ATP hydrolysis and transport (Figure 3.6 D). Therefore, verapamil occupancy at the H-site is positively cooperative with respect to ATP hydrolysis and

transport. At high concentrations, verapamil will occupy both the H and L sites on Pgp as shown in Figure 3.6 E. Occupancy at both sites of Pgp also shifts Pgp into an "intermediate" conformation. In contrast with the H-site, the L-site on Pgp is located within the transmembrane region closer to the NBDs. Verapamil binding to the L-site increases the affinity of ATP to the NBDs. In this case, verapamil and ATP are positively cooperative with respect to binding to Pgp. Occupancy of verapamil at both sites stabilizes the "intermediate" Pgp conformation and prevents ATP from driving Pgp to the "closed" conformation in Figure 3.6 F. This reduces verapamil transport and verapamil-stimulated ATP hydrolysis by Pgp. In this case, verapamil occupancy at both sites on Pgp is negatively cooperative with respect to ATP hydrolysis and transport.

CHAPTER 4

NMR-DERIVED MODEL OF DIGOXIN BOUND TO P-GLYCOPROTEIN

4.1. OVERVIEW

The P-glycoprotein (Pgp) transporter is a membrane-bound protein that acts as a "gatekeeper" to several physiological barriers to drive drug translocation across the cell membrane from the cytosol to the extracellular space. This mechanism is particularly intriguing from the clinical perspective because of Pgp's ability to confer multidrug resistance in cancer cells, to mediate drug-drug interactions (DDIs) and to influence drug disposition. One of the hallmarks of Pgp function is its drug promiscuity. With the Pgp substrate recognition count encompassing a significant portion of clinically relevant drugs, identifying key molecular features of drug substrates and their corresponding binding site(s) on the transporter is essential for developing ways to modulate Pgp function. One drug that has been extensively studied with the Pgp transporter due to its central involvement in Pgp-mediated DDIs is the cardiac glycoside digoxin. Despite numerous *in vitro* and *in vivo* studies with digoxin and Pgp, the location of the digoxin-binding site on Pgp and its corresponding molecular interactions are unknown. To pinpoint the digoxin binding site on the Pgp transporter, paramagnetic relaxation enhancement (PRE) NMR was used to determine the distance between paramagnetically-labelled cysteine residues on Pgp and the binding site of digoxin. These distances were used as experimental restraints for docking digoxin to the X-ray crystal structure of Pgp with the High Ambiguity Driven DOCKing (HADDOCK) software and the Crystallography & NMR System (CNS).

Molecular docking using HADDOCK revealed a digoxin-binding site near residue G181 on Pgp. Tryptophan fluorescence was used to determine digoxin's drug binding affinity and the conformational changes induced by digoxin with Pgp. This work represents the first NMR-derived model of a Pgp-drug complex.

4.2. INTRODUCTION

The ATP-binding cassette (ABC) superfamily comprise a group of molecular "efflux" pumps that use energy from ATP hydrolysis to drive drug export across cell membranes back to the extracellular space (Sharom, 2011). The ABC transporter P-glycoprotein (ABCB1, Pgp) is a key component to many physiological barriers. Pgp is localized to tissues such as the liver, intestines, kidneys and the blood-brain and placental barrier where it plays a significant role in mediating drug disposition, drug pharmacokinetics and drug bioavailability (Aszalos, 2007; International Transporter *et al.*, 2010). The Pgp transporter is widely recognized for its ability to bind chemically and functionally diverse substrates (Callaghan, 2015; S. F. Zhou, 2008). This drug promiscuity poses challenges in the clinic because Pgp confers multidrug resistance (MDR) in cancer cells and mediates drug-drug interactions (DDIs) (Boumendjel *et al.*, 2009; Sharom, 2008). Both Pgp-mediated mechanisms have significant clinical consequences that lead to patients developing resistance to anticancer therapies or lead to undesired adverse drug reactions (ADRs) that often result in patient death (Owens, 2005). There is biochemical and structural information available on the Pgp transporter, but the promiscuous nature of Pgp still remains enigmatic.

Most of our structural understanding of Pgp is based on the X-ray crystal structure of the analogous mouse Pgp transporter (87% sequence identity and 95% sequence similarity to human

Pgp) and Pgp structures from *Caenorhabditis (C.) elegans* and bacterial transporters (MsbA, SAV1866) (Aller *et al.*, 2009; Dawson and Locher, 2007; Esser *et al.*, 2017; Jin *et al.*, 2012; J. Li *et al.*, 2014). The X-ray crystal structures of the 140 kD (170 kD when glycosylated) mouse Pgp transporter revealed a 6000 $Å^3$ binding cavity within the lipid bilayer framed by two pseudosymmetric halves each consisting of one transmembrane domain (TMD) and one nucleotide binding domain (NBD) (Aller *et al.*, 2009; J. Li *et al.*, 2014). Each TMD consists of 6 transmembrane helices (TMHs) that connect to one of the NBDs, which have significant homology and feature the conserved Walker A, Walker B and signature amino acid sequence motifs (Suresh V. Ambudkar *et al.*, 2006; S. V. Ambudkar *et al.*, 2006). In all the X-ray crystal structures that have been solved to date, the NBDs are separated by ~ 35-45 Å, which has been designated the "open" conformation due to the exposure of residues within the transmembrane region of the transporter (Aller *et al.*, 2009; Esser *et al.*, 2017; J. Li *et al.*, 2014). Both domains can bind and hydrolyze ATP, which triggers a series of conformational changes that promote drug binding and transport. Most recently, a 3.3 Å crystal structure of mouse Pgp with a mutated linker region showed ATP bound to one of the NBDs in an asymmetric fashion and, in the absence of drug, prefers one NBD over the other (Esser *et al.*, 2017). This suggests that despite the homology between both NBDs, ATP binds each NBD in a distinct manner with different affinities (Esser *et al.*, 2017).

Pgp structures have been co-crystalized with the cyclic peptide inhibitors, a marine pollutant and a mouse Pgp nanobody (Aller *et al.*, 2009; J. Li *et al.*, 2014; A. B. Ward *et al.*, 2013). The X-ray crystal structures with the non-therapeutic peptide inhibitors showed that there were distinct drug binding sites within the internal cavity and that these sites were stereoselective (Aller *et al.*, 2009; J. Li *et al.*, 2014). A marine pollutant co-crystalized with mouse Pgp also

bound within the internal cavity and 11 out of the 15 interacting residues were distinct from the interactions observed with the peptide inhibitors (Nicklisch *et al.*, 2016). The nanobody NB592 co-crystalized with mouse Pgp showed a specificity for NBD1 and revealed a unique epitope on NBD1 despite the high sequence similarity to NBD2 (A. B. Ward *et al.*, 2013). Although these structures have given insight into the structural features of Pgp in complex with inhibitors, we still lack information on distinct drug-bound locations and the structural properties governing drug interactions with Pgp (Callaghan, 2015). Continuous effort towards understanding the structural basis of drug binding and multi-drug recognition by Pgp is essential for the rational design of drugs and Pgp inhibitors and for better predictions of safe multidrug regimens that bypass Pgp-mediated DDIs in the clinic.

Pgp-mediated ADRs are often observed from DDIs observed with cardiovascular ion channel inhibitors because of their relatively low therapeutic indices (Niayesh Mohebbi *et al.*, 2010; Mowry *et al.*, 2015). Pgp-mediated DDIs associated with cardiovascular drugs represents a major roadblock to effective treatment because many cardiovascular drugs are Pgp substrates, inhibitors and in some cases, inducers of the Pgp transporter (Wessler *et al.*, 2013). As a result of the low therapeutic indices of cardiovascular ion channel inhibitors, small increases in drug exposure can significantly increase the potential for drug toxicity (Ledwitch and Roberts, 2016; Wessler *et al.*, 2013). One of the most studied Pgp substrates is the cardiac glycoside digoxin. Digoxin is an ion channel inhibitor widely administered to treat atrial fibrillation (Hauptman and Kelly, 1999; Ziff and Kotecha, 2016) and has been involved in many preventable DDIs (Karimzadeh *et al.*, 2011). This cardiovascular drug has been the central focus of many *in vitro* and *in vivo* studies because it is transported by Pgp and has been involved in Pgp-mediated DDIs

that result in digoxin toxicity (Cavet *et al.*, 1996; Fenner *et al.*, 2009; Gozalpour *et al.*, 2016; Pauli-Magnus *et al.*, 2001; Schwartz, 1988).

In a recent study by our group with Pgp reconstituted in liposomes, we showed that verapamil has low-affinity binding site that competitively displaces digoxin (Ledwitch, Barnes*, et al.*, 2016). Another study showed that a G185V mutation in human Pgp affects the low affinity site of verapamil, but not the high affinity site (Omote *et al.*, 2004). More recently, it was shown that digoxin was a transported substrate by Pgp in a conditionally immortalized proximal tubule epithelial cells (ciPTEC) but not in a Madine Darby Canine Kidney (MDCK)-Pgp cell line (Gozalpour *et al.*, 2016). This loss of digoxin transport in the MDCK-Pgp cell line was due to a G181V point mutation in mouse Pgp (Gozalpour *et al.*, 2016). Therefore, we hypothesized that digoxin's binding site was near this glycine (Ledwitch, Barnes*, et al.*, 2016).

Currently, the distinct location of the digoxin drug binding site and the corresponding molecular interactions between digoxin and Pgp are unknown. To test the hypothesis that digoxin binds near a specific glycine, we determined its location on the Pgp transporter by NMR. To build an accurate digoxin-Pgp model, we probed digoxin's interactions with the transporter and determined the effects of digoxin on Pgp conformation. Quenching of intrinsic Pgp tryptophan fluorescence was used to determine digoxin's affinity to the transporter. Acrylamide quenching was used to investigate Pgp's conformation in the presence of digoxin. Paramagnetic relaxation enhancement (PRE) NMR with paramagnetically-labeled single cysteine mutants was used to determine digoxin's relative distance from the labels. These NMR-derived distances were used as experimental restraints to drive the docking of digoxin to Pgp using High Ambiguity Driven DOCKing protocols with the Crystallography & NMR System (HADDOCK/CNS). This digoxin-Pgp bound complex deduced by NMR is the first experimentally-derived model

demonstrating the location of a drug on the transporter. This drug-bound complex and the conformational changes deduced by acrylamide quenching were used to build a model of digoxin transport by Pgp.

4.3. MATERIALS AND METHODS

4.3.1. Materials

Digoxin was purchased from Alfa Aesar (Tewksbury, MA) and colchicine was purchased from Acros Organics (Pittsburgh, PA). The detergent *n*-dodecyl-*β*-*D*-maltoside (DDM), which is used in protein purification, was purchased from EMD Millipore Corporation (San Diego, CA). *Escherichia coli* (*E. Coli*) total lipid extract powder was purchased from Avanti Polar Lipids Inc. (Alabaster, AL) and cholesterol was purchased from Amresco (Solon, OH) for liposome preparations. Disodium ATP (Na_2ATP) was purchased from Amresco (Solon, OH) and sodium orthovanadate (Na_3VO_4) was purchased from Enzo Life Sciences (Farmingdale, NY) for the ATPase activity assays. Acrylamide was purchased from Calbiochem (San Diego, CA) for the acrylamide quenching experiments. $MnCl_2$ (99.999%) and $CaCl_2$ hydrate (99.999%) were purchased from Sigma Aldrich (Milwaukee, WI). The N-[S-(2-pyridyldithio)cysteinyl]ethylenediamine-N,N,N',N'-tetraacetic acid monamine (EDTA) used for labeling single cysteine-Pgp mutants with the Mn^{2+} or Ca^{2+} ion was purchased from Toronto Research Chemicals (Toronto, ON, Canada). Deuterium oxide (D_2O) and deuterated (d_{11})-Tris was purchased from Cambridge Isotope Laboratories (Tewksbury, MA) and deuterated (d_{10}) dithiothreitol (DTT) was purchased from CDN Isotopes (Quebec, Canada) for NMR experiments. 600 MHz NMR tubes for all NMR studies were purchased from Wilmad-LabGlass (Vineland, NJ). DTT was purchased from Gold Biotechnology (St. Louis, MO). HEPES was

purchased from Calbiochem (San Diego, CA). Tris-HCl was purchased from Amresco (Solon, OH). $MgCl_2$ and NaCl were purchased from J.T Baker (Center Valley, PA). NH_4Cl was purchased from Sigma Aldrich (Milwaukee, WI). $MgSO_4$ and NaN_3 were both purchased from Thermo Fisher Scientific (Waltham, MA).

4.3.2. Single cysteine mutant constructs

The single cysteine Pgp mutant was provided by Dr. Ina L. Urbatsch of Texas Tech University. Briefly, the site-specific cysteine residue C1070 was introduced in cysteine-free mouse Pgp where all nine natural cysteine residues were converted to alanine as previously described (Tombline *et al.*, 2006). The C1070 mutant was expressed in *Pichia* (*P.*) *pastoris* as previously described (Lerner-Marmarosh *et al.*, 1999).

4.3.3. Pgp purification and reconstitution

The wild-type (wt) his-tagged mouse Pgp transporter (mdr1a, ABCB1) and both single cysteine mutants were purified from *P. pastoris* with the detergent *n*-dodecyl-*β*-*D*-maltoside (DDM) as described previously (Bai *et al.*, 2011; Lerner-Marmarosh *et al.*, 1999). For the specific ATPase activity assays, wt Pgp and Pgp mutants were reconstituted into liposomes as described previously (Bai *et al.*, 2011; Ledwitch, Gibbs*, et al.*, 2016). Briefly, the liposomes used for Pgp reconstitution were composed of 80% w/v Avanti *Escherichia* (*E.*) *coli* Total Lipid Extract and 20% w/v cholesterol. The final lipid to protein ratio for all preparations was 0.16 mg ml^{-1} liposomes per μM^{-1} of Pgp. These proteoliposomes were stored in aliquots at -80^{o}C in HEPES buffer (20 mM HEPES, 100 mM NaCl, 5 mM $MgCl_2$, 2 mM DTT, pH 7.4). The

concentration of Pgp was determined using the extinction coefficient of 1.28 ml mg^{-1} cm^{-1} (0.181 μM^{-1} cm^{-1}) (Bai *et al.*, 2011) or the DC Protein Assay Kit II (Bio-Rad, Hercules, CA).

4.3.4. Measurement of Colchicine and Digoxin-Stimulated ATPase Activity

The specific ATPase activity of wt Pgp was measured using the Chifflet colorimetric assay as described previously (Chifflet *et al.*, 1988). The rate of colchicine or digoxin-stimulated ATP hydrolysis was determined by measuring the amount of free inorganic phosphate (P_i) generated in the presence of 3.2 mM ATP. The P_i generated in the reaction conjugates with ammonium molybdate, and this *Pi*-molybdenum complex produces a strong absorbance signal at 850 nm. The absorbance was measured in a 96-well plate on a FlexStation 3 spectrometer (Molecular Devices, Sunnyvale, CA). The ATPase activity with colchicine, digoxin and ATP was measured with 50 nM Pgp reconstituted in liposomes in Chifflet buffer (150 mM NH_4Cl, 5 mM $MgSO_4$, 0.02% w/v NaN_3, 50 mM Tris-HCl, 2 mM DTT, pH 7.4). All kinetic curves were monophasic and the Michaelis-Menten constant (K_m) was estimated with the modified Michaelis-Menten equation (equation 1):

$$v = \frac{V_{MAX}\,[L]}{K_m + [L]} + v_{basal} \qquad (1)$$

where v is the ATP hydrolysis rate, V_{MAX} is the maximum ATP hydrolysis rate, [L] is the concentration of drug and v_{basal} is the basal activity in the absence of drug.

4.3.5. Fluorescence Spectroscopy

Fluorescent quenching of intrinsic Pgp tryptophan residues has been widely used to characterize drug binding affinities and drug-induced conformational changes of Pgp (Liu *et al.*, 2000; Sharom *et al.*, 2003; Sonveaux *et al.*, 1999). To determine the binding affinity of digoxin

to Pgp, digoxin-induced quenching of detergent solubilized Pgp was investigated on an Olis DM 45 spectrofluorimeter (Olis Corp, Bogart, GA). The acrylamide quenching of tryptophan fluorescence was used to probe the digoxin-induced Pgp conformation for wt and all single cysteine Pgp mutants. All fluorescence samples contained 1 μM detergent solubilized Pgp or Pgp mutant in Chifflet buffer with 0.01% DDM (pH 7.4). Fluorescence emission was measured at 333 nm following excitation at 295 nm. Fluorescence (*F*) in the presence of digoxin and acrylamide were corrected for background fluorescence, dilution and inner filter effects as described previously with the following equation (Lakowicz, 1999; Ledwitch, Gibbs*, et al.*, 2016):

$$F_{corrected} = (F - B)10^{\frac{(\varepsilon_{ex} b_{ex} + \varepsilon_{em} b_{em})[Q]}{2}} \qquad (2)$$

where *F* is the measured protein fluorescence, *B* is the background and *[Q]* is the quenching ligand concentration. The extinction coefficients (ε) for excitation and emission are ε_{ex} and ε_{em}, respectively. Digoxin is transparent above 250 nm, so interference from digoxin absorbance was not an issue for these experiments. The pathlength (*b*) along the excitation and emission axes are b_{ex} and b_{em}, respectively. Fluorescent quenching relating to a drug's complexation with a protein is known as static quenching, and quenching related to random drug collisions with the protein is known as dynamic quenching (Lakowicz, 1999). The fluorescence quenching curves were fit to the following equation regardless of the nature of quenching (Lakowicz, 1999):

$$F_{corrected} = \frac{F_{0,L}}{1 + K_L[Q]} + \frac{F_{0,H}}{1 + K_H[Q]} + F_{unquenched} \qquad (3)$$

where $F_{corrected,0}$ is the protein fluorescence in the absence of a quenching ligand, $F_{0,L}$ and $F_{0,H}$ are the fluorescence amplitudes and K_H and K_L are the apparent equilibrium constants at low and high concentrations, respectively. The *K* value either represents the association constant (K_A) relating to a static quenching process or the Stern-Volmer quenching constant (K_{SV}) relating to a

dynamic quenching process. These two quenching mechanisms were differentiated by performing the fluorescence titration experiments at two different temperatures as described previously (Ledwitch, Gibbs*, et al.*, 2016). To determine the Stern-Volmer quenching constants, $F_{corrected,0}/F_{corrected}$ was plotted as a function of the acrylamide concentration. The degree of dynamic tryptophan quenching was estimated from the slopes of the Stern-Volmer curves and is related to the K_{SV} by the following equation (Lakowicz, 1999):

$$\frac{F_{corrected,0}}{F_{corrected}} = 1 + K_{SV}[Q] \qquad (4)$$

4.3.6. Paramagnetic Relaxation Enhancement (PRE) NMR

PRE is a powerful tool used to sample long-range distances up to ~50 Å in biological systems by NMR (Clore, 2015). This technique was used to determine the location of the digoxin binding site by covalently attaching a thiol-specific disulfide paramagnetic label to a single cysteine Pgp mutant. This allowed us to determine the distance-dependent longitudinal (R_1) and transverse (R_2) relaxation rates (Clore, 2015; Clore and Iwahara, 2009; Gueron, 1975). The relaxation rates and the T_1 relaxation times were measured using an inversion recovery sequence with a composite 180° pulse and WATER suppression with GrAdient tailored excitation (WATERGATE) to remove the background water resonance from the ^{1}H NMR spectra (Cameron *et al.*, 2007; Kowalewski and Maler, 2006; Martial Piotto *et al.*, 1992). The ^{1}H- T_2 relaxation rates were measured using a spin echo experiment with a Carr-Purcell-Meiboom-Gill (CMPG) pulse sequence with a relaxation delay of 10s as described in (Carr and Purcell, 1954; Junji Iwahara *et al.*, 2007; Meiboom and Gill, 1958).

EDTA (N-[S-(2-pyridyldithio)cysteinyl]ethylenediamine-N,N,N',N'-tetraacetic acid monamine) was incubated with either the paramagnetic Mn^{2+} or diamagnetic Ca^{2+} metal ion at a

1:1.1 ratio. Prior to attaching the labels, all protein preparations were incubated with an excess of $CaCl_2$ hydrate to displace any paramagnetic metals. The protein was extensively washed by ultrafiltration with a high ionic strength buffer (20 mM Tris-HCl and 0.5 M NaCl, pH 6.8) to remove any trace metal ion containments. Then, a 10-fold molar excess of the paramagnetic or diamagnetic label was incubated with Pgp overnight at 4°C. Excess label was removed by extensively washing the EDTA-metal Pgp complex with 20 mM Tris-HCl and 20 mM NaCl, pH 6.8. Tris-HCl buffers at pH 6.8 were used to prevent metal precipitation. All final samples were made in buffer containing 20 mM Tris-HCl and 20 mM NaCl (80% D_2O to 20% H_2O, pD 7.4) with a protein to digoxin ratio of 1:60.

4.3.7. NMR Analysis

All NMR experiments were performed on a 600 MHz Varian INOVA spectrometer at 25^{o}C equipped with a 5 mm z-gradient $^{1}H\{^{13}C/^{15}N\}$ cryoprobe. The ^{1}H NMR peaks for digoxin were assigned using standard ^{1}H 1D and 2D NMR techniques. The molecular structure of digoxin with the nuclei labeled and ^{1}H NMR peak assignments for digoxin are shown in Fig. 4A and 4B, respectively, and were essentially identical to previous ^{1}H NMR assignments (Aulabaugh *et al.*, 1992). All NMR spectra were processed using the iNMR software package (http://www.inmr.net) and analyzed using Igor Pro 6.2 (Wavemetrics, Tigard, OR).

4.3.8. Distance calculations

The apparent paramagnetic relaxation rate (R_p) is calculated by taking the difference between the diamagnetic relaxation rate (R_{Ca}^{2+}) and the paramagnetic relaxation rate (R_{Mn}^{+2}) and can be represented by the equation $R_p = R_{Ca}^{2+} - R_{Mn}^{2+}$, where R_p represents paramagnetic

relaxation from longitudinal ($R_{p,1}$) or transverse ($R_{p,2}$) relaxation (Clore and Iwahara, 2009). To calculate the $R_{p,1}$ relaxation rate, the $R_{p,1}$ relaxation curves were fit with the following modified inversion recovery equation (Arthur G. Roberts *et al.*, 2011):

$$M_z(t) = M_{Z,eq}(1 - 2fe^{\frac{-t}{T_1}}) \qquad (5)$$

where M_z is the z component of nuclear spin magnetization, $M_{Z,eq}$ is the M_z at thermal equilibrium, T_1 is the spin-lattice decay constant, t is the time and f is used to adjust small errors in the inversion recovery pulse. The $R_{p,1}$ relaxation rate is related to the distance by the Solomon-Bloembergen equation:

$$R_{p,1} = \alpha \frac{2}{15}\left(\frac{\mu_0}{4\pi}\right)\frac{\Upsilon_N^2 g_e^2 \mu_B^2 S(S+1)}{r_{app}^6}\left[\frac{\tau_C}{1+(\omega_N-\omega_E)^2\tau_C^2} + \frac{3\tau_C}{1+\omega_N^2\tau_C^2} + \frac{6\tau_C}{1+(\omega_N+\omega_E)^2\tau_C^2}\right] \qquad (6)$$

where μ_0 is the magnetic permeability of free space, γ_N is the nuclear gyromagnetic ratio, g_e is the electronic g-factor, μ_B is the Bohr magneton, r_{app} is the apparent time-averaged electron-nuclear distance, τ_C is the correlation time, S is the electron spin quantum number and ω_N and ω_E are the radial frequencies of the nucleus and electron, respectively. To account for the effects of internal motion emerging from the linker (EDTA) connecting the paramagnetic metal to Pgp, the S^2order parameter was calculated using the following equation:

$$S^2 = \frac{4\pi}{5}\langle r^{-6}\rangle^{-1} \sum_{m=-2}^{2}\left|\langle\frac{\Upsilon_2^m(\Omega^{mol})}{r^3}\rangle\right| 2 \qquad (7)$$

where $\Upsilon_2^m(\Omega)$ are second order spherical harmonics and Ω^{mol} are Euler angles in the molecular frame (Clore and Iwahara, 2009; Lipari and Szabo, 1981). The paramagnetic relaxation rate ($R'_{p,1}$) that accounts for internal motion of the label is calculated using the following modified Solomon-Bloembergen equation:

$$R'_{p,1} = S^2 R_{p,1}(\tau_s, \tau_R) + (1 - S^2)R_{p,1}(\tau_s, \tau_R, \tau_i) \qquad (8)$$

where τ_s is spin relaxation time, τ_R is rotational correlation time and τ_i is internal motion.

To calculate the $R_{p,2}$ relaxation rates and associated errors, the $R_{p,2}$ relaxation rates were determined using the two-time point approach for transverse relaxation as described in (Junji Iwahara *et al.*, 2007) using the following equations:

$$R_{p,2} = R_{Ca^{2+}} - R_{Mn^{2+}} = \frac{1}{T_b - T_a} ln \frac{I_{Ca^{2+}}(T_b) I_{Mn^{2+}}(T_a)}{I_{Ca^{2+}}(T_a) I_{Mn^{2+}}(T_b)} \qquad (9)$$

$$\sigma(R_{p,2}) = \frac{1}{T_b - T_a} x \sqrt{\left\{\frac{\sigma_{Ca^{2+}}}{I_{Ca^{2+}}(T_a)}\right\}^2 + \left\{\frac{\sigma_{Ca^{2+}}}{I_{Ca^{2+}}(T_b)}\right\}^2 + \left\{\frac{\sigma_{Mn^{2+}}}{I_{Mn^{2+}}(T_a)}\right\}^2 + \left\{\frac{\sigma_{Mn^{2+}}}{I_{Mn^{2+}}(T_b)}\right\}^2} \qquad (10)$$

where $I_{Ca^{2+}}$ and $I_{Mn^{2+}}$ are the peak intensities for the diamagnetic and paramagnetic states, respectively. The two time points are represented by T_a *(T=0)* and T_b (ΔT). For the error calculation, $\sigma_{Ca^{2+}}$ and $\sigma_{Mn^{2+}}$ are the standard deviations of the noise in the spectra recorded for the diamagnetic and paramagnetic states, respectively. The $R_{p,2}$ relaxation rate is related to the distance from a proton to the paramagnetic center of the metal by the following Solomon-Bloembergen equation.

$$R_{p,2} = \frac{1}{15}\left(\frac{\mu_0}{4\pi}\right)^2 \Upsilon_N^2 g_e^2 \mu_B^2 S(S+1) {r_{app}}^{-6} \left\{4\tau_C + \frac{3\tau_C}{1+(\omega_H \tau_C)^2}\right\} \qquad (11)$$

Both Solomon-Bloembergen equations for $R_{p,1}$ and $R_{p,2}$ assumes that all chemically equivalent protons are equidistant from the paramagnetic label. The following equation relates r_{app} to the minimum distance of a group of chemically equivalent protons r_{min}:

$$r_{app}^{-6} = \frac{1}{n}\sum_0^n r_n^{-6} \cong \frac{1}{n} r_{min}^{-6} \qquad (12)$$

where ${r_{min}}^{-6}$ is approximately equal to the sum of ${r_n}^{-6}$. The number and distances of those chemically equivalent protons are represented by n and r_n, respectively.

4.3.9. Experimentally-restrained docking using HADDOCK/CNS

Digoxin was docked to the mouse Pgp crystal structure using AutoDock Vina and experimentally-restrained docking protocols through the HADDOCK/CNS software (Brünger *et al.*, 1998; S. J. de Vries *et al.*, 2007). Various types of experimental data sets can be used within the HADDOCK/CNS software to drive molecular docking (Dominguez *et al.*, 2003; Hennig *et al.*, 2012; van Zundert *et al.*, 2016). Here, the PRE NMR distance restraints generated from the C1070 Pgp mutant were used to drive the docking of digoxin to Pgp.

4.3.9.1. Parameterizing the Mn-EDTA label for HADDOCK

The EDTA-Mn^{2+} cysteine label was built and parameterized for the PARALLHDG force field to be used for molecular docking in HADDOCK and CNS/Xplor using parameters derived from (Clore and Iwahara, 2009; Linge and Nilges, 1999). The EDTA-Mn^{2+} cysteine label was built and the geometry was optimized using the Ghemical force field in Avogadro 1.1.1 (Hanwell *et al.*, 2012). Force field parameters for the EDTA group and Mn^{2+} of the EDTA-Mn^{2+} cysteine label was obtained from deoxythymine labeled with Mn^{2+} chelated by EDTA (dT-EDTA-Mn^{2+}) in (J. Iwahara *et al.*, 2004). The cysteine group of the label used parameters from cysteine in the PARALLHDG force field (Linge and Nilges, 1999). These force field parameters were integrated in to the PARALLHDG force field of CNS/Xplor. Then the EDTA-Mn^{2+} cysteine label replaced appropriate cysteine residues in the X-ray crystal structure of mouse Pgp (PDB ID:4M1M) (J. Li *et al.*, 2014) using a script written in the Python programming language and the Biopython module (Cock *et al.*, 2009).

The Mn^{2+} and the surrounding nitrogen and oxygen atoms were given partial Mulliken charges of 0.762, -0.068 and -0.282, respectively, as described previously for a Mn Schiff base

complex in the ground state (Abdallah *et al.*, 2009). The C6 and C12 Lennard-Jones (LJ) parameters for the Mn^{2+} were 3.63119 x 10^{-5} kJ mol^{-1} nm^6 and 1.21636 x 10^{-8} kJ mol^{-1} nm^{12}, respectively, and were calculated using a distance between atoms at their lowest potential energy of 0.2635 ± 0.0072 nm and a well depth of 0.02710042 ± 0.01063420 kJ mol^{-1} averaged from several water models (P. Li *et al.*, 2013). The rest of the EDTA-Mn^{2+} cysteine label was given force field parameters derived from cysteine or functional groups from the GROMOS 53A6 force field (Oostenbrink *et al.*, 2005). To estimate the S^2 order parameter and internal correlation time (τ_i) of the EDTA-Mn^{2+} cysteine label, a 100 ns molecular dynamic simulation (GROningen MAchine for Chemical Simulations (GROMACS) (Oostenbrink *et al.*, 2005) of the label and surrounding residues to 12 Å in a TIP3P water shell was performed in a GROMOS 53A6 force field (Van Der Spoel *et al.*, 2005). The S^2 order parameter for the label was between 0.7 and 0.8, which was determined using a customized 48 node Linux cluster and a molecular dynamic (MD) simulation time of 100 ns.

4.3.9.2. Preparation of Pgp and digoxin coordinates

When modeling protein-ligand complexes, successful docking is highly dependent on the receptor's protonation state and functional groups in the binding pocket (Bas *et al.*, 2008). To prepare mouse Pgp for ligand docking, Chain A was extracted from the PDB file (J. Li *et al.*, 2014). This file is then processed through the PROPKA force field and the PARSE force field to give the correct protonation state of Pgp at pH 7.4 (Bas *et al.*, 2008). Most molecular docking programs give atoms partial charges including AutoDock 4.0 (Morris *et al.*, 2009). In contrast, AutoDock Vina treats charges as hydrogen bond donors or acceptors (Trott and Olson, 2010). To approximate a +2 charge on the Manganese in AutoDock Vina, an additional dummy Manganese

atom was added to the coordinates as described in (Roberts *et al.*, 2015).The digoxin file was obtained from PubChem and parameterized using the small-molecule topology generator server PRODRG 2.0 with full charges (S. Kim *et al.*, 2016; Schuttelkopf and van Aalten, 2004).

4.3.9.3. Initial docking using AutoDock Vina

The initial docking of digoxin to Pgp with the files prepared above was achieved by AutoDock Vina to prevent the drug binding in remote crevasses far from the actual drug binding site and to provide better control during initial rigid docking, which is stochastic in HADDOCK/CNS. AutoDock Vina was customized to allow 1000 drugs to be bound simultaneously to the transporter. This process coats the entire surface and binding cavities with digoxin molecules. The AutoDock-derived docked digoxin models were filtered and scored through HADDOCK using the experimental distance restraints calculated from the PRE NMR data. For the PRE NMR restraints, the minimum and maximum distances between the label and digoxin's protons are explicitly defined in Table 4.1 and 4.2. The HADDOCK score is related to the total binding energy reflecting the sum of the energies from the distance restraints, buried surface area and desolvation (S. J. de Vries *et al.*, 2007). The top 20 lowest scoring HADDOCK digoxin-Pgp complexes generated through AutoDock Vina are sent through HADDOCK docking protocols for refinement.

4.3.9.4. Refinement docking through HADDOCK

The top 20 digoxin molecules with the lowest HADDOCK scores go through 10 MD simulations each for a total of 200 MD simulations for further refinement. The MD simulations consist of three successive stages for the docking protocol. First, the docked structures are energy

minimized (EM) in AutoDock Vina. Then, the side chains are allowed to move by semi-flexible simulated annealing (SA). Last, explicit waters are included for Cartesian dynamics refinement (Brünger *et al.*, 1998; S. J. de Vries *et al.*, 2007; Sjoerd J. de Vries *et al.*, 2010; Dominguez *et al.*, 2003). After all the steps were completed, the lowest weighted HADDOCK score for the digoxin-Pgp complex was 89.

4.4. RESULTS AND DISCUSSION

4.4.1. The effect of digoxin and colchicine on wt Pgp-mediated ATP hydrolysis

Figure 4.1 shows the wt Pgp-coupled activation of ATP hydrolysis for digoxin (closed squares) and colchicine (open squares) in the presence of saturating ATP (3.2 mM). The digoxin-induced kinetics were monophasic and gave a V_{max} and K_m value of 1344 ± 150 nmol min^{-1} mg^{-1} and 240 ± 68 μM, respectively, when fit to the Michaelis-Menten equation (equation 1). The ~2-fold activation of Pgp-mediated ATP hydrolysis by digoxin is within the range of previous observations (Matsunaga *et al.*, 2006; Rebbeor and Senior, 1998; von Richter *et al.*, 2009) and our K_m value agrees well with the K_m value of 385 μM that was determined for digoxin transport in Caco-2 cells for human Pgp (Hansen and Nilsen, 2009).

The colchicine-induced kinetics were also monophasic and fitting to the Michaelis-Menten equation (equation 1) gave a V_{max} and K_m of 265 ± 93 nmol min^{-1} mg^{-1} and 246 ± 193 μM, respectively. The ~20% increase in Pgp-mediated ATP hydrolysis is similar to previous observations (al-Shawi and Senior, 1993; Sharom *et al.*, 1993). The K_m for colchicine determined for wt human Pgp in *sf9* insect cells was 163 ±18 μM (Rao, 1995), which is consistent with our determinations for wt mouse Pgp. Purified wt human Pgp reconstituted in lipids had a K_m that was considerably higher at 680 μM (Omote *et al.*, 2004). This discrepancy may be a result of

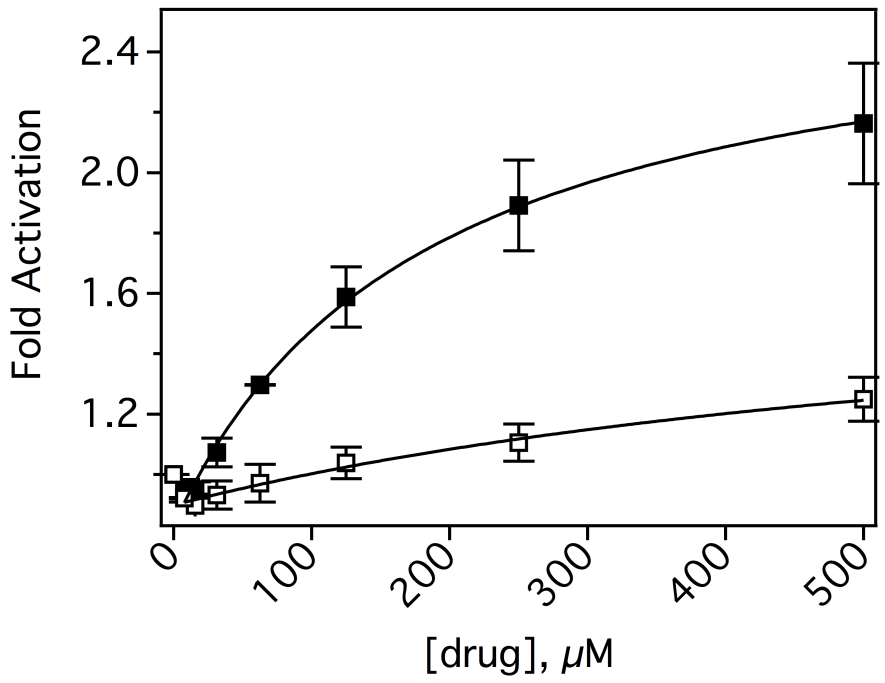

Figure 4.1. Digoxin and colchicine-stimulated ATPase Activity of wild-type Pgp. The digoxin (closed squares) and colchicine (open squares) stimulated ATPase activity was measured over a range of concentrations with wild-type mouse Pgp. The kinetic curves were fit to the Michaelis-Menten equation (equation 1) and are represented as a solid line. Error bars represent the standard deviation and the points are an average of three independent experiments.

residual detergents remaining during Pgp reconstitution, which were recently shown to reduce drug binding affinity (Shukla *et al.*, 2017).

4.4.2. Detergent does not significantly interfere with digoxin's interactions with Pgp

To compare our NMR-derived model with X-ray crystal and cryo-EM structures (Aller *et al.*, 2009; Frank *et al.*, 2016; J. Li *et al.*, 2014; A. B. Ward *et al.*, 2013), we isolated and prepped Pgp under approximately the same DDM detergent conditions for our PRE NMR experiments. The DDM detergent is known to affect drug binding to the Pgp transporter (Tip W. Loo and Clarke, 2017; Shukla *et al.*, 2017). To determine the effect of detergent on digoxin binding to Pgp, digoxin-induced quenching of Pgp fluorescence was monitored as we have done previously (Ledwitch, Barnes*, et al.*, 2016).

Figure 4.2A shows the effect of digoxin on the intrinsic tryptophan fluorescence of detergent solubilized Pgp over a range of digoxin concentrations after exciting the protein at 280 nm. The fluorescence amplitude for detergent solubilized Pgp (closed squares) and Pgp reconstituted in liposomes (open squares) at 333 nm was corrected for inner filter effects and background fluorescence with equation 2 and plotted as a function of digoxin concentration in Figure 4.2B. At saturating digoxin concentrations Pgp is quenched ~15% with a biphasic titration curve giving a K_L and K_H value of 0.0140 ± 0.0034 μM^{-1} and 9.45 ± 6.27 μM^{-1} after fitting to equation 3. At higher temperature, the K_L value decreased to 0.0089 μM^{-1} while the K_H value increased, suggesting that the low concentration phase is a result of static quenching. This allowed us to calculate a K_D for digoxin binding to detergent solubilized Pgp of 71 ± 30 μM. This binding affinity is very similar to the K_D determined for Pgp reconstituted in liposomes of

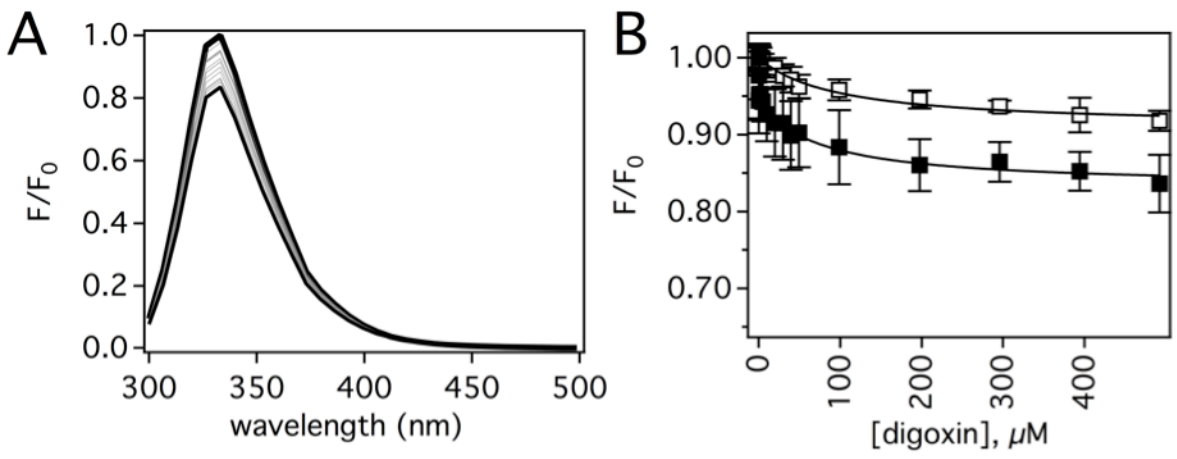

Figure 4.2. Binding affinity of digoxin to Pgp probed by intrinsic tryptophan fluorescence. (A) Detergent solubilized Pgp fluorescence spectra in the presence of a range of digoxin concentrations after exciting at 280 nm with 0 μM digoxin (thick line) to 500 μM digoxin (thin line) and intermediate concentrations shown in grey. (B) Corrected fluorescence emission spectra for detergent solubilized Pgp (closed squares) and Pgp reconstituted in proteoliposomes (open squares) over a range of digoxin concentrations. Error bars represent the standard deviation and the points are an average of three independent experiments.

100 ± 18 μM (Ledwitch, Barnes*, et al.*, 2016). This result suggests that the DDM detergent does not significantly disrupt digoxin interactions with Pgp.

4.4.3. The effect of DDM on Pgp conformation with digoxin

To determine the effect of DDM on Pgp conformation in the absence and presence of digoxin, acrylamide quenching was used to probe conformational changes and compared to previous observations in proteoliposomes (Ledwitch, Barnes*, et al.*, 2016). Acrylamide quenching of tryptophan residues has been widely used to determine ligand, nucleotide and detergent-induced changes in the tertiary conformation of Pgp (Sharom *et al.*, 2003). Figure 4.3 shows the Stern-Volmer plots for Pgp reconstituted in liposomes and detergent solubilized Pgp where the slopes represent the degree of acrylamide quenching of tryptophan residues. Decreases in the slopes of the Stern-Volmer plots suggest that tryptophan residues are less exposed and implies that Pgp shifts to a "closed" conformation where the NBDs come together. Increases in the slope suggest that tryptophan's are more exposed and implies that Pgp shifts to an "open" conformation where the NBDs are a part like the Pgp X-ray crystal structure (A. B. Ward *et al.*, 2013). These differences between the slopes represent relative changes in the protein's conformation and cannot be used to assign distinct Pgp conformations.

The slope of the Stern-Volmer plot for Pgp reconstituted in liposomes (Figure 4.3A, open squares) increased from 1.55 ± 0.04 M^{-1} to 2.89 ± 0.23 M^{-1} for detergent solubilized Pgp (Figure 4.3A, closed squares) (Ledwitch, Barnes*, et al.*, 2016). This increase is consistent with a shift to an "open" Pgp conformation, which correlated well with X-ray crystallographic observations (J. Li *et al.*, 2014). In the presence of digoxin, the K_{SV} value remains relatively constant in the presence of DDM with a K_{SV} value of 2.63 ± 0.20 M^{-1} (Figure 4.3B, closed squares) and 2.29 ±

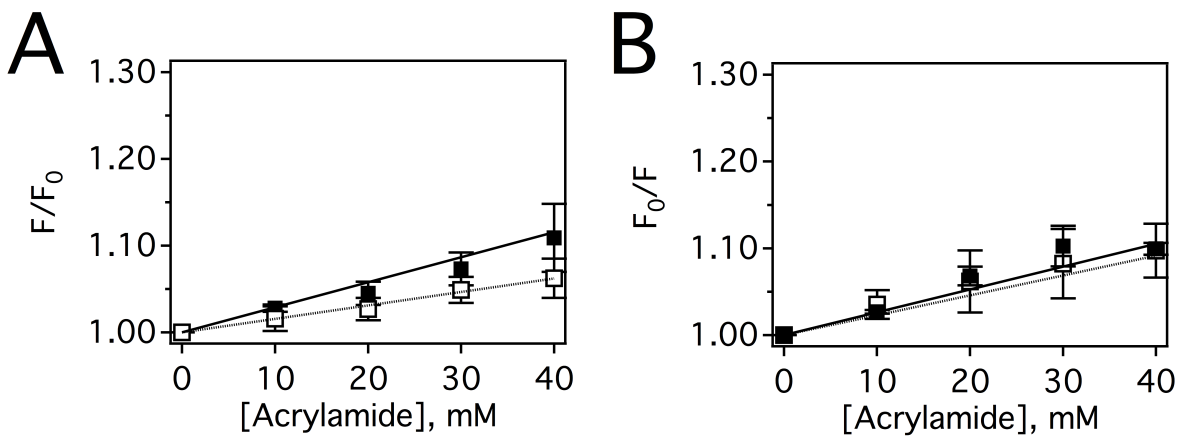

Figure 4.3. The effect of detergent and liposomes on the conformation of Pgp and in the absence and presence of digoxin. (A) The Stern-Volmer plots for detergent solubilized Pgp (closed squares) and Pgp reconstituted in proteoliposomes (open squares) in the absence of drug. (B) The Stern-Volmer plots for detergent solubilized Pgp (closed squares) and Pgp reconstituted in proteoliposomes (open squares) in the presence of 250 μM digoxin. Error bars represent the standard deviation and the points are an average of three independent experiments.

0.12 M^{-1} for Pgp in proteoliposomes (Figure 4.3B, open squares). This is consistent with the fact that the digoxin affinities are similar in the absence and presence of DDM. Therefore, the "open" conformation with the NDBs separated was used for molecular docking.

4.4.3. PRE NMR-derived distance restraints of digoxin to Pgp

PRE NMR was used to determine the distance-dependent relaxation rates of digoxin from a paramagnetically-labeled single cysteine mutant on Pgp. Figure 4.4A shows a waterfall plot of the individual 1D proton NMR spectra of digoxin as a function of T_1 relaxation time with the background and baseline subtracted. The plot shows that at short inversion recovery times the digoxin peaks are positive and become negative at higher inversion recovery times. Figure 4.4B shows the analysis of proton s, a methyl group emanating from the furan-2 one functional group of digoxin, as a function of inversion recovery time. Figure 4.4C shows the change in amplitude at two different time points for proton v, t and s for a T_2 relaxation NMR experiment.

Table 4.1 shows the $R_{p,1}$ relaxation rates and calculated distances that were determined from the analysis for C1070. The first three columns show the R_{Ca}^{2+} (diamagnetic), R_{Mn}^{2+} (paramagnetic) and the $R_{p,1}$, which is the difference (i.e. $R_p = R_{Ca}^{2+} - R_{Mn}^{2+}$). The $R_{p,1}$ is related to the calculated distances using the Solomon-Bloembergen equation (equation 6). We calculated the model-dependent relaxation (R_M) rate using the relationship $R_{p,1} = \alpha R_M$, where α is the fraction of ligand bound to the protein. The K_D for digoxin is 71 μM and was used to determine the fraction of ligand bound to the protein by $[E]/(K_D + L)$. The distances r_{min}, r_{max} and r_{avg} were calculated for each proton using equation 6 with the highest, lowest and average R_M, respectively, as described (Arthur G. Roberts *et al.*, 2011).

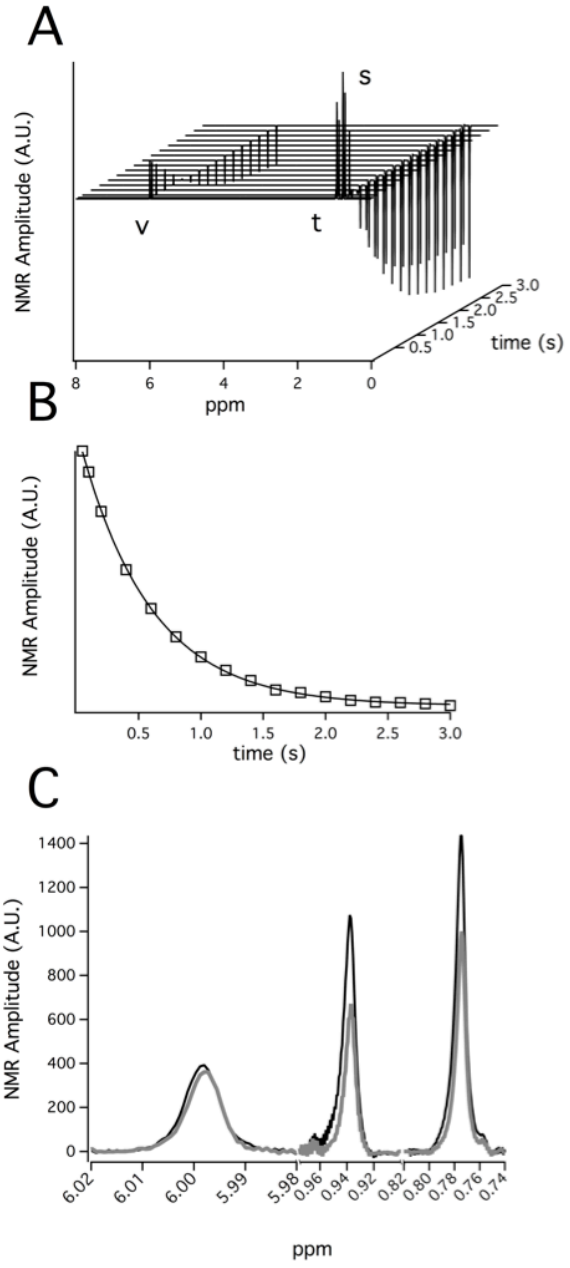

Figure 4.4. NMR relaxation of 300 μM digoxin in the presence of 5 μM C1070 Pgp. (A) Stacked plot of the ^{1}H- T_1 relaxation of digoxin. (B) T_1 relaxation decay curve of proton s emanating from the furan-2-one functional group of digoxin. (C) T_2 relaxation spectra and the amplitudes associated with the two time points, T_a=0s (black) and T_b=0.02s (grey), used to calculate the $R_{p,2}$ relaxation rate for proton v, t and s from high to low ppm, respectively.

Table 4.1. $R_{p,1}$ and distance calculations for digoxin ^{1}H peaks with diamagnetic and paramagnetic ions.

Peak	R_{Ca}^{2+} (sec^{-1})	R_{Mn}^{2+} (sec^{-1})	$R_{p,1}$ (sec^{-1})	r_{min}[a] (Å)	r_{max}[b] (Å)	r_{avg}[c] (Å)
C1070						
v	1.269±0.090	1.247±0.060	0.0144±0.069	12.92	100.00	17.30
t	0.527±0.003	0.514±0.004	0.0463±0.018	13.49	15.47	14.25
s	0.588±0.008	0.573±0.005	0.0459±0.028	13.17	16.74	14.27

[a] r_{min} was calculated based on chemical equivalence using eq. 6.

[b] r_{max} was calculated based on chemical equivalence using eq. 6.

[c] r_{avg} was calculated using eq. 6.

Abbreviations: R_{Ca}^{2+}, paramagnetic relaxation rate (sec^{-1}); R_{Mn}^{2+}, diamagnetic relaxation rate (sec^{-1}); R_p, apparent paramagnetic relaxation rate (i.e. $R_p = R_{Ca}^{2+} - R_{Mn}^{2+}$). The distances were calculated with a τ_C of 1.94×10^{-9} sec.

Table 4.2 shows the amplitude intensities for $I_{Ca^{2+}}$ and $I_{Mn^{2+}}$ at two different time points $T_a = 0s$ and $T_b = 0.02s$ used in equation 8 to calculate the $R_{p,2}$ relaxation rate. $R_{p,2}$ is related to the calculated distances using equation 10. This two-time point approach for a T_2 NMR experiment is advantageous because it does not require curve fitting procedures and the use of two time points versus many time points maximizes the signal to noise ratio (S/N) over a given period of time (Junji Iwahara *et al.*, 2007). The distances r_{min}, r_{max} and r_{avg} were calculated as described above except with equation 10.

4.4.5. Distance-restrained model of digoxin bound to P-glycoprotein

Figure 4.5 shows the bound orientation and location of digoxin to the Pgp transporter determined by the calculated distances from the $R_{p,1}$ and $R_{p,2}$ values. The top 20 scored digoxin-Pgp complexes are shown space filled in green on the left and a close-up of the lowest scoring complex of 89 is shown on the right. The interacting residues E180, K177, D173 and E898 stemming from the intracellular domains of TM3 and TM10 are also depicted. The G181 residue is space filled in red (left) and shown alongside the interacting residues (right) to demonstrate the proximity of G181 to the bound location of digoxin on Pgp.

Lack of structures showing the location of and how a drug-bound substrate interacts with the Pgp transporter stagnates progress towards understanding the molecular basis for these drug-protein interactions. Ultimately, this limits strategies to eradicate Pgp-mediated multidrug resistance and drug toxicities. Alternative techniques to X-ray crystallography have been adopted in attempts to map the locations of these drug-binding sites. These techniques include

Table 4.2. Peak intensities for the paramagnetic and diamagnetic samples at two time points (T_a and T_b) used to determine the $R_{p,2}$ relaxation rates and calculated distances for digoxin ^{1}H peaks.

Peak	$I_{Ca^{2+}}(T_a)$	$I_{Mn^{2+}}(T_a)$	$I_{Ca^{2+}}(T_b)$	$I_{Mn^{2+}}(T_b)$	$R_{p,2}$ (sec^{-1})	r_{min}[a] (Å)	r_{max}[b] (Å)	r_{avg}[c] (Å)
C1070								
v	412.9	364.5	393.0	336.2	1.568±0.26	14.19	14.99	14.55
t	1158.7	998.2	722.3	590.8	2.595±0.12	13.28	13.49	13.38
s	1471.7	1333.5	1042.8	887.84	3.113±0.09	12.92	13.04	12.98

[a] r_{min} was calculated based on chemical equivalence using eq. 10.

[b] r_{max} was calculated based on chemical equivalence using eq. 10.

[c] r_{avg} was calculated using eq. 10.

Abbreviations: $I_{Ca^{2+}}$, diamagnetic peak intensity; $I_{Mn^{2+}}$ paramagnetic peak intensity; T_a time = 0; T_b time = 0.02; R_p, apparent paramagnetic relaxation rate (i.e. $R_p = R_{Ca}^{2+} - R_{Mn}^{2+}$). The distances were calculated with a τ_C of 1.94 x 10^{-9} sec.

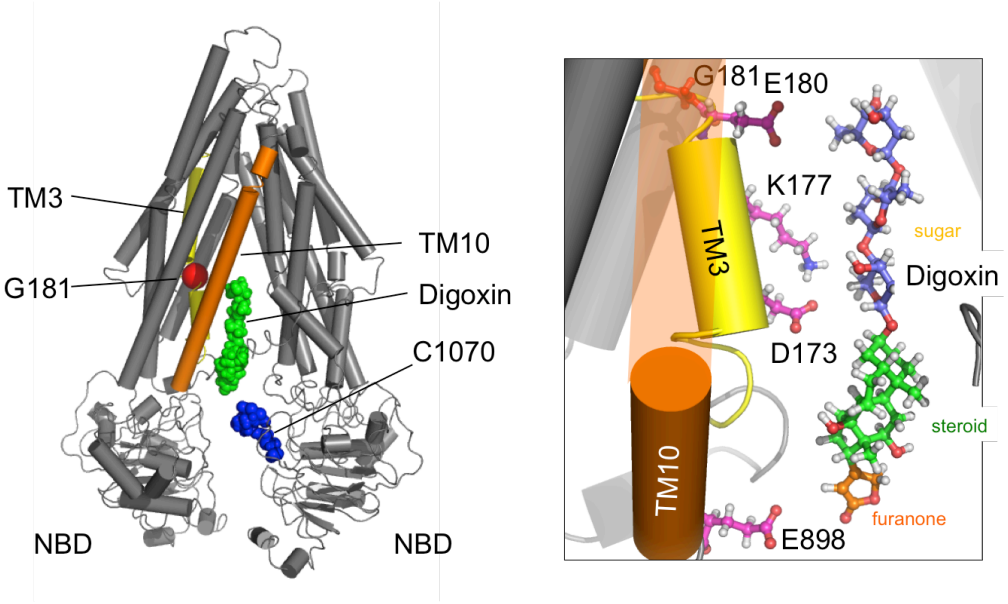

Figure 4.5. HADDOCK/CNS derived model of digoxin bound to Pgp using experimentally-derived NMR restraints. The highest scored docked conformation of digoxin to Pgp is space filled (green) and the G181 residue is labeled (orange). The inset shows a close-up of the highest scored docked conformation of digoxin (green) and the interacting residues labeled (magenta).

cysteine/arginine scanning mutagenesis (Tip W. Loo and Clarke, 1995; T. W. Loo and Clarke, 2015; Tip W. Loo and Clarke, 2017) photoaffinity analogues (Dey *et al.*, 1997; Greenberger, 1993; Raviv *et al.*, 1990; Ahmad R Safa, 1992; Tamai and Safa, 1991) and fluorescence spectroscopy (Sonveaux *et al.*, 1999; Vigano *et al.*, 2002). Here, we present a different approach to locate and model Pgp drug binding sites using PRE NMR to get distance restraints to drive molecular docking in HADDOCK/CNS.

Figure 4.5 shows the bound location of the drug digoxin to the Pgp transporter deduced by NMR-derived distance restraints summarized in Table 4.1 and 4.2. In a study by our group, we demonstrated by STDD NMR that the digoxin protons emanating from the sugar groups and proton v on the furan-2-one functional group (cf. 2.1B for reference) had the strongest interactions with Pgp (Ledwitch, Barnes*, et al.*, 2016). These interactions agree well with the orientation and proximity of digoxin's sugar group protons and proton v when bound to Pgp shown in Figure 4.5 (left). Another study investigating binding interactions of digitalis-like compounds (DLCs) to Pgp determined that the sugar moiety and the δ-lactone ring (i.e. the furan functional group) are important in digoxin binding (Gozalpour *et al.*, 2013), which is also consistent with our model.

It was recently shown that digoxin transport by human Pgp was not observed in a ciPTEC cell line due to a G185V point mutation (Gozalpour *et al.*, 2016). In our digoxin-Pgp complex, digoxin binds within ~11 Å measured from the 6' methyl protons to the G181 (mouse equivalent to G185) residue, which is shown space filled in red. The effect of the G181V/G185V Pgp mutation on drug binding, ATPase activity and transport has been well characterized for a number of substrates (Bruggemann *et al.*, 1992; Choi *et al.*, 1988; Müller *et al.*, 1996; Omote *et al.*, 2004; Rao, 1995; A. R. Safa *et al.*, 1990a, 1990b; Watanabe *et al.*, 2000). The mutant was

first identified in a colchicine-resistant cell line where the replacement of glycine with valine resulted in an increase in colchicine transport (Choi *et al.*, 1988). The opposite effect was observed for vinblastine where the mutant caused a decrease in transport (A. R. Safa *et al.*, 1990a). For colchicine, the transport rate increased ~2 fold with human G1815V Pgp reconstituted in lipids compared to wt Pgp and resulted in an increase of the K_m from 680 to 5800 μM (Omote *et al.*, 2004). In contrast, the G185V Pgp mutant did not affect the K_m for verapamil or valinomycin (Omote *et al.*, 2004). However, the K_i for verapamil more than doubled from 0.64 mM to 1 mM, suggesting that the G185V Pgp mutant affects a secondary verapamil binding site (Omote *et al.*, 2004). We demonstrated that digoxin is competitively displaced at verapamil's secondary binding site (i.e. low-affinity binding site) as discussed in Chapter 2, which further supports digoxin's location bound to Pgp in this model (Ledwitch, Barnes*, et al.*, 2016).

This G185 residue is located on TM3 and has been a targeted region for mutagenesis studies due to the emergence of the G185V Pgp mutant and its effect on drug interactions with Pgp. In general, this region plays an important role in substrate specificities, ATPase activity, transport and membrane targeting (Choi *et al.*, 1988; T W Loo and Clarke, 1994; Müller *et al.*, 1996; Rao, 1995; A. R. Safa *et al.*, 1990b). In our model, digoxin interacts with and is bound to close proximity of the amino acids that make up TM3, which are residues 138-185 for mouse Pgp (Aller *et al.*, 2009; J. Li *et al.*, 2014). A study by Loo and Clarke showed that mutating other glycine residues to valine within this region (G141 on TM2 and G187 on TM3) on human Pgp increased resistance to colchicine and adriamycin, but decreased resistance to vinblastine (T W Loo and Clarke, 1994). Another study showed that mouse Pgp mutations to the consecutive residues T169I, R170L, L171P and T172P on TM3 caused a severe loss in overall Pgp function and as a result, are likely important residues in drug binding (Kwan and Gros, 1998). In our

digoxin-Pgp model, these residues are clustered near the digoxin binding site and more specifically, the amino acid T172 is ~6 Å from the 6''' methyl protons on digoxin. Additionally, they also generated a G181R mutant, which showed a near complete loss of activity for verapamil and valinomycin-simulated ATPase activity (Kwan and Gros, 1998).

The G181 residue and the TM3 region are evidently significant in the overall function of Pgp and recognition of drug substrates by Pgp. The structures that are available have identified drug-binding sites preferentially close to the extracellular side within the transmembrane spanning regions of the Pgp transporter (Aller *et al.*, 2009; J. Li *et al.*, 2014). The model in Figure 4.5 reveals that digoxin binds within the TM region of Pgp near G181 and interacts with charged residues E180, K177, D173 and E898. Most of these residues are on the TM3 region of the transporter, which through mutagenesis studies, have been identified as significant residues for Pgp drug recognition and transport. The G181V Pgp mutant was shown to abolish digoxin transport in a ciPTEC cell line and is also a residue within this TM3 region (Gozalpour *et al.*, 2016). With this information, the NMR-derived model of digoxin bound to Pgp is most likely an accurate predication of the digoxin drug-binding site. Future experiments needed to validate this model are presented in Chapter 5.

CHAPTER 5

SUMMARY AND FUTURE DIRECTIONS

5.1. SUMMARY

Since the discovery of the Pgp transporter ~40 years ago, a vast amount of research has been devoted to understanding this enigmatic protein (Gottesman and Ling, 2006; Juliano and Ling, 1976). This ATP-dependent drug pump is widely recognized for its role in multidrug resistance, drug disposition and mediating DDIs (Giacomini *et al.*, 2010; Gottesman and Ling, 2006; Tanigawara, 2000; L. Zhang *et al.*, 2011). These clinical implications make Pgp a sought after therapeutic drug target. However, targeting Pgp remains challenging due to its drug promiscuity and lack of information regarding transport, how drug binding couples to ATP hydrolysis and drug binding site(s).

The overall goal of this research was focused on understanding the mechanism(s) associated with P-glycoprotein mediated cardiovascular drug-drug interactions (DDIs). P-glycoprotein is an efflux transporter responsible for extruding drug substrates from within the lipid bilayer or cytosol to the extracellular space. Cardiovascular drugs have broad substrate specificities for the Pgp transporter and often these molecules have low therapeutic indexes. Therefore, P-glycoprotein serves as a major roadblock for effective cardiovascular drug therapy by altering dug disposition and subsequently promoting toxicity through DDIs.

My research was focused on DDIs between the calcium channel antagonist verapamil and the cardiac glycoside digoxin. Verapamil is known to inhibit P-glycoprotein-mediated digoxin

transport at the apical membrane of the kidneys where digoxin elimination is prevented causing a spike in digoxin plasma concentrations. Although we know the mechanism of how the verapamil-digoxin DDI occurs *in vivo*, what lacks is an understanding of this Pgp-mediated DDI on a molecular and structural level.

This dissertation project had three objectives: 1) define the mechanism by which verapamil modulates Pgp-mediated transport of digoxin, 2) determine how verapamil binding is coupled to ATP hydrolysis and 3) determine the digoxin binding site on the Pgp transporter. To satisfy the first objective of this project, we determined that verapamil, at low concentrations, non-competitively inhibits digoxin transport and both cardiovascular drugs can occupy the transporter simultaneously. Our results and previous transport studies were combined into a comprehensive molecular and mechanistic model of verapamil-digoxin DDIs with Pgp. These molecular details are essential for defining a general DDI mechanism, identifying therapeutics that have a high probability for exhibiting DDIs and ultimately, decreasing the risk and associated toxicities with DDIs in the clinic.

The second objective of this project was to determine how verapamil binding is coupled to Pgp-mediated ATP hydrolysis. In the presence of saturating ATP concentrations (i.e. 3.2 mM), verapamil kinetics were biphasic. However, in the presence of subsaturating ATP, verapamil kinetics switched from biphasic to monophasic. We determined that this switch in kinetic behavior occurs in a cooperative fashion. Essentially, occupancy of verapamil at the high affinity binding site is non-cooperative with ATP and verapamil occupancy at the low affinity site is cooperative with ATP.

The third objective of this project was to identify the bound location of digoxin to the Pgp transporter. Typically, determining locations of bound substrates to receptor molecules are done

through X-ray crystallography. Our approach utilized NMR to determine long-range distance restraints from a label on Pgp to the bound location of the drug. Using this approach in combination with molecular docking protocols, we were able to successfully model the digoxin-Pgp complex employing experimentally-derived distance restraints generated from C1070 Pgp mutant PRE NMR data. To further validate this proposed model, current progress and future directions are given in the next section.

.

5.2. CURRENT PROGRESS AND FUTURE DIRECTIONS

This section describes current progress and future experimental considerations for validating the NMR derived model of digoxin bound to Pgp presented in Chapter 4. The experiments and the significance they have on validating the proposed model are summarized below. Additionally, any current work and preliminary data supporting the feasibility of each experiment is included and discussed.

5.2.1. Progress on creating a G181V Pgp mutant, obtaining expression and determining its effect on digoxin-induced Pgp-mediated ATPase activity

The G185V human Pgp mutation was first identified in a colchicine-resistant KB cell line (Choi *et al.*, 1988) where the replacement of glycine with a bulky valine group results in an energetically more efficient manner of transport for the drug colchicine (Omote *et al.*, 2004). The cardiac glycoside digoxin is a well-characterized Pgp substrate but was recently shown to not be transported in a MDCK-Pgp cell line coding for the G185V point mutation (Gozalpour *et al.*, 2016). To validate the bound location of digoxin on Pgp, the effect of the G181V (the residue equivalent to human) Pgp mutant on digoxin-induced ATP hydrolysis will be investigated and

compared to wt activity. Colchicine will be used as a control to show the effect of the G181V point mutation on Pgp-mediated colchicine ATPase activity.

The G181V Pgp mutant was generated at the Bioexpression and Fermentation Facility, University of Georgia. Briefly, the pPICZ A vector (Invitrogen, Carlsbad, CA) was used as the expression vector for G181V. The codon optimized plasmid was transformed into XL1 Blue competent cells using a Qiagen Miniprep Kit. The entire mdr3 gene sequence was confirmed with primers designed using the GenScript Sequencing Primer Design website. The point mutation for changing glycine to valine at position 181 was introduced using QuikChange II XL Site-Directed Mutagenesis Kit. The primers used to create the mutation were 'CCG ATC TTG TCA CCG ATT ACT TCG TTA ATC TTG GAC A' (forward) and 'TGT CCA AGA TTA ACG AAG TAA TCG GTG ACA AGA TCG G' (reverse) and were also designed using the GeneScript Sequencing Primer design website. The mutant plasmid was transformed into XL1 Blue competent cells, isolated using the Qiagen mini-prep Kit and confirmed again with the above primers.

The XL1 Blue cells containing the mutant were spread on Low Salt LB plates (10g bactotryptone, 5g yeast extract, 5g NaCl and 15g Agar, 50 µg/ml zeocin, pH 7.5) plates. A single colony was inoculated in a 10 ml culture tube in Low Salt LB media (50 µg/ml zeocin) and grown overnight in an incubator shaker at 37 ^{o}C. The XL1 Blue cells with the G181V mutant were re-inoculated in a 500 ml of Low Salt LB media (50 µg/ml zeocin) at a 1:2000 dilution and grown overnight at 37 ^{o}C. Cells were pelleted down and the G181V plasmid DNA was isolated using a Maxi Prep Kit, linearized and transformed into electrocompetent KM71H *P. Pastoris* yeast cells as described in (Weidner *et al.*, 2010). Zeocin-resistant tranformants were selected out on YPDS (1% yeast extract, 2% peptone, dextrose and agar, pH 7.5) plates containing 100, 500

and 1000 μg/ml of zeocin. Colonies that were resistant to 1000 μg/ml of zeocin were selected out and purified on MGY plates for inoculation in MGY media and methanol induction as described previously (Lerner-Marmarosh *et al.*, 1999).

With these high zeocin resistant colonies, there was not any detectable G181V protein expression post 72 hrs of methanol induction tested by SDS-PAGE and small-scale protein purification as described in (Lerner-Marmarosh *et al.*, 1999). The purpose of using high zeocin concentrations is to screen and select out colonies with multi-(gene) copies integrated into the *P. Pastoris* genome (Aw and Polizzi, 2013). Theoretically, the clones able to survive at higher concentrations of zeocin would indicate an increase in a higher number of antibiotic resistance genes into the genome (Sunga *et al.*, 2008). It has been reported that multi-(gene) copy integrations do not always have a linear correlation with increased protein expression and that proteins do not necessarily have the same copy integration threshold for producing maximal expression (Hohenblum *et al.*, 2004; Whyteside *et al.*, 2011). A possible explanation is that lack of protein yield is related to cellular stress from over saturation of the secretory pathway (i.e. increased traffic through the secretion pathway) (Whyteside *et al.*, 2011). Another possibility is that the DNA is inserted in a location where induction of the gene of interest is inefficient. Due to the negative effects observed with expressing the G181V Pgp mutant, it is possible that screening numerous colonies at lower levels of zeocin may be of interest to achieve expression levels of the protein.

5.2.2. Feasibility of using C713 and C133 as two additional cysteine mutants to triangulate the bound location of digoxin to Pgp

In addition to the Pgp single cysteine mutant C1070, two additional cysteine mutants,

C713 and C133, will be used to triangulate in on the bound location of digoxin to Pgp. Figure 5.1 shows the location on Pgp of each single cysteine mutant and their proximity to the bound location of digoxin determined with the C1070 PRE NMR data as mentioned in Chapter 4. The expected distances for C713 to proton v on digoxin's steroid ring is ~26 Å and to the first 6' methyl protons on the sugar group is ~26 Å. The expected distances for C133 to proton labeled 'v' on digoxin's steroid ring is ~43 Å and to the first 6' methyl protons on the sugar group is ~4 Å. For both single cysteine mutants, these distances are within the measurable range of ~50 Å and would provide additional distance restraints used in the docking protocols to verify the digoxin binding site on the Pgp transporter.

5.2.3. Progress on using diffusion-ordered spectroscopy (DOSY) PRE NMR to isolate distances for protons on digoxin's sugar group

One of the challenges with the PRE NMR experiments with digoxin and detergent solubilized Pgp is overlap between the digoxin sugar groups and the *n*-dodecyl-β-*D*-maltoside (DDM) detergent maltoside sugar group. The methyl proton peaks emanating from DDM's sugar group directly overlaps digoxin's 6', 6'' and 6''' methyl proton peaks shown in Figure 2.1 and supplementary Figure 2.8B. This overlap prevents getting distance-dependent relaxation measurements from the opposite side of the digoxin molecule when bound to Pgp. These measurements will provide further support that digoxin is bound away from the extracellular side of Pgp as shown in Figure 4.5.

Diffusion-ordered spectroscopy (DOSY) is a technique used to separate out individual NMR spectra from a mixture of compounds based on differences in diffusion coefficients (Johnson, 1999; Nicolay *et al.*, 2001). In order to isolate the digoxin sugar proton peaks from the

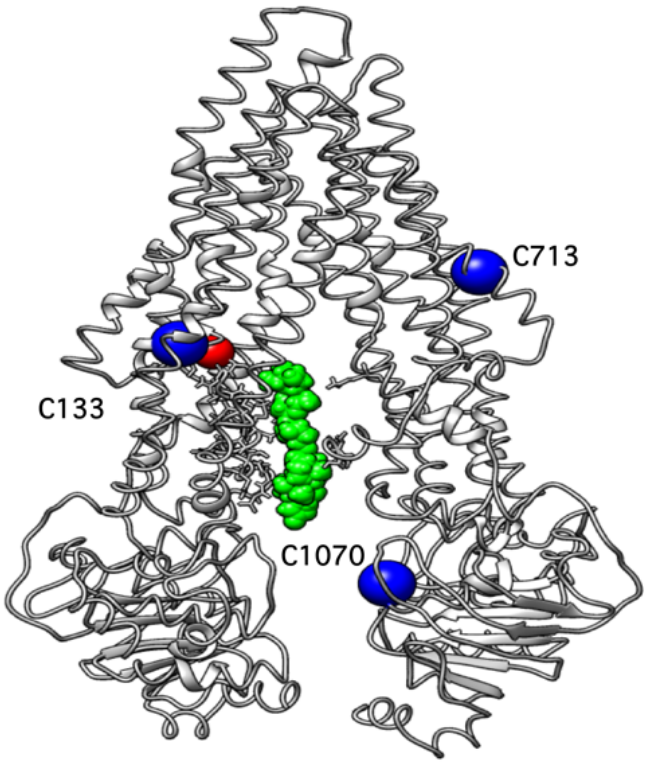

Figure 5.1. The structure of Pgp showing the locations of the single cysteine mutants (blue) for triangulating the location of digoxin bound to Pgp by PRE NMR. The G181 residue (red) is shown for reference and the bound location of digoxin determined with the C1070 distance restraints are space-filled in green.

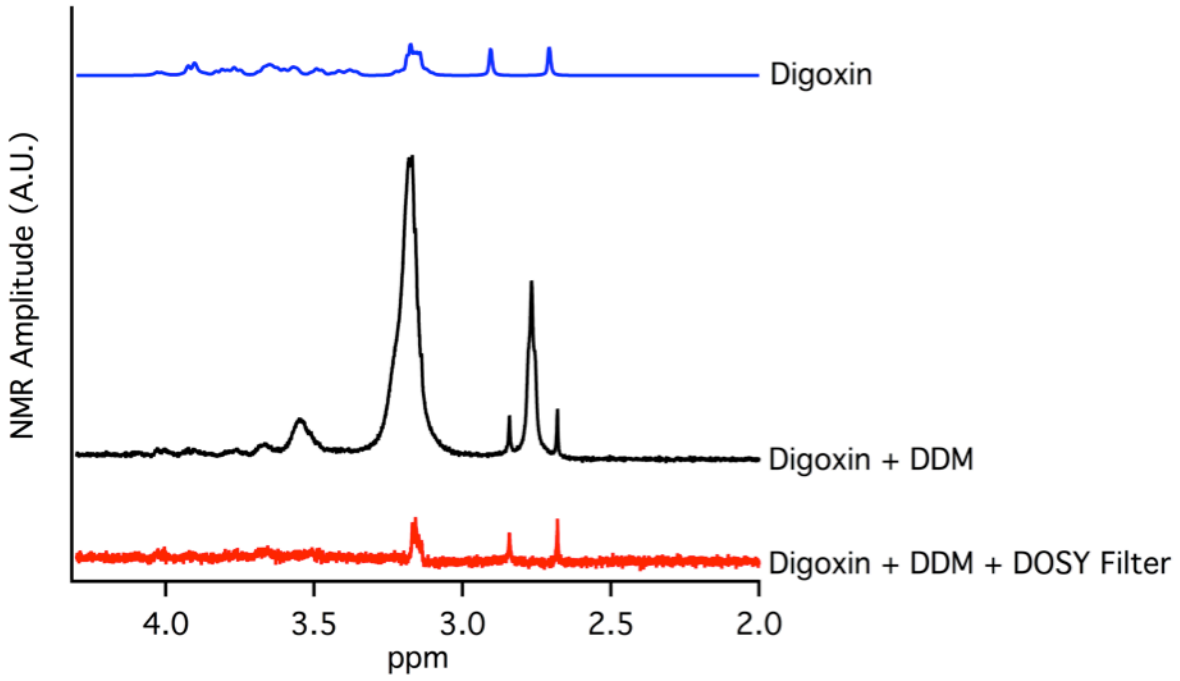

Figure 5.2. ^{1}H NMR spectra of digoxin, a mixture of digoxin and *n*-dodecyl-β-*D*-maltoside (DDM) and the separation achieved using a DOSY filter. 10 mM digoxin ^{1}H NMR spectra is shown in blue, digoxin ^{1}H NMR spectra in the presence of DDM is shown in black and the digoxin ^{1}H NMR spectra in the presence of DDM with the addition of a DOSY filter is show in red.

DDM sugar proton peaks, a DOSY filter can be used to separate the two within the mixture. Figure 5.2 demonstrates the effect of a DOSY filter on the ^{1}H proton NMR spectra of a sample containing both digoxin and DDM. Essentially, the background signals arising from the detergent at 3.2 ppm were completely removed by diffusion editing and WATERGATE using a diffusion-ordered spectroscopy bipolar pulse pair stimulated echo modified with WATERGATE for water suppression (Pelta *et al.*, 1998; Wu *et al.*, 1995). The DOSY filter works by taking two spectra at two different gradient strengths where slowly diffusing features are half the amplitude of the other. The slowly diffusing features are internally subtracted out within the pulse program by phasing the high gradient strength NMR spectrum 180° from the low gradient strength NMR spectrum. Representative digoxin spectra in the absence of DDM, with DDM and with a DOSY filter are shown in Figure 5.2.

5.3. LONG-TERM RESEARCH OUTLOOK

To gain a full understanding of the Pgp-mediated DDI between verapamil and digoxin and how these interactions are coupled to ATP hydrolysis, the drugs and ATP can be simultaneously docked and modeled to the transporter using similar approaches and techniques discussed in this dissertation. This information would provide a complete snapshot of this DDI on a molecular level. It is also of interest to investigate other Pgp-mediated DDIs to determine if some of these mechanisms are generalizable. Such structural knowledge and information will provide a platform for developing safer drug regimens, identifying potential drugs that are susceptible to Pgp-mediated DDIs, and designing novel Pgp inhibitors. Additionally, these types of approaches will provide the first drug-bound Pgp models and can be used as a high throughput method for screening drug compounds for Pgp interactions.

REFERENCES

Aanismaa, P., & Seelig, A. (2007). P-Glycoprotein kinetics measured in plasma membrane vesicles and living cells. *Biochemistry, 46*(11), 3394-3404.

Abdallah, H. H., Gadzhiev, O. B., & Adnan, R. (2009). *Comparative study of theoretical partial charges of Zn and Mn-Schiff base complexes.* Paper presented at the 13th Int. Electron. Conf. Synth. Org. Chem.

al-Shawi, M. K., & Senior, A. E. (1993). Characterization of the adenosine triphosphatase activity of Chinese hamster P-glycoprotein. *Journal of Biological Chemistry, 268*(6), 4197-4206.

Aller, S. G., Yu, J., Ward, A., Weng, Y., Chittaboina, S., Zhuo, R., Harrell, P. M., Trinh, Y. T., Zhang, Q., Urbatsch, I. L., & Chang, G. (2009). Structure of P-glycoprotein reveals a molecular basis for poly-specific drug binding. *Science, 323*(5922), 1718-1722.

Ambudkar, S. V., Kim, I.-W., Xia, D., & Sauna, Z. E. (2006). The A-loop, a novel conserved aromatic acid subdomain upstream of the Walker A motif in ABC transporters, is critical for ATP binding. *FEBS Letters, 580*(4), 1049-1055.

Ambudkar, S. V., Kim, I. W., & Sauna, Z. E. (2006). The power of the pump: mechanisms of action of P-glycoprotein (ABCB1). *Eur J Pharm Sci, 27*(5), 392-400.

Ambudkar, S. V., Lelong, I. H., Zhang, J., Cardarelli, C. O., Gottesman, M. M., & Pastan, I. (1992). Partial purification and reconstitution of the human multidrug-resistance pump: characterization of the drug-stimulatable ATP hydrolysis. *Proc Natl Acad Sci U S A, 89*(18), 8472-8476.

Amin, A. S., Tan, H. L., & Wilde, A. A. (2010). Cardiac ion channels in health and disease. *Heart Rhythm, 7*(1), 117-126.

Aszalos, A. (2007). Drug–drug interactions affected by the transporter protein, P-glycoprotein (ABCB1, MDR1): II. Clinical aspects. *Drug Discovery Today, 12*(19–20), 838-843.

Ataullakhanov, F. I., & Vitvitsky, V. M. (2002). What determines the intracellular ATP concentration. *Biosci Rep, 22*(5-6), 501-511.

Atlas, S. A. (2007). The renin-angiotensin aldosterone system: pathophysiological role and pharmacologic inhibition. *J Manag Care Pharm, 13*(8 Suppl B), 9-20.

Aulabaugh, A. E., Crouch, R. C., Martin, G. E., Ragouzeos, A., Shockcor, J. P., Spitzer, T. D., Farrant, R. D., Hudson, B. D., & Lindon, J. C. (1992). The conformational behaviour of the

cardiac glycoside digoxin as indicated by NMR spectroscopy and molecular dynamics calculations. *Carbohydr Res, 230*(2), 201-212.

Aw, R., & Polizzi, K. M. (2013). Can too many copies spoil the broth? *Microbial Cell Factories, 12*(1), 128.

Bai, J., Swartz, D. J., Protasevich, II, Brouillette, C. G., Harrell, P. M., Hildebrandt, E., Gasser, B., Mattanovich, D., Ward, A., Chang, G., & Urbatsch, I. L. (2011). A gene optimization strategy that enhances production of fully functional P-glycoprotein in Pichia pastoris. *PLoS One, 6*(8), e22577.

Bailey, D. G., & Dresser, G. K. (2004). Interactions between grapefruit juice and cardiovascular drugs. *Am J Cardiovasc Drugs, 4*(5), 281-297.

Baker, A. F., & Dorr, R. T. (2001). Drug interactions with the taxanes: clinical implications. *Cancer Treat Rev, 27*(4), 221-233.

Baltes, S., Gastens, A. M., Fedrowitz, M., Potschka, H., Kaever, V., & Loscher, W. (2007). Differences in the transport of the antiepileptic drugs phenytoin, levetiracetam and carbamazepine by human and mouse P-glycoprotein. *Neuropharmacology, 52*(2), 333-346.

Bas, D. C., Rogers, D. M., & Jensen, J. H. (2008). Very fast prediction and rationalization of pKa values for protein–ligand complexes. *Proteins: Structure, Function, and Bioinformatics, 73*(3), 765-783.

Beaudet, L., & Gros, P. (1995). Functional dissection of P-glycoprotein nucleotide-binding domains in chimeric and mutant proteins. Modulation of drug resistance profiles. *J Biol Chem, 270*(29), 17159-17170.

Becker, J. P., Depret, G., Van Bambeke, F., Tulkens, P. M., & Prevost, M. (2009). Molecular models of human P-glycoprotein in two different catalytic states. *BMC Struct Biol, 9*, 3.

Becquemont, L., Funck-Brentano, C., & Jaillon, P. (1999). Mibefradil, a potent CYP3A inhibitor, does not alter pravastatin pharmacokinetics. *Fundam Clin Pharmacol, 13*(2), 232-236.

Borgnia, M. J., Eytan, G. D., & Assaraf, Y. G. (1996). Competition of hydrophobic peptides, cytotoxic drugs, and chemosensitizers on a common P-glycoprotein pharmacophore as revealed by its ATPase activity. *J Biol Chem, 271*(6), 3163-3171.

Boumendjel, A. n., Boutonnat, J., & Robert, J. (2009). *ABC transporters and multidrug resistance*. Hoboken, N.J.: John Wiley & Sons.

Bruggemann, E. P., Currier, S. J., Gottesman, M. M., & Pastan, I. (1992). Characterization of the azidopine and vinblastine binding site of P-glycoprotein. *J Biol Chem, 267*(29), 21020-21026.

Brünger, A. T., Adams, P. D., Clore, G. M., DeLano, W. L., Gros, P., Grosse-Kunstleve, R. W., Jiang, J.-S., Kuszewski, J., Nilges, M., & Pannu, N. S. (1998). Crystallography & NMR system:

a new software suite for macromolecular structure determination. *Acta Crystallographica Section D: Biological Crystallography, 54*(5), 905-921.

Buckley, N., Dawson, A., & Whyte, I. (2007). Calcium channel blockers. *Medicine, 35*(11), 599-602.

Callaghan, R. (2015). Providing a molecular mechanism for P-glycoprotein; why would I bother? *Biochem Soc Trans, 43*(5), 995-1002.

Cameron, M. D., Wen, B., Roberts, A. G., Atkins, W. M., Campbell, A. P., & Nelson, S. D. (2007). Cooperative binding of acetaminophen and caffeine within the P450 3A4 active site. *Chem Res Toxicol, 20*(10), 1434-1441.

Cao, X., Yu, L. X., Barbaciru, C., Landowski, C. P., Shin, H. C., Gibbs, S., Miller, H. A., Amidon, G. L., & Sun, D. (2005). Permeability dominates in vivo intestinal absorption of P-gp substrate with high solubility and high permeability. *Mol Pharm, 2*(4), 329-340.

Carr, H. Y., & Purcell, E. M. (1954). Effects of Diffusion on Free Precession in Nuclear Magnetic Resonance Experiments. *Physical Review, 94*(3), 630-638.

Cascorbi, I., Paul, M., & Kroemer, H. K. (2004). Pharmacogenomics of heart failure -- focus on drug disposition and action. *Cardiovasc Res, 64*(1), 32-39.

Catterall, W. A. (2011). Voltage-gated calcium channels. *Cold Spring Harb Perspect Biol, 3*(8), a003947.

Cavet, M. E., West, M., & Simmons, N. L. (1996). Transport and epithelial secretion of the cardiac glycoside, digoxin, by human intestinal epithelial (Caco-2) cells. *Br J Pharmacol, 118*(6), 1389-1396.

Ceckova-Novotna, M., Pavek, P., & Staud, F. (2006). P-glycoprotein in the placenta: expression, localization, regulation and function. *Reprod Toxicol, 22*(3), 400-410.

Chifflet, S., Torriglia, A., Chiesa, R., & Tolosa, S. (1988). A method for the determination of inorganic phosphate in the presence of labile organic phosphate and high concentrations of protein: application to lens ATPases. *Anal Biochem, 168*(1), 1-4.

Choi, K., Chen, C.-j., Kriegler, M., & Roninson, I. B. (1988). An altered pattern of cross-resistance in multidrug-resistant human cells results from spontaneous mutations in the mdr1 (P-glycoprotein) gene. *Cell, 53*(4), 519-529.

Chung, F. S., Eyal, S., Muzi, M., Link, J. M., Mankoff, D. A., Kaddoumi, A., O'Sullivan, F., Hsiao, P., & Unadkat, J. D. (2010). Positron emission tomography imaging of tissue P-glycoprotein activity during pregnancy in the non-human primate. *Br J Pharmacol, 159*(2), 394-404.

Chung, J. W., Yang, S. H., & Choi, J. S. (2010). Effects of lovastatin on the pharmacokinetics of nicardipine in rats. *Biopharm Drug Dispos, 31*(7), 436-441.

Claasen, B., Axmann, M., Meinecke, R., & Meyer, B. (2005). Direct observation of ligand binding to membrane proteins in living cells by a saturation transfer double difference (STDD) NMR spectroscopy method shows a significantly higher affinity of integrin $\alpha_{IIb}\beta_3$ in native platelets than in liposomes. *J Am Chem Soc, 127*(3), 916-919.

Clore, G. M. (2015). Practical Aspects of Paramagnetic Relaxation Enhancement in Biological Macromolecules. *Methods Enzymol, 564*, 485-497.

Clore, G. M., & Iwahara, J. (2009). Theory, practice, and applications of paramagnetic relaxation enhancement for the characterization of transient low-population states of biological macromolecules and their complexes. *Chem Rev, 109*(9), 4108-4139.

Cock, P. J., Antao, T., Chang, J. T., Chapman, B. A., Cox, C. J., Dalke, A., Friedberg, I., Hamelryck, T., Kauff, F., Wilczynski, B., & de Hoon, M. J. (2009). Biopython: freely available Python tools for computational molecular biology and bioinformatics. *Bioinformatics, 25*(11), 1422-1423.

Cook, P. F., & Cleland, W. W. (2007). *Enzyme kinetics and mechanism*. London; New York: Garland Science.

Couture, L., Nash, J. A., & Turgeon, J. (2006). The ATP-binding cassette transporters and their implication in drug disposition: a special look at the heart. *Pharmacol Rev, 58*(2), 244-258.

Davydov, D. R., Botchkareva, A. E., Davydova, N. E., & Halpert, J. R. (2005). Resolution of Two Substrate-Binding Sites in an Engineered Cytochrome P450eryF Bearing a Fluorescent Probe. *Biophys J, 89*(1), 418-432.

Dawson, R. J., Hollenstein, K., & Locher, K. P. (2007). Uptake or extrusion: crystal structures of full ABC transporters suggest a common mechanism. *Mol Microbiol, 65*(2), 250-257.

Dawson, R. J., & Locher, K. P. (2007). Structure of the multidrug ABC transporter Sav1866 from Staphylococcus aureus in complex with AMP-PNP. *FEBS Lett, 581*(5), 935-938.

de Vries, S. J., van Dijk, A. D., Krzeminski, M., van Dijk, M., Thureau, A., Hsu, V., Wassenaar, T., & Bonvin, A. M. (2007). HADDOCK versus HADDOCK: new features and performance of HADDOCK2.0 on the CAPRI targets. *Proteins, 69*(4), 726-733.

de Vries, S. J., van Dijk, M., & Bonvin, A. M. J. J. (2010). The HADDOCK web server for data-driven biomolecular docking. *Nat. Protocols, 5*(5), 883-897.

Dey, S., Ramachandra, M., Pastan, I., Gottesman, M. M., & Ambudkar, S. V. (1997). Evidence for two nonidentical drug-interaction sites in the human P-glycoprotein. *Proceedings of the National Academy of Sciences, 94*(20), 10594-10599.

Dimmeler, S. (2011). Cardiovascular disease review series. *EMBO Mol Med, 3*(12), 697.

Dixon, A. J., & Wall, G. C. (2001). Probable colchicine-induced neutropenia not related to intentional overdose. *Ann Pharmacother, 35*(2), 192-195.

Doige, C. A., Yu, X., & Sharom, F. J. (1993). The effects of lipids and detergents on ATPase-active P-glycoprotein. *Biochim Biophys Acta, 1146*(1), 65-72.

Dominguez, C., Boelens, R., & Bonvin, A. M. (2003). HADDOCK: a protein-protein docking approach based on biochemical or biophysical information. *J Am Chem Soc, 125*(7), 1731-1737.

Doppenschmitt, S., Spahn-Langguth, H., Regardh, C. G., & Langguth, P. (1998). Radioligand-binding assay employing P-glycoprotein-overexpressing cells: testing drug affinities to the secretory intestinal multidrug transporter. *Pharm Res, 15*(7), 1001-1006.

Dunn, B., & Wobbe, C. R. (2001). Preparation of protein extracts from yeast. *Curr Protoc Mol Biol, Chapter 13*, Unit13 13.

Edwards, D. J., Lavoie, R., Beckman, H., Blevins, R., & Rubenfire, M. (1987). The effect of coadministration of verapamil on the pharmacokinetics and metabolism of quinidine. *Clin Pharmacol Ther, 41*(1), 68-73.

Ehle, M., Patel, C., & Giugliano, R. P. (2011). Digoxin: clinical highlights: a review of digoxin and its use in contemporary medicine. *Crit Pathw Cardiol, 10*(2), 93-98.

Eijkelkamp, N., Linley, J. E., Baker, M. D., Minett, M. S., Cregg, R., Werdehausen, R., Rugiero, F., & Wood, J. N. (2012). Neurological perspectives on voltage-gated sodium channels. *Brain, 135*(Pt 9), 2585-2612.

Elsby, R., Surry, D. D., Smith, V. N., & Gray, A. J. (2008). Validation and application of Caco-2 assays for the in vitro evaluation of development candidate drugs as substrates or inhibitors of P-glycoprotein to support regulatory submissions. *Xenobiotica, 38*(7-8), 1140-1164.

Elsherbiny, M. E., El-Kadi, A. O., & Brocks, D. R. (2008). The metabolism of amiodarone by various CYP isoenzymes of human and rat, and the inhibitory influence of ketoconazole. *J Pharm Pharm Sci, 11*(1), 147-159.

Emi, Y., Tsunashima, D., Ogawara, K.-I., Higaki, K., & Kimura, T. (1998). Role of P-glycoprotein as a secretory mechanism in quinidine absorption from rat small intestine. *Journal of Pharmaceutical Sciences, 87*(3), 295-299.

Englund, G., Hallberg, P., Artursson, P., Michaelsson, K., & Melhus, H. (2004). Association between the number of coadministered P-glycoprotein inhibitors and serum digoxin levels in patients on therapeutic drug monitoring. *BMC Med, 2*, 8.

Esser, L., Zhou, F., Pluchino, K. M., Shiloach, J., Ma, J., Tang, W. K., Gutierrez, C., Zhang, A., Shukla, S., Madigan, J. P., Zhou, T., Kwong, P. D., Ambudkar, S. V., Gottesman, M. M., & Xia, D. (2017). Structures of the Multidrug Transporter P-glycoprotein Reveal Asymmetric ATP Binding and the Mechanism of Polyspecificity. *J Biol Chem, 292*(2), 446-461.

Eyal, S., Hsiao, P., & Unadkat, J. D. (2009). Drug interactions at the blood-brain barrier: fact or fantasy? *Pharmacol Ther, 123*(1), 80-104.

Faassen, F., Vogel, G., Spanings, H., & Vromans, H. (2003). Caco-2 permeability, P-glycoprotein transport ratios and brain penetration of heterocyclic drugs. *Int J Pharm, 263*(1-2), 113-122.

Feng, Q., Wilke, R. A., & Baye, T. M. (2012). Individualized risk for statin-induced myopathy: current knowledge, emerging challenges and potential solutions. *Pharmacogenomics, 13*(5), 579-594.

Fenner, K. S., Troutman, M. D., Kempshall, S., Cook, J. A., Ware, J. A., Smith, D. A., & Lee, C. A. (2009). Drug–Drug interactions mediated through P-glycoprotein: Clinical relevance and in vitro–in vivo correlation using digoxin as a probe drug. *Clinical Pharmacology & Therapeutics, 85*(2), 173-181.

Fleckenstein, A. (1977). Specific pharmacology of calcium in myocardium, cardiac pacemakers, and vascular smooth muscle. *Annu Rev Pharmacol Toxicol, 17*, 149-166.

Frank, G., Shukla, S., Rao, P., Borgnia, M. J., Bartesaghi, A., Merk, A., Mobin, A., Esser, L., Earl, L. A., Gottesman, M. M., Xia, D., Ambudkar, S. V., & Subramaniam, S. (2016). Cryo-EM analysis of the conformational landscape of human P-glycoprotein (ABCB1) during its catalytic cycle. *Molecular Pharmacology*.

Fromm, M. F., Kim, R. B., Stein, C. M., Wilkinson, G. R., & Roden, D. M. (1999). Inhibition of P-glycoprotein-mediated drug transport: A unifying mechanism to explain the interaction between digoxin and quinidine [seecomments]. *Circulation, 99*(4), 552-557.

Fuerstenwerth, H. (2014). On the differences between ouabain and digitalis glycosides. *Am J Ther, 21*(1), 35-42.

Gajewski, C. D., Yang, L., Schon, E. A., & Manfredi, G. (2003). New Insights into the Bioenergetics of Mitochondrial Disorders Using Intracellular ATP Reporters. *Molecular Biology of the Cell, 14*(9), 3628-3635.

Gatlik-Landwojtowicz, E., Aanismaa, P., & Seelig, A. (2006). Quantification and characterization of P-glycoprotein-substrate interactions. *Biochemistry, 45*(9), 3020-3032.

Gholami, K., Ziaie, S., & Shalviri, G. (2008). Adverse drug reactions induced by cardiovascular drugs in outpatients. *Pharm Pract (Granada), 6*(1), 51-55.

Giacomini, K. M., Huang, S. M., Tweedie, D. J., Benet, L. Z., Brouwer, K. L., Chu, X., Dahlin, A., Evers, R., Fischer, V., Hillgren, K. M., Hoffmaster, K. A., Ishikawa, T., Keppler, D., Kim, R. B., Lee, C. A., Niemi, M., Polli, J. W., Sugiyama, Y., Swaan, P. W., Ware, J. A., Wright, S. H., Yee, S. W., Zamek-Gliszczynski, M. J., & Zhang, L. (2010). Membrane transporters in drug development. *Nat Rev Drug Discov, 9*(3), 215-236.

Giovannitti, J. A., Jr., Thoms, S. M., & Crawford, J. J. (2015). Alpha-2 adrenergic receptor agonists: a review of current clinical applications. *Anesth Prog, 62*(1), 31-39.

Giudicessi, J. R., & Ackerman, M. J. (2012). Potassium-channel mutations and cardiac arrhythmias--diagnosis and therapy. *Nat Rev Cardiol, 9*(6), 319-332.

Glaeser, H. (2011). Importance of P-glycoprotein for drug-drug interactions. *Handb Exp Pharmacol*(201), 285-297.

Gordon, M., & Goldenberg, L. M. (1986). Clinical digoxin toxicity in the aged in association with co-administered verapamil. A report of two cases and review of the literature. *J Am Geriatr Soc, 34*(9), 659-662.

Gottesman, M. M., & Ling, V. (2006). The molecular basis of multidrug resistance in cancer: The early years of P-glycoprotein research. *FEBS Letters, 580*(4), 998-1009.

Gould, B. A., Mann, S., Kieso, H., Subramanian, V. B., & Raftery, E. B. (1982). The 24-hour ambulatory blood pressure profile with verapamil. *Circulation, 65*(1), 22-27.

Gozalpour, E., Wilmer, M. J., Bilos, A., Masereeuw, R., Russel, F. G., & Koenderink, J. B. (2016). Heterogeneous transport of digitalis-like compounds by P-glycoprotein in vesicular and cellular assays. *Toxicol In Vitro, 32*, 138-145.

Gozalpour, E., Wittgen, H. G., van den Heuvel, J. J., Greupink, R., Russel, F. G., & Koenderink, J. B. (2013). Interaction of digitalis-like compounds with p-glycoprotein. *Toxicol Sci, 131*(2), 502-511.

Grant, A. O. (2009). Cardiac ion channels. *Circ Arrhythm Electrophysiol, 2*(2), 185-194.

Greenberger, L. M. (1993). Major photoaffinity drug labeling sites for iodoaryl azidoprazosin in P-glycoprotein are within, or immediately C-terminal to, transmembrane domains 6 and 12. *Journal of Biological Chemistry, 268*(15), 11417-11425.

Gribble, F. M., Loussouarn, G., Tucker, S. J., Zhao, C., Nichols, C. G., & Ashcroft, F. M. (2000). A novel method for measurement of submembrane ATP concentration. *J Biol Chem, 275*(39), 30046-30049.

Gueron, M. (1975). Nuclear relaxation in macromolecules by paramagnetic ions: a novel mechanism. *Journal of Magnetic Resonance (1969), 19*(1), 58-66.

Hafkemeyer, P., Dey, S., Ambudkar, S. V., Hrycyna, C. A., Pastan, I., & Gottesman, M. M. (1998). Contribution to substrate specificity and transport of nonconserved residues in transmembrane domain 12 of human P-glycoprotein. *Biochemistry, 37*(46), 16400-16409.

Hansen, T. S., & Nilsen, O. G. (2009). Echinacea purpurea and P-glycoprotein drug transport in Caco-2 cells. *Phytother Res, 23*(1), 86-91.

Hanwell, M. D., Curtis, D. E., Lonie, D. C., Vandermeersch, T., Zurek, E., & Hutchison, G. R. (2012). Avogadro: an advanced semantic chemical editor, visualization, and analysis platform. *J Cheminform, 4*(1), 17.

Harter, K., Levine, M., & Henderson, S. O. (2015). Anticoagulation drug therapy: a review. *West J Emerg Med, 16*(1), 11-17.

Hartter, S., Sennewald, R., Nehmiz, G., & Reilly, P. (2013). Oral bioavailability of dabigatran etexilate (Pradaxa((R))) after co-medication with verapamil in healthy subjects. *Br J Clin Pharmacol, 75*(4), 1053-1062.

Haselhorst, T., Munster-Kuhnel, A. K., Oschlies, M., Tiralongo, J., Gerardy-Schahn, R., & von Itzstein, M. (2007). Direct detection of ligand binding to Sepharose-immobilised protein using saturation transfer double difference (STDD) NMR spectroscopy. *Biochem Biophys Res Commun, 359*(4), 866-870.

Haslam, I. S., Jones, K., Coleman, T., & Simmons, N. L. (2008). Induction of P-glycoprotein expression and function in human intestinal epithelial cells (T84). *Biochem Pharmacol, 76*(7), 850-861.

Hauptman, P. J., & Kelly, R. A. (1999). Digitalis. *Circulation, 99*(9), 1265-1270.

Helfand, M., Peterson, K., Christensen, V., Dana, T., & Thakurta, S. (2009) *Drug Class Review: Beta Adrenergic Blockers: Final Report Update 4*. Portland (OR).

Hennig, J., de Vries, S. J., Hennig, K. D., Randles, L., Walters, K. J., Sunnerhagen, M., & Bonvin, A. M. (2012). MTMDAT-HADDOCK: high-throughput, protein complex structure modeling based on limited proteolysis and mass spectrometry. *BMC Struct Biol, 12*, 29.

Ho, W. S., Davis, A. J., Chadha, P. S., & Greenwood, I. A. (2013). Effective contractile response to voltage-gated Na+ channels revealed by a channel activator. *Am J Physiol Cell Physiol, 304*(8), C739-747.

Hochman, J. H., Pudvah, N., Qiu, J., Yamazaki, M., Tang, C., Lin, J. H., & Prueksaritanont, T. (2004). Interactions of human P-glycoprotein with simvastatin, simvastatin acid, and atorvastatin. *Pharm Res, 21*(9), 1686-1691.

Hohenblum, H., Gasser, B., Maurer, M., Borth, N., & Mattanovich, D. (2004). Effects of gene dosage, promoters, and substrates on unfolded protein stress of recombinant Pichia pastoris. *Biotechnol Bioeng, 85*.

Hohl, M., Hurlimann, L. M., Bohm, S., Schoppe, J., Grutter, M. G., Bordignon, E., & Seeger, M. A. (2014). Structural basis for allosteric cross-talk between the asymmetric nucleotide binding sites of a heterodimeric ABC exporter. *Proc Natl Acad Sci U S A, 111*(30), 11025-11030.

Holcberg, G., Sapir, O., Tsadkin, M., Huleihel, M., Lazer, S., Katz, M., Mazor, M., & Ben-Zvi, Z. (2003). Lack of interaction of digoxin and P-glycoprotein inhibitors, quinidine and verapamil in human placenta in vitro. *Eur J Obstet Gynecol Reprod Biol, 109*(2), 133-137.

Holtzman, C. W., Wiggins, B. S., & Spinler, S. A. (2006). Role of P-glycoprotein in Statin Drug Interactions. *Pharmacotherapy: The Journal of Human Pharmacology and Drug Therapy, 26*(11), 1601-1607.

Hoops, S., Sahle, S., Gauges, R., Lee, C., Pahle, J., Simus, N., Singhal, M., Xu, L., Mendes, P., & Kummer, U. (2006). COPASI--a COmplex PAthway SImulator. *Bioinformatics, 22*(24), 3067-3074.

Horie, A., Ishida, K., Shibata, K., Taguchi, M., Ozawa, A., Hirono, K., Ichida, F., & Hashimoto, Y. (2014). Pharmacokinetic variability of flecainide in younger Japanese patients and mechanisms for renal excretion and intestinal absorption. *Biopharm Drug Dispos, 35*(3), 145-153.

Hrycyna, C. A., Ramachandra, M., Germann, U. A., Cheng, P. W., Pastan, I., & Gottesman, M. M. (1999). Both ATP sites of human P-glycoprotein are essential but not symmetric. *Biochemistry, 38*(42), 13887-13899.

Huang, H., Zhang, X., Li, S., Liu, N., Lian, W., McDowell, E., Zhou, P., Zhao, C., Guo, H., Zhang, C., Yang, C., Wen, G., Dong, X., Lu, L., Ma, N., Dong, W., Dou, Q. P., Wang, X., & Liu, J. (2010). Physiological levels of ATP negatively regulate proteasome function. *Cell Res, 20*(12), 1372-1385.

Hunt, G., & Bruera, E. (1995). Respiratory depression in a patient receiving oral methadone for cancer pain. *J Pain Symptom Manage, 10*(5), 401-404.

International Transporter, C., Giacomini, K. M., Huang, S. M., Tweedie, D. J., Benet, L. Z., Brouwer, K. L., Chu, X., Dahlin, A., Evers, R., Fischer, V., Hillgren, K. M., Hoffmaster, K. A., Ishikawa, T., Keppler, D., Kim, R. B., Lee, C. A., Niemi, M., Polli, J. W., Sugiyama, Y., Swaan, P. W., Ware, J. A., Wright, S. H., Yee, S. W., Zamek-Gliszczynski, M. J., & Zhang, L. (2010). Membrane transporters in drug development. *Nat Rev Drug Discov, 9*(3), 215-236.

Ito, S., Woodland, C., Harper, P. A., & Koren, G. (1993). The mechanism of the verapamil-digoxin interaction in renal tubular cells (LLC-PK1). *Life Sci, 53*(24), PL399-403.

Iwahara, J., Schwieters, C. D., & Clore, G. M. (2004). Ensemble approach for NMR structure refinement against (1)H paramagnetic relaxation enhancement data arising from a flexible paramagnetic group attached to a macromolecule. *J Am Chem Soc, 126*(18), 5879-5896.

Iwahara, J., Tang, C., & Marius Clore, G. (2007). Practical aspects of 1H transverse paramagnetic relaxation enhancement measurements on macromolecules. *Journal of Magnetic Resonance, 184*(2), 185-195.

Jacobson, T. A. (2004). Comparative pharmacokinetic interaction profiles of pravastatin, simvastatin, and atorvastatin when coadministered with cytochrome P450 inhibitors. *The American Journal of Cardiology, 94*(9), 1140-1146.

Jensen, B. C., O'Connell, T. D., & Simpson, P. C. (2011). Alpha-1-adrenergic receptors: targets for agonist drugs to treat heart failure. *J Mol Cell Cardiol, 51*(4), 518-528.

Jin, M. S., Oldham, M. L., Zhang, Q., & Chen, J. (2012). Crystal structure of the multidrug transporter P-glycoprotein from Caenorhabditis elegans. *Nature, 490*(7421), 566-569.

Johannessen, S. I., & Landmark, C. J. (2010). Antiepileptic drug interactions - principles and clinical implications. *Curr Neuropharmacol, 8*(3), 254-267.

Johnson, C. S. (1999). Diffusion ordered nuclear magnetic resonance spectroscopy: principles and applications. *Progress in Nuclear Magnetic Resonance Spectroscopy, 34*(3), 203-256.

Juliano, R. L., & Ling, V. (1976). A surface glycoprotein modulating drug permeability in Chinese hamster ovary cell mutants. *Biochimica et Biophysica Acta (BBA) - Biomembranes, 455*(1), 152-162.

Kakumoto, M., Takara, K., Sakaeda, T., Tanigawara, Y., Kita, T., & Okumura, K. (2002). MDR1-mediated interaction of digoxin with antiarrhythmic or antianginal drugs. *Biol Pharm Bull, 25*(12), 1604-1607.

Kantor, E. D., Rehm, C. D., Haas, J. S., Chan, A. T., & Giovannucci, E. L. (2015). TRends in prescription drug use among adults in the united states from 1999-2012. *JAMA, 314*(17), 1818-1830.

Karimzadeh, I., Namazi, S., Shalviri, G., & Gholami, K. (2011). Cardiovascular drug adverse reactions in hospitalized patients in cardiac care unit. *African Journal of Pharmacy and Pharmacology, 5*(4), 493-499.

Katoh, M., Nakajima, M., Yamazaki, H., & Yokoi, T. (2001). Inhibitory effects of CYP3A4 substrates and their metabolites on P-glycoprotein-mediated transport. *European Journal of Pharmaceutical Sciences, 12*(4), 505-513.

Ke, A. B., Eyal, S., Chung, F. S., Link, J. M., Mankoff, D. A., Muzi, M., & Unadkat, J. D. (2013). Modeling cyclosporine A inhibition of the distribution of a P-glycoprotein PET ligand, 11C-verapamil, into the maternal brain and fetal liver of the pregnant nonhuman primate: impact of tissue blood flow and site of inhibition. *J Nucl Med, 54*(3), 437-446.

Keefe, D. L. (2001). Anthracycline-induced cardiomyopathy. *Semin Oncol, 28*(4 Suppl 12), 2-7.

Kennedy, H. J., Pouli, A. E., Ainscow, E. K., Jouaville, L. S., Rizzuto, R., & Rutter, G. A. (1999). Glucose generates sub-plasma membrane ATP microdomains in single islet beta-cells. Potential role for strategically located mitochondria. *J Biol Chem, 274*(19), 13281-13291.

Kerr, K. M., Sauna, Z. E., & Ambudkar, S. V. (2001). Correlation between steady-state ATP hydrolysis and vanadate-induced ADP trapping in Human P-glycoprotein. Evidence for ADP release as the rate-limiting step in the catalytic cycle and its modulation by substrates. *J Biol Chem, 276*(12), 8657-8664.

Kharasch, E. D., Hoffer, C., Altuntas, T. G., & Whittington, D. (2004). Quinidine as a Probe for the Role of P-Glycoprotein in the Intestinal Absorption and Clinical Effects of Fentanyl. *The Journal of Clinical Pharmacology, 44*(3), 224-233.

Kharasch, E. D., Hoffer, C., & Whittington, D. (2004). The effect of quinidine, used as a probe for the involvement of P-glycoprotein, on the intestinal absorption and pharmacodynamics of methadone. *Br J Clin Pharmacol, 57*(5), 600-610.

Kim, J. B. (2014). Channelopathies. *Korean J Pediatr, 57*(1), 1-18.

Kim, S., Thiessen, P. A., Bolton, E. E., Chen, J., Fu, G., Gindulyte, A., Han, L., He, J., He, S., Shoemaker, B. A., Wang, J., Yu, B., Zhang, J., & Bryant, S. H. (2016). PubChem Substance and Compound databases. *Nucleic Acids Research, 44*(D1), D1202-D1213.

Kimoto, E., Seki, S., Itagaki, S., Matsuura, M., Kobayashi, M., Hirano, T., Goto, Y., Tadano, K., & Iseki, K. (2007). Efflux transport of N-monodesethylamiodarone by the human intestinal cell-line Caco-2 cells. *Drug Metab Pharmacokinet, 22*(4), 307-312.

Klein, H. O., Lang, R., Weiss, E., Di Segni, E., Libhaber, C., Guerrero, J., & Kaplinsky, E. (1982). The influence of verapamil on serum digoxin concentration. *Circulation, 65*(5), 998-1003.

Kowalewski, J., & Maler, L. (2006). *Nuclear spin relaxation in liquids: theory, experiments, and applications*: CRC press.

Kwan, T., & Gros, P. (1998). Mutational analysis of the P-glycoprotein first intracellular loop and flanking transmembrane domains. *Biochemistry, 37*(10), 3337-3350.

Laer, S., Scholz, H., Buschmann, I., Thoenes, M., & Meinertz, T. (1998). Digitoxin intoxication during concomitant use of amiodarone. *Eur J Clin Pharmacol, 54*(1), 95-96.

Lafuente-Lafuente, C., Alvarez, J. C., Leenhardt, A., Mouly, S., Extramiana, F., Caulin, C., Funck-Brentano, C., & Bergmann, J. F. (2009). Amiodarone concentrations in plasma and fat tissue during chronic treatment and related toxicity. *Br J Clin Pharmacol, 67*(5), 511-519.

Lakowicz, J. R. (1983). *Principles of fluorescence spectroscopy*. New York: Plenum Press.

Lakowicz, J. R. (1999). *Principles of fluorescence spectroscopy* (2nd ed.). New York: Kluwer Academic/Plenum.

Latini, R., Tognoni, G., & Kates, R. E. (1984). Clinical pharmacokinetics of amiodarone. *Clin Pharmacokinet, 9*(2), 136-156.

Lattuca, B., Khoueiry, Z., Malcles, G., Davy, J. M., & Leclercq, F. (2013). Drug interactions between non-steroidal anti-inflammatory drugs and cardiovascular treatments (except anti-agregant therapy). *Antiinflamm Antiallergy Agents Med Chem, 12*(1), 36-46.

Lawson, J., O'Mara, M. L., & Kerr, I. D. (2008). Structure-based interpretation of the mutagenesis database for the nucleotide binding domains of P-glycoprotein. *Biochim Biophys Acta, 1778*(2), 376-391.

Leach, A. R., & Hann, M. M. (2011). Molecular complexity and fragment-based drug discovery: ten years on. *Curr Opin Chem Biol, 15*(4), 489-496.

Leatherbarrow, R. J. (1990). Using linear and non-linear regression to fit biochemical data. *Trends in Biochemical Sciences, 15*(12), 455-458.

Ledwitch, K. V., Barnes, R. W., & Roberts, A. G. (2016). Unraveling the complex drug-drug Interactions of the cardiovascular drugs, verapamil and digoxin, with P-glycoprotein. *Bioscience Reports, 36*(2).

Ledwitch, K. V., Gibbs, M. E., Barnes, R. W., & Roberts, A. G. (2016). Cooperativity between verapamil and ATP bound to the efflux transporter P-glycoprotein. *Biochem Pharmacol, 118*, 96-108.

Ledwitch, K. V., & Roberts, A. G. (2016). Cardiovascular Ion Channel Inhibitor Drug-Drug Interactions with P-glycoprotein. *The AAPS Journal*, 1-12.

Lefkowitz, J. M., & Shapiro, M. (1986). Quinine-induced thrombocytopenia. *Can Fam Physician, 32*, 1949-1953.

Leist, M., Single, B., Castoldi, A. F., Kuhnle, S., & Nicotera, P. (1997). Intracellular adenosine triphosphate (ATP) concentration: a switch in the decision between apoptosis and necrosis. *J Exp Med, 185*(8), 1481-1486.

Lerner-Marmarosh, N., Gimi, K., Urbatsch, I. L., Gros, P., & Senior, A. E. (1999). Large scale purification of detergent-soluble P-glycoprotein from Pichia pastoris cells and characterization of nucleotide binding properties of wild-type, Walker A, and Walker B mutant proteins. *J Biol Chem, 274*(49), 34711-34718.

Leuranguer, V., Mangoni, M. E., Nargeot, J., & Richard, S. (2001). Inhibition of T-type and L-type calcium channels by mibefradil: physiologic and pharmacologic bases of cardiovascular effects. *J Cardiovasc Pharmacol, 37*(6), 649-661.

Lewis, G. P., & Holtzman, J. L. (1984). Interaction of flecainide with digoxin and propranolol. *Am J Cardiol, 53*(5), 52B-57B.

Lewis, G. R., Morley, K. D., Lewis, B. M., & Bones, P. J. (1978). The treatment of hypertension with verapamil. *N Z Med J, 87*(612), 351-354.

Lewis, G. R., Morley, K. D., Maslowski, A. H., & Bones, P. J. (1979). Verapamil in the management of hypertensive patients. *Aust N Z J Med, 9*(1), 62-64.

Li, J., Jaimes, K. F., & Aller, S. G. (2014). Refined structures of mouse P-glycoprotein. *Protein Sci, 23*(1), 34-46.

Li, P., Roberts, B. P., Chakravorty, D. K., & Merz, K. M., Jr. (2013). Rational Design of Particle Mesh Ewald Compatible Lennard-Jones Parameters for +2 Metal Cations in Explicit Solvent. *J Chem Theory Comput, 9*(6), 2733-2748.

Liesenfeld, K. H., Lehr, T., Dansirikul, C., Reilly, P. A., Connolly, S. J., Ezekowitz, M. D., Yusuf, S., Wallentin, L., Haertter, S., & Staab, A. (2011). Population pharmacokinetic analysis of the oral thrombin inhibitor dabigatran etexilate in patients with non-valvular atrial fibrillation from the RE-LY trial. *J Thromb Haemost, 9*(11), 2168-2175.

Lin, J. H., & Yamazaki, M. (2003). Role of P-glycoprotein in pharmacokinetics: clinical implications. *Clin Pharmacokinet, 42*(1), 59-98.

Linge, J. P., & Nilges, M. (1999). Influence of non-bonded parameters on the quality of NMR structures: a new force field for NMR structure calculation. *J Biomol NMR, 13*(1), 51-59.

Lipari, G., & Szabo, A. (1981). Nuclear magnetic resonance relaxation in nucleic acid fragments: models for internal motion. *Biochemistry, 20*(21), 6250-6256.

Litman, T., Nielsen, D., Skovsgaard, T., Zeuthen, T., & Stein, W. D. (1997). ATPase activity of P-glycoprotein related to emergence of drug resistance in Ehrlich ascites tumor cell lines. *Biochim Biophys Acta, 1361*(2), 147-158.

Litman, T., Zeuthen, T., Skovsgaard, T., & Stein, W. D. (1997a). Competitive, non-competitive and cooperative interactions between substrates of P-glycoprotein as measured by its ATPase activity. *Biochim Biophys Acta, 1361*(2), 169-176.

Litman, T., Zeuthen, T., Skovsgaard, T., & Stein, W. D. (1997b). Structure-activity relationships of P-glycoprotein interacting drugs: kinetic characterization of their effects on ATPase activity. *Biochim Biophys Acta, 1361*(2), 159-168.

Liu, R., Siemiarczuk, A., & Sharom, F. J. (2000). Intrinsic fluorescence of the P-glycoprotein multidrug transporter: sensitivity of tryptophan residues to binding of drugs and nucleotides. *Biochemistry, 39*(48), 14927-14938.

Loo, T. W., Bartlett, M. C., & Clarke, D. M. (2002). The "LSGGQ" motif in each nucleotide-binding domain of human P-glycoprotein is adjacent to the opposing walker A sequence. *J Biol Chem, 277*(44), 41303-41306.

Loo, T. W., Bartlett, M. C., & Clarke, D. M. (2003a). Drug binding in human P-glycoprotein causes conformational changes in both nucleotide-binding domains. *J Biol Chem, 278*(3), 1575-1578.

Loo, T. W., Bartlett, M. C., & Clarke, D. M. (2003b). Permanent activation of the human P-glycoprotein by covalent modification of a residue in the drug-binding site. *J Biol Chem, 278*(23), 20449-20452.

Loo, T. W., Bartlett, M. C., & Clarke, D. M. (2003c). Simultaneous binding of two different drugs in the binding pocket of the human multidrug resistance P-glycoprotein. *J Biol Chem, 278*(41), 39706-39710.

Loo, T. W., Bartlett, M. C., Detty, M. R., & Clarke, D. M. (2012). The ATPase activity of the P-glycoprotein drug pump is highly activated when the N-terminal and central regions of the nucleotide-binding domains are linked closely together. *J Biol Chem, 287*(32), 26806-26816.

Loo, T. W., & Clarke, D. M. (1994). Functional consequences of glycine mutations in the predicted cytoplasmic loops of P-glycoprotein. *Journal of Biological Chemistry, 269*(10), 7243-7248.

Loo, T. W., & Clarke, D. M. (1995). Membrane Topology of a Cysteine-less Mutant of Human P-glycoprotein. *Journal of Biological Chemistry, 270*(2), 843-848.

Loo, T. W., & Clarke, D. M. (1996). Inhibition of oxidative cross-linking between engineered cysteine residues at positions 332 in predicted transmembrane segments (TM) 6 and 975 in predicted TM12 of human P-glycoprotein by drug substrates. *J Biol Chem, 271*(44), 27482-27487.

Loo, T. W., & Clarke, D. M. (1997). Drug-stimulated ATPase Activity of Human P-glycoprotein Requires Movement between Transmembrane Segments 6 and 12. *Journal of Biological Chemistry, 272*(34), 20986-20989.

Loo, T. W., & Clarke, D. M. (2015). Mapping the Binding Site of the Inhibitor Tariquidar That Stabilizes the First Transmembrane Domain of P-glycoprotein. *J Biol Chem, 290*(49), 29389-29401.

Loo, T. W., & Clarke, D. M. (2017). Thiol-reactive drug substrates of human P-glycoprotein label the same sites to activate ATPase activity in membranes or dodecyl maltoside detergent micelles. *Biochem Biophys Res Commun, 488*(4), 573-577.

Lowes, S., Cavet, M. E., & Simmons, N. L. (2003). Evidence for a non-MDR1 component in digoxin secretion by human intestinal Caco-2 epithelial layers. *Eur J Pharmacol, 458*(1-2), 49-56.

Luepker, R. V. (2011). Cardiovascular disease: rise, fall, and future prospects. *Annu Rev Public Health, 32*, 1-3.

Lum, B. L., & Gosland, M. P. (1995). MDR expression in normal tissues. Pharmacologic implications for the clinical use of P-glycoprotein inhibitors. *Hematol Oncol Clin North Am, 9*(2), 319-336.

Maccotta, A., Scibona, G., Valensin, G., Gaggelli, E., Botre, F., & Botre, C. (1991a). Nuclear magnetic resonance investigations of calcium antagonist drugs. II: Conformational and dynamic features of verapamil in [2H6]DMSO. *J Pharm Sci, 80*(6), 586-589.

Maccotta, A., Scibona, G., Valensin, G., Gaggelli, E., Botre, F., & Botre, C. (1991b). Nuclear magnetic resonance investigations of calcium antagonist drugs. II: Conformational and dynamic features of verapamil in [2H6]DMSO. *Journal of Pharmaceutical Sciences, 80*(6), 586-589.

Mahar Doan, K. M., Humphreys, J. E., Webster, L. O., Wring, S. A., Shampine, L. J., Serabjit-Singh, C. J., Adkison, K. K., & Polli, J. W. (2002). Passive permeability and P-glycoprotein-mediated efflux differentiate central nervous system (CNS) and non-CNS marketed drugs. *J Pharmacol Exp Ther, 303*(3), 1029-1037.

Maines, L. W., Antonetti, D. A., Wolpert, E. B., & Smith, C. D. (2005). Evaluation of the role of P-glycoprotein in the uptake of paroxetine, clozapine, phenytoin and carbamazapine by bovine retinal endothelial cells. *Neuropharmacology, 49*(5), 610-617.

Makinson, A., Martelli, N., Peyriere, H., Turriere, C., Le Moing, V., & Reynes, J. (2007). Profound neutropenia resulting from interaction between antiretroviral therapy and vinblastine in a patient with HIV-associated Hodgkin's disease. *Eur J Haematol, 78*(4), 358-360.

Manfredi, G., Yang, L., Gajewski, C. D., & Mattiazzi, M. (2002). Measurements of ATP in mammalian cells. *Methods, 26*(4), 317-326.

Marchetti, S., Mazzanti, R., Beijnen, J. H., & Schellens, J. H. (2007). Concise review: Clinical relevance of drug drug and herb drug interactions mediated by the ABC transporter ABCB1 (MDR1, P-glycoprotein). *Oncologist, 12*(8), 927-941.

Martens, J. R., & Gelband, C. H. (1998). Ion channels in vascular smooth muscle: alterations in essential hypertension. *Proc Soc Exp Biol Med, 218*(3), 192-203.

Martin, R. B. (1997). Disadvantages of Double Reciprocal Plots. *Journal of Chemical Education, 74*(10), 1238.

Mateti, U. V., Rajakannan, T., Nekkanti, H., Rajesh, V., Mallaysamy, S. R., & Ramachandran, P. (2011). Drug–drug interactions in hospitalized cardiac patients. *Journal of Young Pharmacists, 3*(4), 329-333.

Matsunaga, T., Kose, E., Yasuda, S., Ise, H., Ikeda, U., & Ohmori, S. (2006). Determination of p-glycoprotein ATPase activity using luciferase. *Biol Pharm Bull, 29*(3), 560-564.

Mayer, M., & Meyer, B. (2001a). Group epitope mapping by saturation transfer difference NMR to identify segments of a ligand in direct contact with a protein receptor. *Journal of the American Chemical Society, 123*(25), 6108-6117.

Mayer, M., & Meyer, B. (2001b). Group epitope mapping by saturation transfer difference NMR to identify segments of a ligand in direct contact with a protein receptor. *J Am Chem Soc, 123*(25), 6108-6117.

McDonagh, M. S., Eden, K. B., & Peterson, K. (2005). *Drug Class Review: Calcium Channel Blockers: Final Report*. Portland, OR.

Meiboom, S., & Gill, D. (1958). Modified Spin-Echo Method for Measuring Nuclear Relaxation Times. *Review of Scientific Instruments, 29*(8), 688-691.

Meissner, K., Sperker, B., Karsten, C., Meyer Zu Schwabedissen, H., Seeland, U., Bohm, M., Bien, S., Dazert, P., Kunert-Keil, C., Vogelgesang, S., Warzok, R., Siegmund, W., Cascorbi, I., Wendt, M., & Kroemer, H. K. (2002). Expression and localization of P-glycoprotein in human heart: effects of cardiomyopathy. *J Histochem Cytochem, 50*(10), 1351-1356.

Mendell, J., Zahir, H., Matsushima, N., Noveck, R., Lee, F., Chen, S., Zhang, G., & Shi, M. (2013). Drug-drug interaction studies of cardiovascular drugs involving P-glycoprotein, an efflux transporter, on the pharmacokinetics of edoxaban, an oral factor Xa inhibitor. *Am J Cardiovasc Drugs, 13*(5), 331-342.

Mohebbi, N., Shalviri, G., Salarifar, M., Salamzadeh, J., & Gholami, K. (2010). Adverse drug reactions induced by cardiovascular drugs in cardiovascular care unit patients. *Pharmacoepidemiology and Drug Safety, 19*(9), 889-894.

Mohebbi, N., Shalviri, G., Salarifar, M., Salamzadeh, J., & Gholami, K. (2010). Adverse drug reactions induced by cardiovascular drugs in cardiovascular care unit patients. *Pharmacoepidemiol Drug Saf, 19*(9), 889-894.

Morris, G. M., Huey, R., Lindstrom, W., Sanner, M. F., Belew, R. K., Goodsell, D. S., & Olson, A. J. (2009). AutoDock4 and AutoDockTools4: Automated docking with selective receptor flexibility. *J Comput Chem, 30*(16), 2785-2791.

Moss, A. J., Davis, H. T., Conard, D. L., DeCamilla, J. J., & Odoroff, C. L. (1981). Digitalis-associated cardiac mortality after myocardial infarction. *Circulation, 64*(6), 1150-1156.

Mowry, J. B., Spyker, D. A., Brooks, D. E., McMillan, N., & Schauben, J. L. (2015). 2014 Annual Report of the American Association of Poison Control Centers' National Poison Data System (NPDS): 32nd Annual Report. *Clin Toxicol (Phila), 53*(10), 962-1147.

Mui, B., Chow, L., & Hope, M. J. (2003). Extrusion technique to generate liposomes of defined size. *Methods Enzymol, 367*, 3-14.

Müller, M., Bakos, É., Welker, E., Váradi, A., Germann, U. A., Gottesman, M. M., Morse, B. S., Roninson, I. B., & Sarkadi, B. (1996). Altered Drug-stimulated ATPase Activity in Mutants of the Human Multidrug Resistance Protein. *Journal of Biological Chemistry, 271*(4), 1877-1883.

Munafo, A., Buclin, T., Tuto, D., & Biollaz, J. (1992). The effect of a low dose of quinidine on the disposition of flecainide in healthy volunteers. *Eur J Clin Pharmacol, 43*(4), 441-443.

Nagy, H., Goda, K., Arceci, R., Cianfriglia, M., Mechetner, E., & Szabo, G., Jr. (2001). P-Glycoprotein conformational changes detected by antibody competition. *Eur J Biochem, 268*(8), 2416-2420.

Neugebauer, G. (1978). Comparative cardiovascular actions of verapamil and its major metabolites in the anaesthetised dog. *Cardiovasc Res, 12*(4), 247-254.

Nicklisch, S. C., Rees, S. D., McGrath, A. P., Gokirmak, T., Bonito, L. T., Vermeer, L. M., Cregger, C., Loewen, G., Sandin, S., Chang, G., & Hamdoun, A. (2016). Global marine

pollutants inhibit P-glycoprotein: Environmental levels, inhibitory effects, and cocrystal structure. *Sci Adv, 2*(4), e1600001.

Nicolay, K., Braun, K. P., Graaf, R. A., Dijkhuizen, R. M., & Kruiskamp, M. J. (2001). Diffusion NMR spectroscopy. *NMR Biomed, 14*(2), 94-111.

Nishio, S., Watanabe, H., Kosuge, K., Uchida, S., Hayashi, H., & Ohashi, K. (2005). Interaction between amlodipine and simvastatin in patients with hypercholesterolemia and hypertension. *Hypertens Res, 28*(3), 223-227.

Omote, H., & Al-Shawi, M. K. (2002). A novel electron paramagnetic resonance approach to determine the mechanism of drug transport by P-glycoprotein. *J Biol Chem, 277*(47), 45688-45694.

Omote, H., Figler, R. A., Polar, M. K., & Al-Shawi, M. K. (2004). Improved energy coupling of human P-glycoprotein by the glycine 185 to valine mutation. *Biochemistry, 43*(13), 3917-3928.

Oostenbrink, C., Soares, T. A., van der Vegt, N. F., & van Gunsteren, W. F. (2005). Validation of the 53A6 GROMOS force field. *Eur Biophys J, 34*(4), 273-284.

Orlowski, S., Mir, L. M., Belehradek, J., Jr., & Garrigos, M. (1996). Effects of steroids and verapamil on P-glycoprotein ATPase activity: progesterone, desoxycorticosterone, corticosterone and verapamil are mutually non-exclusive modulators. *Biochem J, 317 (Pt 2)*, 515-522.

Owens, J. (2005). Drug resistance: Passing on protection. *Nat. Rev. Drug Discov., 4*, 191.

Padwal, R., Straus, S. E., & McAlister, F. A. (2001). Evidence based management of hypertension. Cardiovascular risk factors and their effects on the decision to treat hypertension: evidence based review. *BMJ, 322*(7292), 977-980.

Pan, A. Z., Dong, X. A., Zhang, S. J., Xiang, T., Chen, Z. X., & Lin, Y. W. (2013). [Study on mRNA and protein expressions of organic anion transporting polypeptide (oatp2b1) in rats with high fat diet and overstrain induced Pi deficiency syndrome]. *Zhongguo Zhong Xi Yi Jie He Za Zhi, 33*(7), 953-957.

Pang, K. S., Rodrigues, A. D., & Peter, R. M. (2010). *Enzyme- and transporter-based drug-drug Interactions : progress and future challenges*. New York: Springer.

Patel, C., Yan, G. X., & Kowey, P. R. (2009). Dronedarone. *Circulation, 120*(7), 636-644.

Pauli-Magnus, C., Murdter, T., Godel, A., Mettang, T., Eichelbaum, M., Klotz, U., & Fromm, M. F. (2001). P-glycoprotein-mediated transport of digitoxin, alpha-methyldigoxin and beta-acetyldigoxin. *Naunyn Schmiedebergs Arch Pharmacol, 363*(3), 337-343.

Pauli-Magnus, C., von Richter, O., Burk, O., Ziegler, A., Mettang, T., Eichelbaum, M., & Fromm, M. F. (2000). Characterization of the major metabolites of verapamil as substrates and inhibitors of P-glycoprotein. *J Pharmacol Exp Ther, 293*(2), 376-382.

Pedersen, K. E., Christiansen, B. D., Klitgaard, N. A., & Nielsen-Kudsk, F. (1983). Effect of quinidine on digoxin bioavailability. *Eur J Clin Pharmacol, 24*(1), 41-47.

Pedersen, K. E., Dorph-Pedersen, A., Hvidt, S., Klitgaard, N. A., & Nielsen-Kudsk, F. (1981). Digoxin-verapamil interaction. *Clin Pharmacol Ther, 30*(3), 311-316.

Pedersen, K. E., Dorph-Pedersen, A., Hvidt, S., Klitgaard, N. A., & Pedersen, K. K. (1982). The long-term effect of verapamil on plasma digoxin concentration and renal digoxin clearance in healthy subjects. *Eur J Clin Pharmacol, 22*(2), 123-127.

Pelta, M. D., Barjat, H., Morris, G. A., Davis, A. L., & Hammond, S. J. (1998). Pulse sequences for high-resolution diffusion-ordered spectroscopy (HR-DOSY). *Magnetic Resonance in Chemistry, 36*(10), 706-714.

Pereira, A., Pfeifer, T. A., Grigliatti, T. A., & Andersen, R. J. (2009). Functional cell-based screening and saturation transfer double-difference NMR have identified haplosamate A as a cannabinoid receptor agonist. *ACS Chem Biol, 4*(2), 139-144.

Piazza, G., Nguyen, T. N., Cios, D., Labreche, M., Hohlfelder, B., Fanikos, J., Fiumara, K., & Goldhaber, S. Z. (2011). Anticoagulation-associated adverse drug events. *Am J Med, 124*(12), 1136-1142.

Piotto, M., Saudek, V., & Sklenar, V. (1992). Gradient-tailored excitation for single-quantum NMR spectroscopy of aqueous solutions. *Journal of Biomolecular NMR, 2*(6), 661-665.

Piotto, M., Saudek, V., & Sklenář, V. (1992). Gradient-tailored excitation for single-quantum NMR spectroscopy of aqueous solutions. *Journal of Biomolecular NMR, 2*(6), 661-665.

Polli, J. W., Wring, S. A., Humphreys, J. E., Huang, L., Morgan, J. B., Webster, L. O., & Serabjit-Singh, C. S. (2001). Rational use of in vitro P-glycoprotein assays in drug discovery. *J Pharmacol Exp Ther, 299*(2), 620-628.

Potschka, H., & Loscher, W. (2001). In vivo evidence for P-glycoprotein-mediated transport of phenytoin at the blood-brain barrier of rats. *Epilepsia, 42*(10), 1231-1240.

Prueksaritanont, T., Chu, X., Gibson, C., Cui, D., Yee, K. L., Ballard, J., Cabalu, T., & Hochman, J. (2013). Drug-drug interaction studies: regulatory guidance and an industry perspective. *AAPS J, 15*(3), 629-645.

Qu, Q., Russell, P. L., & Sharom, F. J. (2003). Stoichiometry and affinity of nucleotide binding to P-glycoprotein during the catalytic cycle. *Biochemistry, 42*(4), 1170-1177.

Ramachandra, M., Ambudkar, S. V., Gottesman, M. M., Pastan, I., & Hrycyna, C. A. (1996). Functional characterization of a glycine 185-to-valine substitution in human P-glycoprotein by using a vaccinia-based transient expression system. *Molecular Biology of the Cell, 7*(10), 1485-1498.

Ramakrishnan, P. (2003). The role of p-glycoprotein in the blood-brain barrier. *Einstein Quarterly Journal of Biology and Medicine, 19*, 160-165.

Rameis, H. (1985a). On the interaction between phenytoin and digoxin. *Eur J Clin Pharmacol, 29*(1), 49-53.

Rameis, H. (1985b). Quinidine-digoxin interaction: are the pharmacokinetics of both drugs altered? *Int J Clin Pharmacol Ther Toxicol, 23*(3), 145-153.

Ramos, E., & O'Leary M, E. (2004). State-dependent trapping of flecainide in the cardiac sodium channel. *J Physiol, 560*(Pt 1), 37-49.

Ranaldi, F., Vanni, P., & Giachetti, E. (1999). What students must know about the determination of enzyme kinetic parameters. *Biochemical Education, 27*(2), 87-91.

Ranger, S., Sheldon, R., Fermini, B., & Nattel, S. (1993). Modulation of flecainide's cardiac sodium channel blocking actions by extracellular sodium: a possible cellular mechanism for the action of sodium salts in flecainide cardiotoxicity. *J Pharmacol Exp Ther, 264*(3), 1160-1167.

Rao, U. S. (1995). Mutation of glycine 185 to valine alters the ATPase function of the human P-glycoprotein expressed in Sf9 cells. *J Biol Chem, 270*(12), 6686-6690.

Rausl, D., Fotaki, N., Zanoski, R., Vertzoni, M., Cetina-Cizmek, B., Khan, M. Z., & Reppas, C. (2006). Intestinal permeability and excretion into bile control the arrival of amlodipine into the systemic circulation after oral administration. *J Pharm Pharmacol, 58*(6), 827-836.

Rautio, J., Humphreys, J. E., Webster, L. O., Balakrishnan, A., Keogh, J. P., Kunta, J. R., Serabjit-Singh, C. J., & Polli, J. W. (2006). In vitro p-glycoprotein inhibition assays for assessment of clinical drug interaction potential of new drug candidates: a recommendation for probe substrates. *Drug Metab Dispos, 34*(5), 786-792.

Raviv, Y., Pollard, H., Bruggemann, E., Pastan, I., & Gottesman, M. (1990). Photosensitized labeling of a functional multidrug transporter in living drug-resistant tumor cells. *Journal of Biological Chemistry, 265*(7), 3975-3980.

Rebbeor, J. F., & Senior, A. E. (1998). Effects of cardiovascular drugs on ATPase activity of P-glycoprotein in plasma membranes and in purified reconstituted form. *Biochim Biophys Acta, 1369*(1), 85-93.

Remme, C. A., & Bezzina, C. R. (2010). Sodium channel (dys)function and cardiac arrhythmias. *Cardiovasc Ther, 28*(5), 287-294.

Resetar, A. M., & Chalovich, J. M. (1995). Adenosine 5'-(gamma-thiotriphosphate): an ATP analog that should be used with caution in muscle contraction studies. *Biochemistry, 34*(49), 16039-16045.

Riganti, C., Campia, I., Polimeni, M., Pescarmona, G., Ghigo, D., & Bosia, A. (2009). Digoxin and ouabain induce P-glycoprotein by activating calmodulin kinase II and hypoxia-inducible factor-1alpha in human colon cancer cells. *Toxicol Appl Pharmacol, 240*(3), 385-392.

Rigaud, J. L., & Levy, D. (2003). Reconstitution of membrane proteins into liposomes. *Methods Enzymol, 372*, 65-86.

Ritchie, T. K., Grinkova, Y. V., Bayburt, T. H., Denisov, I. G., Zolnerciks, J. K., Atkins, W. M., & Sligar, S. G. (2009). Reconstitution of membrane proteins in phospholipid bilayer nanodiscs *Methods Enzymol* (2009/11/12 ed., Vol. 464, pp. 211-231).

Ritchie, T. K., Kwon, H., & Atkins, W. M. (2011). Conformational analysis of human ATP-binding cassette transporter ABCB1 in lipid nanodiscs and inhibition by the antibodies MRK16 and UIC2. *J Biol Chem, 286*(45), 39489-39496.

Roberts, A. G., Katayama, J., Kaspera, R., Ledwitch, K. V., Le Trong, I., Stenkamp, R. E., Thompson, J. A., & Totah, R. A. (2015). The role of cytochrome P450 BM3 phenylalanine-87 and threonine-268 in binding organic hydroperoxides. *Biochim Biophys Acta, 1860*(4), 669-677.

Roberts, A. G., Sjögren, S. E. A., Fomina, N., Vu, K. T., Almutairi, A., & Halpert, J. R. (2011). NMR-Derived Models of Amidopyrine and Its Metabolites in Complexes with Rabbit Cytochrome P450 2B4 Reveal a Structural Mechanism of Sequential N-Dealkylation. *Biochemistry, 50*(12), 2123-2134.

Roberts, A. G., Yang, J., Halpert, J. R., Nelson, S. D., Thummel, K. T., & Atkins, W. M. (2011). The structural basis for homotropic and heterotropic cooperativity of midazolam metabolism by human cytochrome P450 3A4. *Biochemistry, 50*(50), 10804-10818.

Robinson, K., Johnston, A., Walker, S., Mulrow, J. P., McKenna, W. J., & Holt, D. W. (1989). The digoxin-amiodarone interaction. *Cardiovasc Drugs Ther, 3*(1), 25-28.

Roden, D. M. (2004). Antiarrhythmic drugs: past, present, and future. *Heart Rhythm, 1*(5 Suppl), 57C-66C.

Roden, D. M., Darbar, D., & Kannankeril, P. J. (2007). Antiarrhythmic Drugs. In J. T. Willerson, H. J. J. Wellens, J. N. Cohn, & D. R. Holmes (Eds.), *Cardiovascular Medicine* (pp. 2085-2102). London: Springer London.

Rodriguez, I., Abernethy, D. R., & Woosley, R. L. (1999). P-Glycoprotein in clinical cardiology. *Circulation, 99*(4), 472-474.

Romermann, K., Wanek, T., Bankstahl, M., Bankstahl, J. P., Fedrowitz, M., Muller, M., Loscher, W., Kuntner, C., & Langer, O. (2013). (R)-[(11)C]verapamil is selectively transported by murine and human P-glycoprotein at the blood-brain barrier, and not by MRP1 and BCRP. *Nucl Med Biol, 40*(7), 873-878.

Romsicki, Y., & Sharom, F. J. (1998). The ATPase and ATP-binding functions of P-glycoprotein--modulation by interaction with defined phospholipids. *Eur J Biochem, 256*(1), 170-178.

Romsicki, Y., & Sharom, F. J. (1999). The membrane lipid environment modulates drug interactions with the P-glycoprotein multidrug transporter. *Biochemistry, 38*(21), 6887-6896.

Rosenberg, M. F., Kamis, A. B., Callaghan, R., Higgins, C. F., & Ford, R. C. (2003). Three-dimensional structures of the mammalian multidrug resistance P-glycoprotein demonstrate major conformational changes in the transmembrane domains upon nucleotide binding. *J Biol Chem, 278*(10), 8294-8299.

Roush, G. C., & Sica, D. A. (2016). Diuretics for Hypertension: A Review and Update. *Am J Hypertens*.

Rowland, M., & Tozer, T. N. (2010). *Clinical Pharmacokinetics and Pharmacodynamics: Concepts and Applications* (Fourth ed.). Philadelphia, PA: Lipponcott Williams & Wilkins.

Ruiz-Casado, A., Calzas, J., Garcia, J., Soria, A., & Guerra, J. (2006). Life-threatening adverse drug reaction to paclitaxel. Postmarketing surveillance. *Clin Transl Oncol, 8*(1), 60-61.

Russell, P. L., & Sharom, F. J. (2006). Conformational and functional characterization of trapped complexes of the P-glycoprotein multidrug transporter. *Biochem J, 399*(2), 315-323.

Saeki, T., Shimabuku, A. M., Ueda, K., & Komano, T. (1992). Specific drug binding by purified lipid-reconstituted P-glycoprotein: dependence on the lipid composition. *Biochim Biophys Acta, 1107*(1), 105-110.

Safa, A. R. (1992). Photoaffinity Labeling of P-Glycoprotein in Multidrug-Resistant Cells: New Drugs. *Cancer investigation, 10*(4), 295-305.

Safa, A. R., Stern, R. K., Choi, K., Agresti, M., Tamai, I., Mehta, N. D., & Roninson, I. B. (1990). Molecular basis of preferential resistance to colchicine in multidrug-resistant human cells conferred by Gly-185----Val-185 substitution in P-glycoprotein. *Proc Natl Acad Sci U S A, 87*(18), 7225-7229.

Schenck-Gustafsson, K., & Dahlqvist, R. (1981). Pharmacokinetics of digoxin in patients subjected to the quinidine-digoxin interaction. *Br J Clin Pharmacol, 11*(2), 181-186.

Schinkel, A. H., Mayer, U., Wagenaar, E., Mol, C. A., van Deemter, L., Smit, J. J., van der Valk, M. A., Voordouw, A. C., Spits, H., van Tellingen, O., Zijlmans, J. M., Fibbe, W. E., & Borst, P. (1997). Normal viability and altered pharmacokinetics in mice lacking mdr1-type (drug-transporting) P-glycoproteins. *Proc Natl Acad Sci U S A, 94*(8), 4028-4033.

Schuttelkopf, A. W., & van Aalten, D. M. F. (2004). PRODRG: a tool for high-throughput crystallography of protein-ligand complexes. *Acta Crystallographica Section D, 60*(8), 1355-1363.

Schwab, D., Fischer, H., Tabatabaei, A., Poli, S., & Huwyler, J. (2003). Comparison of in vitro P-glycoprotein screening assays: recommendations for their use in drug discovery. *J Med Chem, 46*(9), 1716-1725.

Schwartz, J. B. (1988). Effects of amlodipine on steady-state digoxin concentrations and renal digoxin clearance. *J Cardiovasc Pharmacol, 12*(1), 1-5.

Schwiebert, E. M., & Zsembery, A. (2003). Extracellular ATP as a signaling molecule for epithelial cells. *Biochim Biophys Acta, 1615*(1-2), 7-32.

Seelig, A. (1998). A general pattern for substrate recognition by P-glycoprotein. *Eur J Biochem, 251*(1-2), 252-261.

Segawa, M., Ogura, J., Seki, S., Itagaki, S., Takahashi, N., Kobayashi, M., Hirano, T., Yamaguchi, H., & Iseki, K. (2013). Rapid stimulating effect of the antiarrhythmic agent amiodarone on absorption of organic anion compounds. *Drug Metab Pharmacokinet, 28*(3), 178-186.

Segel, I. H. (1975). *Enzyme Kinetics: Behavior and Analysis of Rapid Equilibrium and Steady-State Enzyme Systems*. New York: John Wiley & Sons, Inc.

Shapiro, A. B., & Ling, V. (1994). ATPase activity of purified and reconstituted P-glycoprotein from Chinese hamster ovary cells. *J Biol Chem, 269*(5), 3745-3754.

Shapiro, A. B., & Ling, V. (1995). Reconstitution of drug transport by purified P-glycoprotein. *J Biol Chem, 270*(27), 16167-16175.

Shargel, L., Yu, A. B. C., & Wu-Pong, S. (2012). *Applied biopharmaceutics & pharmacokinetics* (6th ed.). New York: McGraw-Hill.

Sharom, F. J. (2008). ABC multidrug transporters: structure, function and role in chemoresistance. *Pharmacogenomics, 9*(1), 105-127.

Sharom, F. J. (2011). The P-glycoprotein multidrug transporter. *Essays Biochem, 50*(1), 161-178.

Sharom, F. J. (2014). Complex interplay between the P-glycoprotein multidrug efflux pump and the membrane: Its role in modulating protein function. *Front Oncol, 4*, 41.

Sharom, F. J., Liu, R., Romsicki, Y., & Lu, P. (1999). Insights into the structure and substrate interactions of the P-glycoprotein multidrug transporter from spectroscopic studies. *Biochim Biophys Acta, 1461*(2), 327-345.

Sharom, F. J., Russell, P. L., Qu, Q., & Lu, P. (2003). Fluorescence techniques for studying membrane transport proteins: the P-glycoprotein multidrug transporter. *Methods Mol Biol, 227*, 109-128.

Sharom, F. J., Yu, X., Chu, J. W., & Doige, C. A. (1995). Characterization of the ATPase activity of P-glycoprotein from multidrug-resistant Chinese hamster ovary cells. *Biochem J, 308 (Pt 2)*, 381-390.

Sharom, F. J., Yu, X., & Doige, C. A. (1993). Functional reconstitution of drug transport and ATPase activity in proteoliposomes containing partially purified P-glycoprotein. *J Biol Chem, 268*(32), 24197-24202.

Sharom, F. J., Yu, X., Lu, P., Liu, R., Chu, J. W., Szabo, K., Muller, M., Hose, C. D., Monks, A., Varadi, A., Seprodi, J., & Sarkadi, B. (1999). Interaction of the P-glycoprotein multidrug transporter (MDR1) with high affinity peptide chemosensitizers in isolated membranes, reconstituted systems, and intact cells. *Biochem Pharmacol, 58*(4), 571-586.

Shirzadi, A., Simpson, M. J., Xu, Y., & Simpson, A. J. (2008). Application of saturation transfer double difference NMR to elucidate the mechanistic interactions of pesticides with humic acid. *Environ Sci Technol, 42*(4), 1084-1090.

Shukla, S., Abel, B., Chufan, E. E., & Ambudkar, S. V. (2017). Effects of a detergent micelle environment on P-glycoprotein (ABCB1)-ligand interactions. *Journal of Biological Chemistry, 292*(17), 7066-7076.

Siarheyeva, A., Liu, R., & Sharom, F. J. (2010). Characterization of an asymmetric occluded state of P-glycoprotein with two bound nucleotides: implications for catalysis. *J Biol Chem, 285*(10), 7575-7586.

Siddoway, L. A. (2003). Amiodarone: guidelines for use and monitoring. *Am Fam Physician, 68*(11), 2189-2196.

Smith, M. E. B., Lee, N. J., Haney, E., & Carson, S. (2009) *Drug Class Review: HMG-CoA Reductase Inhibitors (Statins) and Fixed-dose Combination Products Containing a Statin: Final Report Update 5*. Portland (OR).

Smydo, J. (1979). Delayed respiratory depression with fentanyl. *Anesth Prog, 26*(2), 47-48.

Soltoff, S. P. (1986). ATP and the regulation of renal cell function. *Annu Rev Physiol, 48*, 9-31.

Sonveaux, N., Vigano, C., Shapiro, A. B., Ling, V., & Ruysschaert, J. M. (1999). Ligand-mediated tertiary structure changes of reconstituted P-glycoprotein. A tryptophan fluorescence quenching analysis. *J Biol Chem, 274*(25), 17649-17654.

Staud, F., Cerveny, L., & Ceckova, M. (2012). Pharmacotherapy in pregnancy; effect of ABC and SLC transporters on drug transport across the placenta and fetal drug exposure. *J Drug Target, 20*(9), 736-763.

Stollberger, C., & Finsterer, J. (2015). Relevance of P-glycoprotein in stroke prevention with dabigatran, rivaroxaban, and apixaban. *Herz, 40 Suppl 2*, 140-145.

Suhail, M. (2010). Na, K-ATPase: Ubiquitous Multifunctional Transmembrane Protein and its Relevance to Various Pathophysiological Conditions. *J Clin Med Res, 2*(1), 1-17.

Sunga, A. J., Tolstorukov, I., & Cregg, J. M. (2008). Posttransformational vector amplification in the yeast Pichia pastoris. *FEMS Yeast Res, 8*.

Tabrizchi, R. (2010). Molecular mechanisms of adverse drug reactions in cardiac tissue. *Handb Exp Pharmacol*(196), 77-109.

Tamai, I., & Safa, A. R. (1991). Azidopine noncompetitively interacts with vinblastine and cyclosporin A binding to P-glycoprotein in multidrug resistant cells. *Journal of Biological Chemistry, 266*(25), 16796-16800.

Tanigawara, Y. (2000). Role of P-glycoprotein in drug disposition. *Ther Drug Monit, 22*(1), 137-140.

Taub, M. E., Podila, L., Ely, D., & Almeida, I. (2005). Functional assessment of multiple P-glycoprotein (P-gp) probe substrates: influence of cell line and modulator concentration on P-gp activity. *Drug Metab Dispos, 33*(11), 1679-1687.

Tetreault, S., & Ananthanarayanan, V. S. (1993). Interaction of calcium channel antagonists with calcium: structural studies on verapamil and its Ca2+ complex. *J Med Chem, 36*(8), 1017-1023.

Thein, T., Koene, R. A., & Wijdeveld, P. G. (1977). Orthostatic hypotension due to prazosin. *Lancet, 1*(8007), 363.

Tombline, G., Urbatsch, I. L., Virk, N., Muharemagic, A., White, L. B., & Senior, A. E. (2006). Expression, purification, and characterization of cysteine-free mouse P-glycoprotein. *Arch Biochem Biophys, 445*(1), 124-128.

Trott, O., & Olson, A. J. (2010). AutoDock Vina: improving the speed and accuracy of docking with a new scoring function, efficient optimization, and multithreading. *J Comput Chem, 31*(2), 455-461.

Ulrich, E. L., Akutsu, H., Doreleijers, J. F., Harano, Y., Ioannidis, Y. E., Lin, J., Livny, M., Mading, S., Maziuk, D., Miller, Z., Nakatani, E., Schulte, C. F., Tolmie, D. E., Kent Wenger, R., Yao, H., & Markley, J. L. (2008). BioMagResBank. *Nucleic Acids Res, 36*(Database issue), D402-408.

Urbatsch, I. L., al-Shawi, M. K., & Senior, A. E. (1994). Characterization of the ATPase activity of purified Chinese hamster P-glycoprotein. *Biochemistry, 33*(23), 7069-7076.

Urbatsch, I. L., Sankaran, B., Bhagat, S., & Senior, A. E. (1995). Both P-glycoprotein nucleotide-binding sites are catalytically active. *J Biol Chem, 270*(45), 26956-26961.

Urbatsch, I. L., & Senior, A. E. (1995). Effects of lipids on ATPase activity of purified Chinese hamster P-glycoprotein. *Arch Biochem Biophys, 316*(1), 135-140.

Vahakangas, K., & Myllynen, P. (2009). Drug transporters in the human blood-placental barrier. *Br J Pharmacol, 158*(3), 665-678.

Vallakati, A., Chandra, P. A., Pednekar, M., Frankel, R., & Shani, J. (2013). Dronedarone-induced digoxin toxicity: new drug, new interactions. *Am J Ther, 20*(6), e717-719.

Van Der Spoel, D., Lindahl, E., Hess, B., Groenhof, G., Mark, A. E., & Berendsen, H. J. (2005). GROMACS: fast, flexible, and free. *J Comput Chem, 26*(16), 1701-1718.

van Zundert, G. C., Rodrigues, J. P., Trellet, M., Schmitz, C., Kastritis, P. L., Karaca, E., Melquiond, A. S., van Dijk, M., de Vries, S. J., & Bonvin, A. M. (2016). The HADDOCK2.2 Web Server: User-Friendly Integrative Modeling of Biomolecular Complexes. *J Mol Biol, 428*(4), 720-725.

Venkitakrishnan, R., Benard, O., Max, M., Markley, J., & Assadi-Porter, F. (2012). Use of NMR Saturation Transfer Difference Spectroscopy to Study Ligand Binding to Membrane Proteins. In N. Vaidehi & J. Klein-Seetharaman (Eds.), *Membrane Protein Structure and Dynamics* (Vol. 914, pp. 47-63): Humana Press.

Venkitakrishnan, R. P., Benard, O., Max, M., Markley, J. L., & Assadi-Porter, F. M. (2012). Use of NMR Saturation Transfer Difference Spectroscopy to Study Ligand Binding to Membrane Proteins. In N. Vaidehi & J. Klein-Seetharaman (Eds.), *Membrane Protein Structure and Dynamics: Methods and Protocols* (pp. 47-63). Totowa, NJ: Humana Press.

Verhalen, B., Ernst, S., Borsch, M., & Wilkens, S. (2012). Dynamic ligand-induced conformational rearrangements in P-glycoprotein as probed by fluorescence resonance energy transfer spectroscopy. *J Biol Chem, 287*(2), 1112-1127.

Verschraagen, M., Koks, C. H., Schellens, J. H., & Beijnen, J. H. (1999). P-glycoprotein system as a determinant of drug interactions: the case of digoxin-verapamil. *Pharmacol Res, 40*(4), 301-306.

Vigano, C., Julien, M., Carrier, I., Gros, P., & Ruysschaert, J.-M. (2002). Structural and functional asymmetry of the nucleotide-binding domains of P-glycoprotein investigated by attenuated total reflection Fourier transform infrared spectroscopy. *Journal of Biological Chemistry, 277*(7), 5008-5016.

von Richter, O., Glavinas, H., Krajcsi, P., Liehner, S., Siewert, B., & Zech, K. (2009). A novel screening strategy to identify ABCB1 substrates and inhibitors. *Naunyn Schmiedebergs Arch Pharmacol, 379*(1), 11-26.

Wang, G., Pincheira, R., & Zhang, J. T. (1998). Dissection of drug-binding-induced conformational changes in P-glycoprotein. *Eur J Biochem, 255*(2), 383-390.

Wang, Q., Rager, J. D., Weinstein, K., Kardos, P. S., Dobson, G. L., Li, J., & Hidalgo, I. J. (2005). Evaluation of the MDR-MDCK cell line as a permeability screen for the blood-brain barrier. *Int J Pharm, 288*(2), 349-359.

Ward, A., Reyes, C. L., Yu, J., Roth, C. B., & Chang, G. (2007). Flexibility in the ABC transporter MsbA: Alternating access with a twist. *Proc Natl Acad Sci U S A, 104*(48), 19005-19010.

Ward, A. B., Szewczyk, P., Grimard, V., Lee, C. W., Martinez, L., Doshi, R., Caya, A., Villaluz, M., Pardon, E., Cregger, C., Swartz, D. J., Falson, P. G., Urbatsch, I. L., Govaerts, C., Steyaert, J., & Chang, G. (2013). Structures of P-glycoprotein reveal its conformational flexibility and an epitope on the nucleotide-binding domain. *Proc Natl Acad Sci U S A, 110*(33), 13386-13391.

Watanabe, T., Uchiyama, N., Roninson, I. B., Cohen, D., & Atadja, P. (2000). Altered activity of MDR-reversing agents on KB3-1 cells transfected with Gly(185)-->Val human P-glycoprotein. *Int J Oncol, 17*(3), 579-586.

Wegener, F. T., Ehrlich, J. R., & Hohnloser, S. H. (2006). Dronedarone: an emerging agent with rhythm- and rate-controlling effects. *J Cardiovasc Electrophysiol, 17 Suppl 2*, S17-20.

Weidner, M., Taupp, M., & Hallam, S. J. (2010). Expression of recombinant proteins in the methylotrophic yeast Pichia pastoris. *J Vis Exp*(36).

Welker, E., Szabo, K., Hollo, Z., Muller, M., Sarkadi, B., & Varadi, A. (1995). Drug-stimulated ATPase activity of a deletion mutant of the human multidrug-resistance protein (MDR1). *Biochem Biophys Res Commun, 216*(2), 602-609.

Wessler, J. D., Grip, L. T., Mendell, J., & Giugliano, R. P. (2013). The P-glycoprotein transport system and cardiovascular drugs. *J Am Coll Cardiol, 61*(25), 2495-2502.

Whyteside, G., Alcocer, M. J., Kumita, J. R., Dobson, C. M., Lazarou, M., Pleass, R. J., & Archer, D. B. (2011). Native-state stability determines the extent of degradation relative to secretion of protein variants from Pichia pastoris. *PLoS One, 6*.

Wong, R., Lopaschuk, G., Zhu, G., Walker, D., Catellier, D., Burton, D., Teo, K., Collins-Nakai, R., & Montague, T. (1992). Skeletal muscle metabolism in the chronic fatigue syndrome. In vivo assessment by 31P nuclear magnetic resonance spectroscopy. *Chest, 102*(6), 1716-1722.

Wu, D., Chen, A., & Johnson, C. S. (1995). An improved diffusion-ordered spectroscopy experiment incorporating bipolar-gradient pulses. *Journal of magnetic resonance, Series A, 115*(2), 260-264.

Wulff, H., Castle, N. A., & Pardo, L. A. (2009). Voltage-gated potassium channels as therapeutic targets. *Nat Rev Drug Discov, 8*(12), 982-1001.

Zaidenstein, R., Eyal, S., Efrati, S., Akivison, L., Michowitz, M. K., Nagornov, V., & Golik, A. (2002). Adverse drug events in hospitalized patients treated with cardiovascular drugs and anticoagulants. *Pharmacoepidemiol Drug Saf, 11*(3), 235-238.

Zhang, C., Kwan, P., Zuo, Z., & Baum, L. (2010). In vitro concentration dependent transport of phenytoin and phenobarbital, but not ethosuximide, by human P-glycoprotein. *Life Sci, 86*(23-24), 899-905.

Zhang, L., Huang, S. M., & Lesko, L. J. (2011). Transporter-mediated drug-drug interactions. *Clin Pharmacol Ther, 89*(4), 481-484.

Zhou, S. F. (2008). Structure, function and regulation of P-glycoprotein and its clinical relevance in drug disposition. *Xenobiotica, 38*(7-8), 802-832.

Zhou, Y., Tozzi, F., Chen, J., Fan, F., Xia, L., Wang, J., Gao, G., Zhang, A., Xia, X., Brasher, H., Widger, W., Ellis, L. M., & Weihua, Z. (2012). Intracellular ATP levels are a pivotal determinant of chemoresistance in colon cancer cells. *Cancer Res, 72*(1), 304-314.

Ziff, O. J., & Kotecha, D. (2016). Digoxin: The good and the bad. *Trends Cardiovasc Med*.